ENERGY ANALYSIS OF A FLAT PLATE SOLAR COLLECTOR USING CF-MWCNTS AND NONCF-MWCNTS/WATER NANOFLUIDS: A CFD BASED COMPARISON

2023
MASTER THESIS
MECHANICAL ENGINEERING

Abdulazeez Ahmed HAMEEDI

Thesis Advisors
Assist. Prof. Dr. Cevat ÖZARPA
Assist. Prof. Dr. Omar Assi HUSSEIN

ENERGY ANALYSIS OF A FLAT PLATE SOLAR COLLECTOR USING CF-MWCNTS AND NONCF-MWCNTS/WATER NANOFLUIDS: A CFD BASED COMPARISON

Abdulazeez Ahmed HAMEEDI

Thesis Advisors
Assist. Prof. Dr. Cevat ÖZARPA
Assist. Prof. Dr. Omar Assi HUSSEIN

T.C.
Karabük University
Institute of Graduate Programs
Department of Mechanical Engineering

Prepared as
Master Thesis

KARABÜK
July 2023

I certify that in my opinion, the thesis submitted by Abdulazeez Ahmed HAMEEDI titled "ENERGY ANALYSIS OF A FLAT PLATE SOLAR COLLECTOR USING CF-MWCNTS AND NONCF-MWCNTS/WATER NANOFLUIDS: A CFD BASED COMPARISON" is fully adequate in scope and in quality as a thesis for the degree of Master of Science.

Assist. Prof. Dr. Cevat ÖZARPA .....
Thesis Advisor, Department of Mechanical Engineering

Assist. Prof. Dr. Omar Assi HUSSEIN .....
Second Advisor, Department of Mechanical Engineering, Tikrit University

This thesis is accepted by the examining committee with a unanimous vote in the Department of Mechanical Engineering as a Master of Science thesis.

Examining Committee Members (Institutions)	Signature
Chairman : Prof. Dr. Mehmet ÖZALP (KBU)	….....
Member : Assoc. Prof. Dr. Yusuf BİÇER (HBKU)	.....
Member : Asst. Prof. Dr. Cevat ÖZARPA (KBU)	.....

The degree of Master of Science by the thesis submitted is approved by the Administrative Board of the Institute of Graduate Programs, Karabük University.

Prof. Dr. Müslüm KUZU .....
Director of the Institute of Graduate Programs

This thesis contains information that I have gathered and presented in a manner that is consistent with academic regulations and ethical principles, and I affirm that I have appropriately cited any and all sources that are not my own work.

Abdulazeez Ahmed HAMEEDI

ABSTRACT

M. Sc. Thesis

ENERGY ANALYSIS OF A FLAT PLATE SOLAR COLLECTOR USING CF-MWCNTS AND NONCF-MWCNTS/WATER NANOFLUIDS: A CFD BASED COMPARISON

Abdulazeez Ahmed HAMEEDI

Karabük University
Institute of Graduate Programs
The Department of Mechanical Engineering

Thesis Advisors:
Assist. Prof. Dr. Cevat ÖZARPA
Assist. Prof. Dr. Omar Assi HUSSEIN
July 2023, 125 pages

Adding metallic particles to thermal fluid systems is a promising approach to enhance heat transfer, but the poor stability of suspensions containing micro-sized particles limits their applications. This study explores the use of newly developed mono nanofluids to replace conventional water-based fluids in flat plate solar collectors. The nanofluids assessed in this study are a combination of covalently functionalized-multi-walled carbon nanotubes (CF-MWCNTs) and non-covalently functionalized-multi-walled carbon nanotubes (NCF-MWCNTs) in distilled water as a base fluid, are expected to enhance fluid conductivity and boost thermal efficiency. The study examines the physical and thermal properties of the mono nanofluids, including stability, thermal conductivity, viscosity, specific heat capacity, and density.Various techniques such as FESEM, FTIR, Raman, and XRD characterized

the morphology and dispersion stability of the functionalized materials. At the ultrasonic test time, the highest stability of nanofluids was achieved at 60 min. The measurement confirmed that covalent functionalization nanofluids (CF-MWCNTs) thermal conductivity was higher than non-covalent functionalization (NCF-MWCNTs), higher than distilled water. In conclusion, the growth in thermal conductivity and stability of (CF-MWCNTs) was higher than (NCF-MWCNTs), and the lowest viscosity was 6.4% higher than distilled water, while the best thermal conductivity improvement was (30.3%). The thermal efficiency of flat plate solar collectors with different working fluids, with and without nanoparticles, was tested at various volumetric flow rates (2 L/min, 3 L/min, and 4 L/min), using ASHRAE standard 93-2010. ANSYS software was used for simulation and multi-objective optimization of the performance of nanofluid-filled flat plate solar collectors. Indoor experiments were conducted to characterize CF-MWCNTs. The obtained results showed that the thermal efficiency of the flat plate solar collector was improved by 18.7% and 10.4% with 0.10 wt.% and 0.05 wt.% nanofluids, respectively, at an absorber flow rate of 4 L/min. The use of nanofluid at a flow rate of 4 L/min improved the thermal efficiency of the solar collector by 84% compared to conventional water-based fluids. Increasing the weight percentage of nanoparticles enhanced thermal energy gain and resulted in a higher fluid outlet temperature.

Keywords **:** Computational flhuid dynamic, Covalent Functionalization, NON Covalent Functionalization, Multi-walled carbon nanotubes, Flat plate solar collectors

Science Code : 91411

ÖZET

Yüksek Lisans Tezi

DÜZ PLAKA GÜNEŞ KOLLEKTÖRÜNÜN CF-MWCNTS VE NNCF-MWCNTS/SU NANOSIVILAR KULLANARAK ENERJİ ANALİZİ: CFD TABANLI KARŞILAŞTIRMA

Abdulazeez Ahmed HAMEEDI

Karabük Üniversitesi
Lisansüstü Eğitim Enstitüsü
Makine Mühendisliği Anabilim Dalı

Tez Danışmanları:
Dr. Öğr. Üyesi Cevat ÖZARPA
Dr. Öğr. Üyesi Omar Assi HUSSEIN
Temmuz 2023, 125 sayfa

Termik akışkan sistemlerine metalik parçacıklar eklemek, ısı transferini artırmak için umut verici bir yaklaşımdır, ancak mikro boyutlu parçacıklar içeren süspansiyonların zayıf stabilitesi, uygulamalarını sınırlar. Bu çalışmada, düz plaka güneş kollektörlerinde geleneksel su bazlı sıvıların yerini almak için yeni geliştirilen mono nanoakışkanların kullanımı araştırılmıştır. Bu çalışmada değerlendirilen nanoakışkanlar, kovalent olarak işlevselleştirilmiş çok duvarlı karbon nanotüplerin (CF-MWCNT'ler) ve kovalent olarak işlevselleştirilmemiş çok duvarlı karbon nanotüplerin (NCF-MWCNT'lerin) bir baz sıvısı olarak damıtılmış suda bir kombinasyonu olup sıvı iletkenliğini ve termal verimliliği artırması beklenmektedir. Çalışma, kararlılık, termal iletkenlik, viskozite, özgül ısı kapasitesi ve yoğunluk dahil olmak üzere mono nano sıvıların fiziksel ve termal özellikleri incelenmiştir. FESEM,

FTIR, Raman ve XRD gibi çeşitli teknikler, işlevselleştirilmiş malzemelerin morfolojisini ve dağılım stabilitesini karakterize etti. Ultrasonik test süresinde, nanoakışkanların en yüksek kararlılığı 60 dakikada elde edilmiştir. Ölçüm, kovalent işlevselleştirme nanoakışkanlarının (CF-MWCNT'ler) termal iletkenliğinin kovalent olmayan işlevselleştirmeden (NCF-MWCNT'ler) ve damıtılmış sudan daha yüksek olduğunu doğruladı. Sonuç olarak, (CF-MWCNT'ler)'in ısıl iletkenliği ve kararlılığındaki artış (NCF-MWCNT'ler)'den daha yüksekti ve en düşük viskozite, saf sudan 6,4% daha yüksekken, en iyi ısıl iletkenlik gelişimi (30,3%) oldu Nanoparçacıklı ve nanoparçacıksız farklı çalışma sıvılarına sahip düz plakalı güneş kollektörlerinin termal verimliliği, ASHRAE standardı 93-2010 kullanılarak çeşitli hacimsel akış hızlarında (2 L/dk, 3 L/dk ve 4 L/dk) test edilmiştir. Nanoakışkan dolgulu düz levha güneş kollektörlerinin performansının simülasyonu ve çok amaçlı optimizasyonu için ANSYS yazılımı kullanılmıştır. CF-MWCNT'leri karakterize etmek için iç mekân deneyleri yapılmıştır. Sonuçlar, düz levha güneş kollektörünün ısıl veriminin, 4 L/dak'lık bir soğurucu akış hızında, ağırlıkça %0,10 ve ağırlıkça %0,05 nano sıvı ile sırasıyla %18,7 ve %10,4 oranında iyileştiğini göstermiştir. 4 L/dk debide nano akışkan kullanımı, güneş kollektörünün ısıl verimini geleneksel su bazlı akışkanlara kıyasla %84 oranında iyileştirmiştir. Nanoparçacıkların ağırlık yüzdesinin arttırılması, termal enerji kazanımını arttırmış ve daha yüksek bir akışkan çıkış sıcaklığı ile sonuçlanmıştır.

Anahtar Kelimeler **:** Hesaplamalı akışkanlar dinamiği, Kovalent İşlevselleştirme, NON Kovalent İşlevselleştirme, Çok duvarlı karbon nanotüpler, Düz plakalı güneş kollektörleri

Bilim Kodu **:** 91411

ACKNOWLEDGEMENT

Praise be to God and thanks be to Him for His many blessings, for the blessing of Islam and for health and security. Thanks to our great Messenger, our first and last teacher, Muhammad, may God bless him and grant him peace, for illuminating our path and removing darkness from our hearts before our sight. My thanks go out to every teacher who helped me to know him from the first stages of this study until this moment. I would also like to extend a word of thanks, respect and appreciation to my esteemed teachers, Assist. Prof. Dr. Cevat Özarpa and Assist. prof. Dr. Omar Assi Hussein, I wish them all the best and success. I also thank the Head of the Department of Mechanical Engineering Prof. Dr. Kamil Arslan and his staff for the help they provided me. I dedicate my achievement to my beloved country, Iraq, to our dear people, and to the dear Republic of Turkey for the assistance it provided us. And many thanks to the man who taught me, supported me and inspired me, my dear father, may God prolong his life, to the source of security and tenderness, my beloved mother, may God prolong your life, to those who supported me and helped me, my beloved wife and my young children, the smile of life, you, thank you for your patience, may God protect you, to my brothers And my sisters and relatives and everyone who helped me and stood with me even with a word. Finally, I can only pray to God Almighty to benefit the country and the people and grant us guidance, chastity, more knowledge, and knowledge, and inspire me with more determination and strength to advance my scientific thesis and study for a doctorate, God willing.

CONTENTS

Page

Page

Page

Page

TABLE OF FIGURES

Page

Page

Page

LIST OF TABLES

Page

SYMBOLS AND ABBREVITIONS INDEX

SYMBOLS

CFD	: Computational fluid dynamic
NPs	: Nanoplatelets
CF- MWCNTS	: Covalent Functionalization mwcnts
SDBS	: Sodium dodecyl benzene sulfonate
NONCF- MWCNTS	: NON-Covalent Functionalization mwcnts
T_a	: Ambient temperature (C°)
MWCNTS	: Multi-walled carbon nanotubes
SDS	: Sodium dodecyl sulfate
FPSCS	: Flat plate solar collectors
C_p	: Specific heat (J/kgk)
DW	: Distilled water
FESEM	: Field emission scanning electron microscopy
GA	: Gum arabic
Ctab	: Cetyltrimethylammonium bromide
TX-100	: Tritonx-100
G_t	: Global radiation (W/m^2)
ASHRAE	: American society of heating, refrigerating and air-conditioning engineers
M*	: Mass flow rate (l/m)
Fe_3O_4	: Iron (II, III) oxide (ferrous ferric oxide)
UV–vis	: Ultraviolet–visible spectrophotometry
EXP	: Experimental
CNT_S	: Carbon nanotubes
THEO	: Theoretical
DSC	: Differential scanning calorimeter
TIO_2	: Titanium dioxide (titania)

EG	: Ethylene glycol
Al_2O_3	: Aluminum dioxide
FTIR	: Fourier transform infrared spectroscopy
Tga	: Thermo-gravimetric analysis
P-MWCNT$_S$	: Pristine mwcnts
Edx	: Energy dispersive spectroscopy
R^2	: Regression coefficient
η_i	: Efficiency of flat-plate solar collector
Tw-80	: Tween-80
HNO_3	: Nitric acid
H_2SO_4	: Sulfuric acid
-OH	: Surface hydroxyl group
Sl	: Sodium laureate
PVP	: Polyvinylpyrrolidone
DSC	: Differential scanning calorimetry

PART 1

INTRODUCTION

The increase in renewable energy generation using natural resources has become very important. To work on this and see the important strategies and procedures for storing this continuous and vital sustainability. The guiding principle enables us to exploit and change renewable energy from one source to another, thus enabling us to store the converted energy and reuse it when needed to keep pace with our daily lives. The basic energy capacity can be classified into several systems: 1- Magnetic: In these systems, the attractive energy is characterized by superconductivity (Li *et al.*, 2022). 2- Electrochemical: these systems use batteries, fuel cells and supercapacitors (Abdisattar *et al*., 2022). 3- Hydro: these systems use water pumps (Prasojo *et al.*, 2020). 4- Pneumatic: In these systems, the wind speed is controlled by air compressors (Postol & Struchaiev, 2020). 5- Mechanical: In these systems, flywheels are used (Mahmoud *et al.,* 2020). 6- Thermal: In these systems, liquid salt, water, or oil radiators are used (Ramasamy *et al.*, 2020). To select energy capacity measures, researchers and analysts used several distinct criteria, and the main objectives that must be taken into account are: 1- the natural resources that can be accessed to obtain energy, 2- the necessary energy and the purpose of its application, 3- energy storage and its efficiency, 4- the cost used for energy storage, 5- the infrastructure and the method of storing its energy, 6- other necessary factors that must be taken into account during the application.

Based on the cleanliness of the environment and the safety of the desired atmosphere resulting from solar energy, its use has become widely accepted, and it aims to greatly reduce environmental impacts, which are less than any other renewable energy source (Verma & Kundan, 2013). Solar energy is the best available resource by exploiting renewable energy in any form of energy conversion, including direct and indirect. Solar energy converters exploit part of the sun's rays, and the second

part is transferred to the atmosphere to maintain environmental balance and sustainability. Whereas, if 0.1% of this photovoltaic solar energy is exploited, it is converted with an efficiency of 10%. It can generate about 3,000 gigawatts, which is about four times the current total generation capacity of the entire world (Thirugnanasambandam *et al.*, 2010).

1.1. RESEARCH BACKGROUND

As developing countries strive for progress and improvement, their energy needs increase daily. Because of this increase, and due to the scarcity of traditional fuel used for energy production and its continued depletion and environmentally and economically harmful waste, and to overcome that, it was necessary to search for an alternative. Renewable energy was considered the alternative source for that. It is considered from renewable energy sources that solar energy is abundant, sustainable, renewable, low-cost energy and environmental pollution or non-existent. In order to exploit this, solar collectors must be commonly used to harvest that available energy. The traditional liquids (water) used as a medium for transferring the converted energy in the solar collectors suffer from weak absorption and transmission properties. Through the performance results of several experiments conducted by the researchers on the collectors using conventional fluids, they reached a solution that shows that normal or traditional liquids have limited portability for carry and heat transfer, which reduces its work results from its use as a working fluid. For exploiting that energy, ensuring that it is not lost or reduced, it was noted that concerning the poor performance compared to traditional working fluids, it could be replaced by enhancing the liquid (nanofluid) utilizing nanoparticles, as an ideal alternative, with regard to its improved or thermally distinguished properties. In this present study, we will try to enhance the performance efficiency of flat plate solar collectors by using MWCNTs / water as a working fluid, as it is considered one of the modern technologies. There is some literature or previous research that talks about the use of carbon nanofluids in fpsc. This leads to the development of this research proposal, which aims to further enhance the thermal efficiency of flat plate solar collectors using a new type of liquid called "nanofluid".

1.2. SIGNIFICANCE OF THE STUDY

The importance of the study comes in light of the increasing conditions of development witnessed by developed countries, generally concerning heating and industry. In line with development and growth, there has become an increasing demand for energy daily, especially from fossil fuels, considered scarce and depleted sources, and harmful waste on the resulting environment. About fuel use from air pollution, global warming, and others. Therefore, it has become extremely necessary to work to find necessary and sustainable alternatives to renewable energy from those renewable energies, namely solar energy and the resulting radiation. Solar energy is abundant, and solar energy collectors are widely used to harvest and exploit that energy and convert it into useful energy for daily purposes.

1.3. PROBLEM STATEMENT

Distilled water, ethylene glycol, and motor oil are frequently used working fluids in various mechanical equipment and engineering operations. The heat transfer process, represented in electronic device coolers by fans, power generation, solar energy collectors, chemical processors, and various heat exchange devices, is crucial and effective in most disciplines. Furthermore, conventional heat transfer fluids have a relatively low thermal conductivity, making transmitting heat at high rates in thermal applications impossible. Mechanical equipment with higher pressure and efficiency can be developed, resulting in cost savings in both capital and labor due to improved heat transfer of the working fluids used. The study's methodological issues include the following:

- Using metallic oxide nanofluids in solar collectors provided very low efficiency compared to conventional base fluids.
    - The multi-walled carbon nanofluids based on the nanostructure will be used theoretically in this study by developing a new test platform.
- Lack of uniform the dispersion and the stability of the nano additives in suspensions. Agglomeration of nano additives in nanofluids occurs due to the high surface tension and high surface area of the nano-material associated

with the effects the electrostatic forces of Van der Wall‟s forces between the nanoparticles/additives. Such phenomena will cause the nanoparticle to settle and block the flow channels, and as a sequence, will decrease the thermal conductivity of the nanofluids.

1.4. OBJECTIVES OF THE RESEARCH

This research proposal has the following objectives:

- To experimentally measure the thermophysical properties of covalent and non-covalent multi-walled carbon nanotubes at different temperatures.
- To compare the thermal performance of CF-MWCNTs and non-CF-MWCNTs suspended in water as heat transfer fluids in a flat plate solar collector.
- To carry out numerical simulations using ANSYS-FLUENT software to solve the governing equations in the thermal and flow fields of the carbon nanofluid in the FPSC. A comparison will be made between the experimental and numerical results under different conditions.

1.5. RESEARCH SCOPE

- Two types of nanopowders will be studied; CF-MWCNTs and non-CF-MWCNTs.
- The exploratory test run will be conducted using different values of mass flow rate in the range (2, 3 and 4 L/min) and inlet fluid temperature in the range (20°C to 60°C).
- The concentration and weight of different nanoparticles are examined. They are in the range of (0.02%, 0.05%, 0.08% and 0.1%) of the nanomaterial in the base fluid.
- The Reynolds number varies from 100 to 500 to cover a laminar flow system.

1.6 Research Hypothesis

From the theoretical indications, it was proved that the multi-walled carbon tubes with the covalent bond increase the dispersion and stability, and there is an excellent improvement in the performance efficiency of the flat solar collector.

PART 2

LITERATURE REVIEW

This chapter summarizes the results of earlier investigations in the research or literature on nanofluids' usage in flat solar panel collectors. Additionally, it will be demonstrated how nanofluids' thermal performance and flow properties in large-scale solar collectors are achieved in this chapter and in the earlier writings. Current studies and nanofluid preparation techniques, stability evaluation, thermophysical characteristics, and measurement tools will also be addressed.

2.1. SOLAR THERMAL COLLECTORS

The purpose of solar thermal collectors (STCs) aim to increase the working fluid's temperature by converting the radiation energy (sunlight) obtained from the sun into thermal energy. This is the best option for utilizing and conserving energy. Temperature and the amount of this conversion are dependent on the collector method (Jesko 2008). Generally solar thermal collectors are classified into two broad categories: non-concentrating and concentrating types according to the degree of radiative heat concentration. Concentrating collector technology is categorized as medium concentration, for example, the parabolic cylinder and as high concentration, for example, the paraboloidal collectors. A concentrating collector consists of a parabolic-shaped surface to reflect and concentrate the sun's energy to a focal point where the absorber is positioned. They can be designed as a fixed device or rotating reflectors to track the sun position in the sky for maximum solar capture..

These complexes can cover temperatures ranging from 150 to 500 and up to 1500 degrees Celsius later. However, NCSP can roughly encompass the temperature range between 1 and 200°C thanks to FPSC and evacuated tube technology. The division of solar heat collectors is depicted in Fig. (2.1).

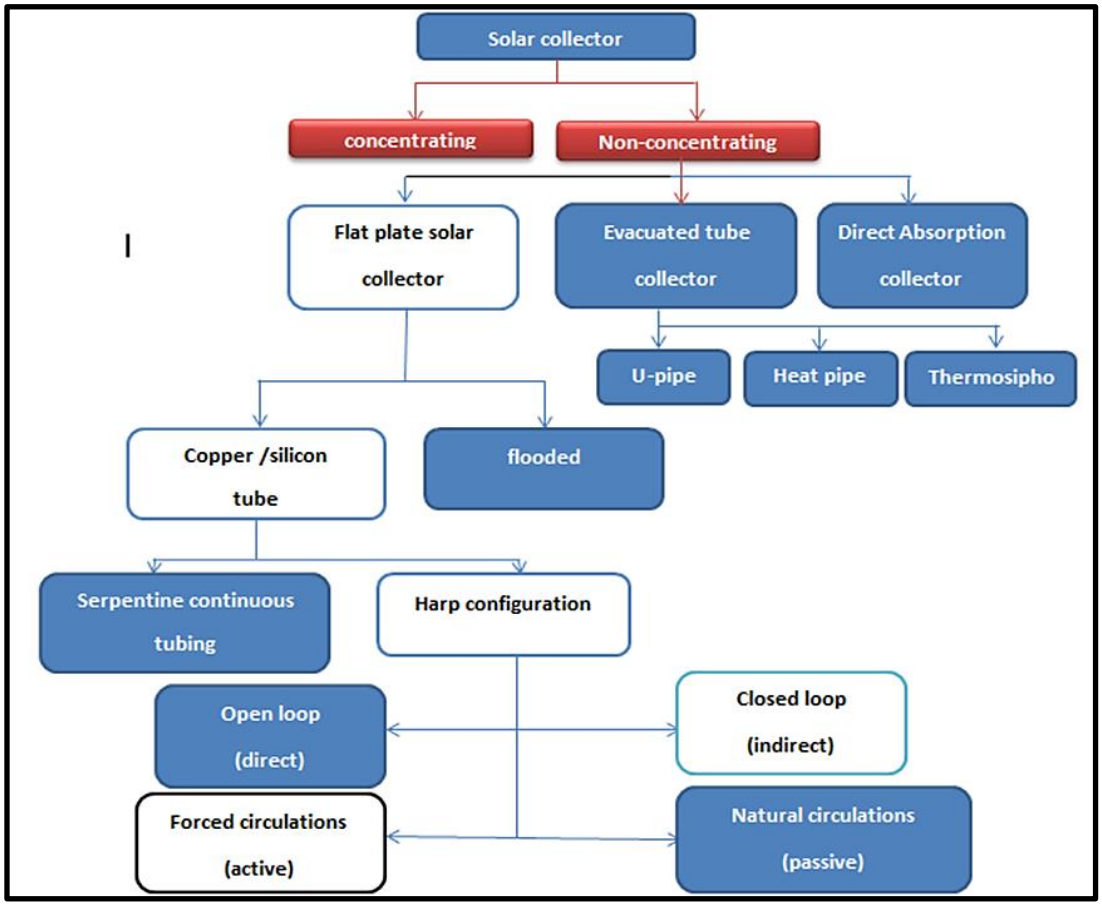

Figure 2.1. Solar-collector section (Jesko 2008).

A non-concentrated direct absorption collector's (DAC) main function is to capture most or all of the solar radiation. In designs, there is frequently no barrier between solar radiation and the moving working fluid. (Qin *et al*., 2017).

FPSCs are among the most widely used collectors worldwide and in various applications, including industrial, commercial and domestic, water heating and solar heating (Jesko 2008). Researchers and various populations around the world benefit from solar radiation, and despite the low financial costs of maintaining the solar system, these collectors could not track the spread of solar radiation. The ability to effectively shed snow and rain, even when placed in arctic and tropical climates with high snow and rain, makes FPSCs practical technologies that have good benefits over other kinds. There are two categories of flat plate solar collectors: tubular and submerged. Parts of an FPSCS The absorber in a submerged type has two parallel metal sheets that enable the working fluid to flow between them. The surface area

affects the efficiency gain. FPSCS are composed of a sinuous and lyre-shaped tube. Serpentine FPSCs offer an effective, continuous S-shaped absorbent that the heated heat transfer fluid travels through from one end to the other.

2.2. FLAT PLATE SOLAR COLLECTOR (FPSC)

It is intended to capture the heat produced by the absorber plate and send it to the FPSCs working fluid, improving the system's thermal efficiency. Due to its superior thermal properties, the nanoscale working fluid is used as an alternative to the frequently used working fluids to increase the collector's overall efficiency. Despite the positive outcomes it produces, there are a few things to keep in mind, including when using nanofluids for solar energy gain uses. One such element is the stable state of the nanofluid, in which solid nanoparticles (NPs) cannot diffuse completely or stay suspended in the working fluid for an extended period of time. (Hordy *et al.*, 2014). The high surface area to volume ratio of NPs can lead to their tendency to agglomerate (Chaji *et al*., 2013). Under normal conditions, the agglomerated NP system has an undesirable problem. The agglomeration property not only clogs the flow channels but may also impede the thermal conductivity of the nanofluid. In order to avoid this, it is necessary to solve the problem of potential factors that can affect the dispersion stability of heat transfer NPs (Chen *et al*., 2009). One important consideration is the cost because nanofluids are very expensive (Saidur *et al.*, 2011).

2.3. CONCEPT OF FPSC

The FPSCs system has several parts, and among those components for the FPSCs are the cover, the absorber and the lifter together, and the insulation(Raj & Subudhi, 2018), as shown in figure (2.2).

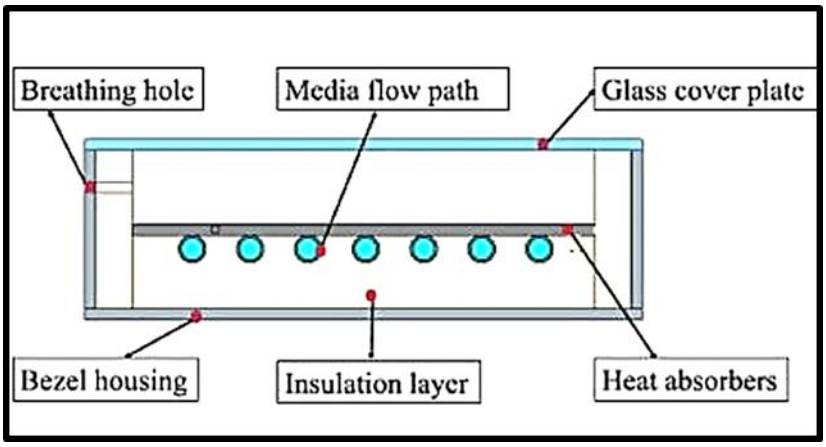

Figure 2.2. The schematic diagram of a FPSCs structure (Wang *et al.*, 2022).

The glass that aids in capturing diffused sunlight is one of the elements of the flat solar panel collection. The flat absorber plate, a spectral absorber plate used to utilize the radiation emitted by the sun by absorbing and reducing the emission, is where the solar energy obtained by the glass is then focused. The heat gathered from the sun's rays is transmitted by the absorption plate to the ascending pipes, where the liquid flows after being transformed from radiant energy into thermal energy. For the heat transfer process to extract water in the system, the liquid is driven into the system's ascending pipes by a pump (forced convection) in pump-operated collectors or (by natural force - natural convection) in heat pressure systems. One important thing is to provide insulation to prevent or reduce heat loss from the sides of the collector and below the perimeter. Therefore, the complete operation of FPSCs depends on the efficiency and design of these key parts. FPSCs perform their best with a well-designed glass, absorbent pad and proper isolation. In the current research, In order to conduct the mathematical and experimental study, solar conversion units were adopted.

2.4. EFFİCİENCY OF NANOFLUİDİC-BASED THERMAL FPSCs

The method of absorbing heat due to radiation and the amount of energy loss is related to the thermal efficiency of a flat panel solar collector system. The main mathematical equation for the efficiency of the flat plate solar collector can be written as follows (Duffie *et al.*, 1985) :

$$\eta_C = \frac{Q_u}{G_T A_C} = \frac{\dot{m} C_p (T_{out} - T_{in})}{G_T A_C} \quad (2.1)$$

The measured solar radiation quantity GT, the collector's surface area AC, its specific heat capacity Cp, the mass flow rate, and the HTF temperatures at the collector's inlet Tin and outlet Tout, respectively, are key factors in conducting an optimal evaluation of the heat efficiency of a flat plate solar collector. The research was conducted in 1975 using a solar detector and a solution of water and additives. (Minardi & Chuang, 1975). As a current working fluid in the direct absorption collection, some dyes can dissolve in water and interact with it; this fluid is referred to as "black liquid." (DAC). The findings indicated that the collector's heat loss has improved. It was introduced in 2000 (Miller & Koenigsdorff, 2000), 2004 (Bertocchi *et al.*, 2004), 1990 (Kumar & Tien, 1990) and 1979 (Abdelrahman *et al.*, 1979). By (Tyagi *et al.*, 2009), a nanofluid-loaded DAC was tested. To evaluate the performance of the DAC analytically, they used water and aluminum (Al) nanofluid. Their results showed an increase in the performance efficiency, as the radiation absorption increased 9 times higher than that of pure water, which led to an increase in the efficiency of the direct absorption solar panel collector is 10% higher compared to the traditional water-based FPSC.

2.5. NANOFLUİDS APPLİCATİONS İN FPSC

Numerous studies on nanofluids and their impact on thermal performance in the flat solar collector have been carried out experimentally and theoretically by numerous researchers and scientists. This was done using NPs with different concentrations and particle diameters, multiple preparation methods and samples. The influence of the thermo-physical properties of the working fluid on the performance of FPSCs, such as thermal conductivity, viscosity, specific heat capacity and density, was also investigated. This part of the study is devoted to reviewing the ongoing thermal efficiency studies focusing on substituting cutting-edge nanofluids for conventional working fluids in FPSCs.

The efficiency of the flat plate solar collector is determined by the characteristic of energy balance, in which the incoming energy from sunlight is changed into optical losses, useful energy gain, and thermal losses. A mathematical model was proposed to evaluate the thermal performance of the flat solar panel collector, and it was later included by ASHRAE as Standard ASHRAE 93 (2003) (conduction - infrared and convection). Solar collectors are subjected to this kind of interior or external testing and rated based on their thermal efficiency. The following definition of the solar collector's effectiveness:

$$\eta_C = \frac{Actual\ useful\ energy\ collected}{Solar\ energy\ intercepted\ by\ the\ collector\ area} \tag{2.2}$$

The efficacy of FPSCs is enhanced by increasing solar energy absorption. The heat loss to the surrounding atmosphere must be decreased concurrently with this rise to achieve it (conduction, convection, and radiation). There should also be an improvement in the rate of heat exchange between the absorbent pad and the working fluids (nanofluids) (Javadi *et al.*, 2013). The thermal performance of the solar system is anticipated to be greatly improved by using a nanofluid in place of the conventional working fluid, such as water, synthetic oil, or a glycol/water mixture. The solar collector's overall efficiency will increase as a result. (Javadi *et al.*, 2013).

The collector heat removal factor (FR), which is the same as the heat exchanger's effective coefficient, is a vital operational parameter. Energy efficiency, then, describes how much heat the collector can potentially absorb under given circumstances in relation to the maximum useful energy gain suggested by Duffy (Duffie *et al.*, 1985):

$$F_R = \frac{Q_u}{A_c G_t(\tau_g \alpha_{ap}) - A_c U_L(T_{in} - T_a)} = \frac{\dot{m} C_p(T_{out} - T_{in})}{SA_c - A_c U_L(T_{in} - T_a)} \tag{2.3}$$

When F^' is given as a factor of the collector, the heat removal factor efficiency leads to the expression relating it to the design terms of the collector.

$$F_R = \frac{\dot{m}C_p}{A_c U_L}\left[(1 - \exp)\left(-\frac{U_L F' A_c}{\dot{m}C_p}\right)\right] \quad (2.4)$$

$$F' = \frac{{}^{1}/_{U_L}}{W\left[\frac{1}{U_L(D + (W-D)F))} + \frac{1}{C_b} + \frac{1}{\pi D_i h_{fi}}\right]} \quad (2.5)$$

When (Di, D, and w) are defined as the interior diameter, exterior diameter, and separation between the riser tubes, respectively, the expression F indicates the fin-specific efficiency:

Temperature loss factor In Eq. (2.2), which measures the collector's capacity to stop heat loss from the insulated surfaces at the top, back, and edges, UL is another determining element. Consequently, the expected total collector heat loss, UL, is as follows.:

$$U_l = U_t + U_e + U_b \quad (2.6)$$

A large portion of a flat plate solar collector's overall heat loss travels to the collector's top, as indicated by (Heris *et al.*, 2013):

$$U = \frac{1}{\frac{N_g}{\frac{C}{T_{ap}}\left[\frac{T_{ap}-T_a}{N_g+\tau}\right]^{0.33}} + \frac{1}{h_{wind}}} + \frac{\sigma\left(T_{ap}^2+T_a^2\right)\left(T_{ap}+T_a\right)}{\frac{1}{\varepsilon_p+0.05N_g\left(1-\varepsilon_p\right)}+\frac{2N_g+\tau-1}{\varepsilon_g}-N_g} \quad (2.7)$$

Where, $\tau = [1\text{-}0.089h_{wind}\text{+}0.1166h^2_{wind}\varepsilon_p)x(1\text{+}0.078661N)]$

$C = [520\ x(1\text{-}0.000051\ \varphi^2)]$

$e = [\ 0.430\ x\ (1\text{-}100/T_{ap})]$

T_{ap} = the Absorber plate mean temperature

Ng, g, p, and hw are Stefan-Boltzmann constants that represent, respectively, the number and emissivity of glass, the emissivity of an absorbent plate, and the coefficient of wind heat transfer. The heat transfer coefficient due to wind force is

calculated as follows for a given wind speed, Vw, and riser length, L (Eltaweel & Abdel-Rehim 2019):

$$h_w = \frac{8.6V_w^{0.6}}{L^{0.4}} \tag{2.8}$$

Using Fourier's law, from the determined average temperature of the absorbent pad, the reduced heat loss coefficient Ub can be found, which represents the heat loss by conduction away from the absorbent pad to the surroundings:

$$Q_b = [k_{ins(b)} {}^{\chi} A_C \frac{(T_{ap} - T_a)}{thk_{ins(b)}} = U_b {}^{\chi} A_C (T_{ap} - T_a)] \tag{2.9}$$

$$U_b = [\frac{k_{ins[(b)]}}{thk_{ins[(b)]}}] = {}^{T.C\ of\ insulation\ at\ bottom}/_{Insulation\ thickness\ at\ bottom} \tag{2.10}$$

T.C: Thermal condactivity

Similar to this, the FPSC's edge heat leakage to the exterior is:

$$Q_e = [k_{ins(e)} {}^{\chi} A_e \frac{(T_{ap} - T_a)}{thk_{ins(e)}}] \tag{2.11}$$

Taking into consideration all heat loss factors that are mentioned in the same area as those mentioned in the collector area, equation (3.13) has been rewritten as follows:

$$Q_e = [\frac{k_{\ ins\ (e)} {}^{\chi} A_{\ e}}{A_C} {}^{\chi} A_C \frac{(T_{\ a\ p} - T_{\ a})}{thk_{\ ins\ (e)}} = U_e A_C (T_{ap} - T_{\ a})] \tag{2.12}$$

$$U_e = [\frac{k_{\ ins(e)} {}^{\chi} A_{\ e}}{thk_{\ ins\ (e)} {}^{\chi} A_{\ C}}] = \frac{[T.C\ of\ insulation\ at\ edge] \times [Edge\ Area]}{[Insulation\ thickness\ at\ bottom] \times [Collector\ Area]} \tag{2.13}$$

T.C = Thermal condactivity

In the experimental setup, seven ascending tubes touched the FPSC absorbent plate. In the mathematical model, only one pipe is taken for calculation, and it is assumed that the fluid flow rate is uniform across all the collecting risers, which operate in a parallel arrangement.

A critical variable that must be evaluated in light of the thermophysical properties of the working fluid entering the FPSC is the internal convection heat transfer coefficient (h_{fi}), as revealed in Eq. (2.5).

2.5.1. Experimental Studies

(Eltaweel & Abdel-Rehim ,2019) In expremantial Multi-walled carbon nanotubes with a diameter of 10–40 nm and a length of 29 m were used in experiments to test the effectiveness of a flat-plate solar collector at concentrations of 0.01 weight percent, 0.05 weight percent, and 0.1 weight percent. The experiment, which was carried out in Cairo, Egypt, demonstrates that the efficiency increased by 34.13% when 0.1 weight percent MWCNTs were used in comparison to the efficiency reached using pure water.

(Yousefi *et al*., 2012) performed an experiment in a horizontal solar panel collector measuring 2 m^2 using MWCNT and water with a 10 to 30 nm size range. The researchers also performed a second study on a flat-plane solar collector system that uses an Al_2O_3 nanofluid with a particle weight concentration of 0.2 weight percent and 0.4 weight percent of Triton X-100 as a surfactant. The results showed an increase in the efficiency of the FPC of 28.3%, at 0.2% by weight. The addition of surfactant also showed a reasonable improvement effect on FPSC performance (Yousefi *et al.,* 2012). (Yousefi *et al*., 2012) did many experiments adding water-based dispersions from 10 to 30 nm MWCNT. The results of their work showed that using surfactants, the efficiency of FPC will increase, but it decreases without using surfactants. They elucidated that the energy increased by 4.0% by weight and is

higher than a concentration of 2.0%. Thus, it was observed that the surfactant improved the performance result of the flat plate solar collector by 4.0% by weight.

(Vijayakumaar *et al*., 2013) conducted experiments using three different weight concentrations of the carbon nanotubes (CNT) (0.4, 0.5, and 0.6 wt%) with a size of 1.0 nm in order to improve the performance of the solar energy collector. They used Polysorbate 80 surfactant in the experiments. Their experiment showed an increase in performance up to 39% at a concentration of 0.5% by weight.

(Alawi ., *et al* 2021) In flat-plate solar collector (FPSC), Experimental and Theoretical study on the presence of covalently functionalized graphene (Gr) suspended in distilled water as operating fluids were conducted. These tests were carried out under a variety of testing settings, including size nanopartecial concentrations of 0.025 weight percent, 0.05 weight percent, 0.075 weight percent, and 0.1 weight percent, flow rates of 0.5, 1, and 1.5 kg/min, intake temperatures of 30, 40, and 50 C, and heat sources from the sun of 500, 750, and 1000 W/m2. The stability and morphological characteristics of the functionalized nanofluids were characterized using a variety of techniques. The greatest theoretical and experimental heat collection efficiency was 76.13% at 0.1 wt% and 1.5 kg/min, which was 13% and 12.5% higher than compared to pure water.

(Ebrahimnia *et al.*, 2016) conducted an experiment, presenting a trade-off demonstrating improvements in the working fluid's heat transfer (mono and binary), which uses titanium oxide in a solar collector. The researchers have recommended using the smallest NPs as highly thermally conductive materials for heating collectors to achieve maximum performance.

(Alawi *et al*., 2019) Performance testing of the internal FPSC system was carried out thermally, and GNPs were prepared with Pent ethylene Glycol as HTFsThe tests were conducted under a variety of conditions, including different heat flows (500, 750, and 1000 W/m2), different flow rates of the working fluid (0.00833, 0.01667, 0.025 kg/s), different entry temperatures (30, 40, and 50 °C), and different mass

fractions of nanoparticles (0.02, 0.05, 0.008, and 0.1 wt%). Finally, MATLAB code was created to forecast the efficiency coefficients using the regression model.

(Yousefi *et al*., 2012) carried out an investigation to evaluate the effect of MWCNTs/water nanofluids on the performance efficiency of the flat plate solar panel collector when using the average of different (pH) values (3.5, 6.5 and 9.5). In their work, (0.2 wt%) MWCNT nanoparticles were prepared using (Triton X-100) surfactant. The ASHRAE standard proves the thermal performance. The work results showed that the removal agent affected the differences in the elevated temperatures. In contrast, low temperatures were controlled for absorption factor tolerances.

2.5.2. Theoretical Studies

(Faizal *et al*., 2013) A test was conducted to determine the effect of MWCNT / nanofluid water on the thermal efficiency of a flat solar panel collector with a $2m^2$-size, for the flow rates and weight fractions of the two different nanoparticles. Using Equation (2.4), all calculations related to the size of the complex were made.

The working fluid for their experiment was MWCNT/water, and the findings showed that (Yousefi *et al.*, 2012). They found that the collector area dropped by about 37% compared to water using the same fluid exit temperature measured at noon. In order to reduce losses or decreases, the size of a small collector can be manageable without compromising efficiency, which is essential for reducing the cost of solar collectors. The study did not present any types, models, or mathematical methods related to the system, and it only used one equation to calculate the pool's size.

$$A_C = \frac{\dot{m} C_p (T_{out} - T_{in})}{G_T \eta_C} \tag{2.14}$$

The high costs of conducting experiments are another reason that may change the use of nanofluids in FPSCs as an alternative to water, including the costs of both the manufacturing process and renewable energy. An increase in the exit temperature is necessary for increased heat transfer, which calls for a high increase in FPC, which

may eventually lead to higher costs. Like (Sint *et al*., 2017), through a theoretical study using CuO-H_2O nanofluids, the performance of FPSC HTFs has been tested. Given weather conditions, mathematical models and MATLAB symbols for the solar water heating system were generated to ascertain a flat plate solar collector's effectiveness. Due to the high volume fraction of nanoparticle weight (2 volume %), their findings indicated a significant increase in the effectiveness of the composite. Under the same operating conditions, the FPSC performs up to 5% better than CuO-HO as HTF in the system.

(Jouybari *et al*., 2019) Experimental and modeling works were carried out on SiO2-DI water with a diameter of 0.4–0.6 V and a size of 20–30 nm to treat the thermal efficiency of a flat plate solar collector. The energy gain coefficient (FRUL) for DW dropped by 55.2% and 51.7%, respectively, as the nanoparticles' volume fraction ascended from (0.4 to 0.6 by volume%). Therefore, FPSC efficiency gave a more significant output than DW at higher temperature values.

(Alawi & Kamar**;** 2020). To investigate the thermal performance of MWNCTs/H2O nanofluid, simulation studies for flat plate solar collector were carried out using 3D models . nanoparticales szie 0.1 wt% , with in a flow rate range of 0.2 to 0.8 kg/min. Meanwhile, a steady heat flux of 1000 W/m2 was provided at the and the inlet temperature for the DW and MWNCTs/H2O nanofluid was set at 30 °C.As a consequence, for volume flow rates of 0.2–0.8 kg/min, the thermal efficiency of MWCNTs nanofluid increased by 6.080%, 6.322%, 6.311%, 6.337%, 6.450%, and 6.857%.

(Farajzadeh *et al*., 2018) used a mixture ratio of 20 nm alumina and 15 nm titania NPs with water at a nanoparticle size concentration of 0.1 wt% in an FPSC to compare the complex's theoretical and standard performance measures. A Brinkman viscosity model and a cetyltrimethylammonium bromide (CTAB) surfactant were used to test the nanofluid durability. At rates of 0.75, 1, and 1.25 L/m2 min, the hybrid nanofluid at 0.1 wt.% increased the effectiveness of the complex by 19%, 21%, and 26%, respectively. The thermal efficiency increases by 5.0% when increasing the mass weight of the nanoparticles from 0.1 to 0.2 wt%. Unlike alumina,

it is an expensive nanomaterial, therefore. Thus their engineered colloidal mixture cannot make cost-effective nanofluids for applying FPCs.

Al_2O_3-DW nanofluids were used as the HTF in numerical modeling by (Ziyadanogullari *et al*., 2018) to investigate the impact of forced convection flow inside an FPSC. He applied Galerkin's weighted residual diagram with the finite element technique (FEM). The analytical findings demonstrated that the most significant Reynolds number (Re) and Bruntel number experience the greatest heat loss. (Pr). Additionally, an improvement in the percentage increase in solar collector efficiency results from the increase in Re and the reduction in Pr. Additionally, the correlation was designed using the sum of the Nusselt, Reynolds, and Prandtl numbers. In this regard, a quasi-experimental connection with experimental data was acknowledged as reported in the literature.

Numerical research using computational fluid dynamics (CFD) simulations was conducted by (Ekramian *et al*., 2014) to forecast the transfer of heat and FPC thermal efficiency using CuO, Al_2O_3, and MWCNT nanofluids. Three different weight percentages for NPs were selected: 1, 2, and 3.0%. They employed the Maxwell and Einstein viscosity and thermal conductivity theories, respectively. The findings indicated that the copper oxide nanofluid could increase thermal efficiency more than other nanofluids, and they also demonstrated excellent agreement with the current experimental data.

Most of the literature on FPSCs wants to use Al_2O_3 nanofluids and MWCNTs, while some also want to investigate CuO, Ag, Fe_2O_3, ZnO, and SWCNTs, respectively GNPs, MgO, SiO_2, TiO_2, graphene, and hybrid nanofluids. The aqueous dispersion of carbon-based nanostructures maximizes the energy efficacy of FPSCs. Graphene, MWCNTs, GNPs, and SWCNTs in comparatively modest concentrations. Generally speaking, FPSCs with large concentrations of solid, non-carbon NPs as nano-additives perform poorly in terms of energy efficiency. In light of the debate that has come before, it is reasonable to assume that carbon-based aqueous dispersants can effectively enhance the performance of FPSCs at low concentrations. Lower nanofluids amounts may lead to better stability of a suspension, reduced costs of

materials, lower viscosity of the fluid, and certainly a lower level of toxicity. Pressure dropping (pumping force). Tables 2.1, 2.2, and 2.3 summarise earlier experimental, theoretical, and numerical studies on using nanofluids in FPSC systems. The summary figures show that carbon nanostructures and metal nanofluids account for 18% and 7% of the published work, while metal oxide nanofluids account for about 72% of it. Hybrid nanofluids were discovered to be the latest trend, at least (3%).

Table 2.1. Metal oxide nanofluids and their applications as HTFs in FPSCs.

References	Base fluid	Nanofluid			Study	FPSC dimensions(M^2)	Efficiency improvement
		Type	Size (nm)	Concentration (%)			
Mahmoud 2021	water	Al2O3	25nm	2 %	Num	/	It is revealed that the heat transfer coefficient was increased between (45 and 58) % when compared with water.
Michael & Iniyan, 2015	DW	CUO	/	(0.05) vol.	Exp.	/	Increased FPSC efficiency by 6.3%.
Yousefi *et al*., 2012	H_2O	GNPs,SiO_2 ,ZNO	/	0.05,0.1,0.15,0.2wt	Exp.	/	Efficiency incrreased up to 85% for 0.1% wt by harbid nano fluid
Faizal *et al*., 2015	DW	SiO_2	/	(0.2 & 0.4) wt.	Exp.	1.84- m^2	The growth effectiveness when using 0.2% by weight was around 23.5%.
Kang *et al*., 2017	DW	Al_2O_3	20 nm	(1) vol.	Exp.	2.37- m^2	Both FPSCs are equally efficient, at 74.9% and 72.4%, respectively.
Verma *et al*., 2016	DW	MgO	40 nm	(0.25-1.25) vol.	Exp.	0.375- m^2	A 9.34% increase in heat efficiency was achieved compared to a 0.75 vol% weight of nanoparticles.
Kiliç *et al*., 2018	H_2O	TiO_2	44 nm	(2) wt.	Exp.	1.82 m^2	About 48.67% more instantaneous effectiveness was achieved.
Jouybari *et al*., 2017	DW	SiO_2	20–30 nm	(0.2, 0.4 and 0.6)	Exp.	$90 \times 20 \times 7 \times 10^{-6}$-m3	There is an 8.1% increase in thermal performance.
Sundar *et al*., 2018	DW	Al_2O_3	<20 nm	(0.1 and 0.3) vol.	Exp.	2- m^2	Efficiency (without inclusion) at 0.3 vol% was 58% and 76% (H/D = 5).
Ziyadanogullari *et al*., 2018	DW	Al_2O_3, CuO, TiO_2	<50, < 50 & < 25 nm	(0.2, 0.4, and 0.8) vol.	Exp.	/	The highest increases in efficiency were 71%, 87.8%, and 52.2%, correspondingly.
(Kashyap *et al*., 2018	EG: DW	ZnO	50 nm	(0.02)vol.	Exp.	1550 × 345 mm	Using grooved tubes, the highest energy efficiency is approximately 5.95%.
Shojaeizadeh. 2016	DW	Al_2O_3	15 nm	(0.4462, 0.7383 and 0.9267) vol.	Theo.	1.51- m^2	The existence of the storage tank affected the FPSC's input temperature.
Hawwash et al.,2018	water	Al2O3	/	0.1– 3wt	Exp and Theo	/	Increased FPSC efficiency by 16.63 %.
Hajabdollahi *et al*.,2019	water	CuO, Al2O3	20	0.1%	Num.	1.51 m2	CuO likewise had the highest heat loss coefficient, however the effects of heat enhancement outweighed the heat loss.
Bazdidi-Tehrani *et al*., 2018	DW	TiO_2	27 nm	(0-2.04) vol.	Num.	Plate width = 20 cm	Nanofluids and ribbed tubes improved FPSC effectiveness by 10%.

Table 2.2. Metallic nanofluids & their applications as HTFs in FPSCs.

References	Base fluid	Nanoparticles			Study	Dimensions of FPSC	Efficiency improvement
		Type	Size (nm)	Concentration (%)			
Tomy *et al*., 2016	DW	Ag	/	(0.1, 0.3, 0.4) vol.	Num.	/	The difference between the testing data and the numerical data was 2%.
Kiliça et al., 2018	DW	TiO2	40 nm	0.2%	Exp	/	The efficiency of the FPSC increased by 12.5%
He *et al*., 2015	DW	Al_2O_3,CuO,TiO_2	/	(0.2, 0.3) wt.	Exp.	2 m^2	The efficiency of the FPSC increased by 23.83%.
peng *et al*., 2020	DW	Ag	15 nm	(0-4) wt.	Exp	/	More efficiency found with CuO,Al_2O_3,TiO_2/ water

Table 2.3. Carbon-based nanofluids and applications as HTFs in FPSCs.

References	Base fluid	Nanoparticles			Study	Dimensions of FPSC	Efficiency enhancement
		Type	Size (nm	Concentration (%)			
Kumar *et al*.,2021	DW	GNPs	1.5-2μm	(0.025,0.05,0.1 wt).	Exp.	L= 0.51m, t= 0.001m	the energy efficiency (24.09%) for 0.1 wt and 1.5 lpm
Said et al. (2015)	H_2O	SWCNT	20 nm	0. 1% and 0. 3%	Exp.	/	the energy efficiency (53%)
Sadripour 2017	DW	MWCNT	1 nm	0.01% to 0.1%	Num .	/	Compared to 0.1% by weight, efficiency increased by about 12.7%.
Chougule & Sahu, 2015	DW	MWCNTs	10–12 nr	/	Exp.	/	The highest and lowest FRUL and FR readings at 60% F.R.
Said *et al*., 2015	DW	SWCNTs	1–2 nm	(0.1-0.3 vol).	Exp.	1.84 - m^2	The effectiveness of the collector increased by 95.12% at 0.5 kg/min and 0.3% by volume.
Eltaweel & Abdel-Rehim, 2019	DW	MWCNTs	10–40 nr	(0.01, 0.05, 0.1) wt.	Exp.	2-m^2	For weight percentages of 0.01, 0.05, and 0.1, the effectiveness rose by roughly 16%, 21%, and 34.13%, respectively.
Vincely & Natarajan, 2016	DW	GO	/	(0.005, 0.01, 0.02) wt.	Exp.	2-m^2	For the values of 0.0167 kg/s and 0.02 wt%, the rise in FR was 7.3%.
Ahmadi *et al*., 2016	DW	GNPs	/	0.01-0.2 wt.	Exp.	0.47 m×0.27m×0.001m	Thermal effectiveness increased by 18.87%.
sedeghi *et al*.,2019	H_2O	Cuo	50nm	(0.01,0.02,0.03 wt).	EXP& Num	/	efficiency increased by about 51%
Alawi *et at*.,2021	H_2O	GrGNPs	/	0.025-0.1 wt.	EXP	/	The maximum efficiency rise was about 13% and 12.5% experimantally and theoretically at 0.025 kg/s

2.5.3. Heat Transfer Standard

The heat transmission coefficient and the Nusselt number are connected to the Reynolds number, which characterizes the flow regime, and the Brentell number are both correlated.

$$h_{fi} = \frac{Nu\, k_{nf}}{D_i}$$

(2.15)

Once the flow regime of the nanofluid inside the ascending tubes has been established, the appropriate correlation can be calculated to approximate the as-yet-unidentified Nusselt number. Without dimensions, Reynolds and Prandtl numbers are expressed as:

$$Re_{nf} = \frac{\rho_{nf}\, V D_i}{\mu_{nf}} = \frac{4\, \dot{m}_{riser}}{\pi \times D_i \times \mu_{nf}}$$

(2.16)

$$Pr_{nf} = \frac{\mu_{nf}\, c_{p,nf}}{k_{nf}}$$

(2.17)

The above equations show that nanoparticles play an important role in fluid flow thanks to the change in nanofluid thermal and physical properties, so the heat transfer coefficients are dimensionless.

For risers with laminar Reynolds numbers >2300 Re, the thermal performance of a solar system depends on the external thermal limits. At a steady heat flux rate, the local Nusselt number can be determined using the Heton correlation.,(Heris *et al*., 2013):

$$Nu = Nu_{\infty} + \frac{a(Re\,\mathrm{Pr}\,D_h/L)^m}{1+b(Re\,\mathrm{Pr}\,D_h/L)^n} = Nu_{\infty} + \frac{a(\mathrm{Pe}\,D_h/L)^m}{1+b(\mathrm{Pe}\,D_h/L)^n}$$

(2.18)

In Eq. (3.28), D_h and L are the tube hydraulic diameter and length, respectively, and Pe is the Peclet number. The friction factor for the laminar flow is given by:

f = 64 / Re

(2.19)

From equations (2.20) and (2.21), respectively, the pressure drop and pumping force can be calculated by (Eltaweel & Abdel-Rehim, 2019):

$$\Delta P = f \times \frac{\rho V^2}{2} \times \frac{\Delta I}{d} + k\frac{\rho V^2}{2}$$

(2.20)

$$\text{Pumping power} = \left(\frac{\dot{m}}{\rho_{nf}}\right) \times \Delta p$$

(2.21)

2.6. NANOFLUİD COMPOSİTİON

Only one kind of basic fluid and NPs are typically present in nanofluids. As reaveled, adding NPs to the working fluid increases thermal conductivity, allowing the nanofluids to transfer heat in nanoparticle uses. (Ajeena *et al*., 2022). Due to their strong thermal conductivity, most NPs in nanofluids is metal oxides or metals alone, such as alumina (Al_2O_3) and titanium oxide (tio2). Numerous additional NPs varieties, such as carbon and diamond, are used in nanofluids, so there are other options besides these (Olayiwola *et al*., 2019). The NPS enhanced the nanofluids' Nusselt number and thermal conductivity (Elsaid *et al*., 2021).

Common and readily available heat transfer fluids are the basic fluids suitable for use in the fabrication of nanofluids. The base fluid's suitability for uses involving heat transfer is one of the criteria that must be observed when evaluating it. Adding NPs to the base fluids will enhance their thermal capabilities. It can be concluded from the previous literature that adding NPs to a base liquid with low thermal conductivity improves its thermal performance (Khalidi *et al*., 2023). Furthermore, flow channels and pipes may be harmed by nanoparticles larger than a few nanometers due to the development of corrosion.

2.6.1. Preparation and Description of Nanofluids

2.6.1.1. Single-Step Process

The "direct evaporation method" is the first efficient and hopeful technique for making nanofluids. In this process, the vapor phase of nanophase powders was quickly condensed into a moving fluid with little vapor pressure. (Das *et al*., 2007). In order to create non-agglomerated copper in a liquid ethylene glycol base, the direct condensation-evaporation process resulted in the process of uniform distribution of NPs in the base fluid (Eastman *et al*., 1997). the single-step technique in action Fig. shows (2.3).

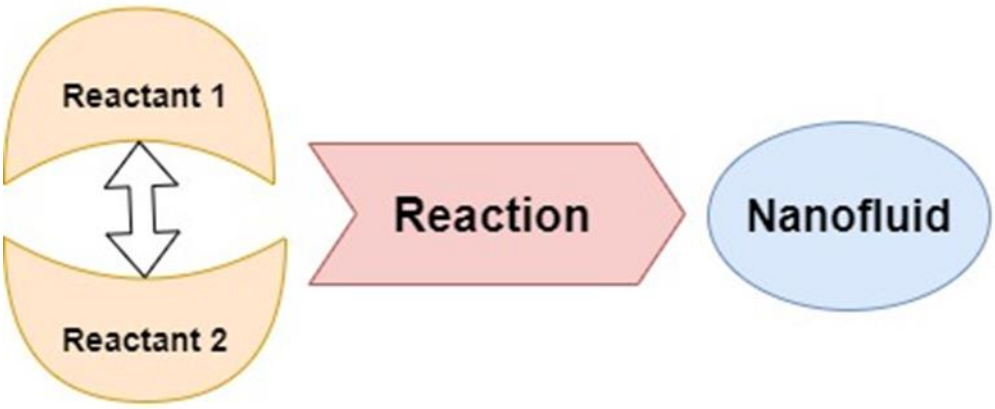

Figure 2.3. Nanofluid preparation in a single process.

2.6.1.2. Two - Step Process

In a typical two-step process, the first stage involves using physical or chemical techniques like chemical vapor deposition and inert gas condensation. The base fluids are then used to spread these produced NPs. According to (Eastman *et al*., 1997), this method is primarily used to create carbon nanotubes and nitrogen oxide nanofluids. Because of the powerful van der Waals attractive forces between the NPs, agglomeration is the primary issue in two-step processes. (Ali *et al*., 2019). It is worth mentioning that the suboptimal dispersion quality of the nanofluids is responsible for their limited thermal conductivity, resulting from this process. To produce monolithic or nearly non-agglomerated nanofluids, a one-step process is recommended in order to increase the thermal conductivity of nanofluids (Liu *et al*., 2005) and (Choi *et al*., 2001) created suspensions of carbon nanotubes using a two-step process. To prevent the aggregation of the carbon NPs, surfactants and ultrasonic agitation were used illustrates a two-step process. Fig (2.4).

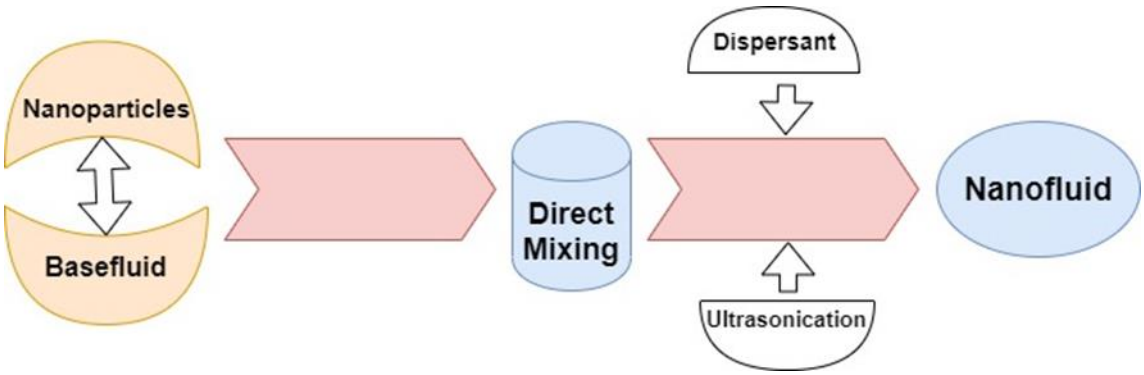

Figure 2.4. illustrates a two-step procedure for creating nanofluids.

The chemical dispersion phase is a second stage of the two-step process that uses electrostatic dispersion, steric dispersion, or functional group coating to block long-range attractive van der Waals forces.

The long-range van der Waals forces cannot surmount the effective distance of the electrostatic method because it charges bound particles with similar charges. This can be accomplished by altering the suspension's pH, which defines the surface of NP. The increased attraction tension between surface hydroxyl groups (-OH) and

potential specific ions will cause the surface charge of the NPs to rise at an ideal pH. The suspension is stable with less aggregation or agglomeration due to the increased electrostatic repelling forces between the particles.

A surfactant is added to a solution during aseptic fixation to avoid caking or accumulation. Surfactants include, for instance, Cetyl trim ethyl ammonium bromide (CTAB), Sodium Laureate (SL), Sodium Dodecyl benzene sulfonate (SDBS), Sodium Dodecyl Sulfate (SDS), TritonX-100, and Gum Arabic (GA). The task involves heating and applying acids to high temperatures to the nanoparticles. The presence of acids will cause the NPs' flaw sites to acquire polar groups in the solution, such as those of -COOH or -OH, increasing their hydrophilicity.

2.6.2. Nanofluid Concentration

There are some concepts used to describe nanofluidic concentrations. According to (Razi et al., 2022), the volume fraction is the first foundation and is calculated as the volume of each component divided by the volume of the entire mixture prior mixing:

$$\phi_i = \frac{V_i}{\sum_j V_j} \tag{2.22}$$

Volume percentage (%vol) is expressed similarly, except that the former is a number without units, and the latter is a percentage. Because the component volumes are additive in an ideal solution, the volume percentage and volume concentration match. (the solution volume is equal to the sum of the volumes of its constituents). The sum of the volume components of a mixture is one:

$$\sum_{i=1}^{N}(V)_i = (V\ );\ \sum_{i=1}^{N}\phi_i = 1 \tag{2.23}$$

The volume percentage is most frequently used when a solution includes a blend of two liquids. However, the proportion is the only additive for ideal gases (Zhu *et al* . 2004). In some cases, solvents and solutes can be classified arbitrarily, like ethanol and water, which combine in all ratios. The mixture has a capacity slightly lower

than the sum of its components. Consequently, when something is described as "40% alcohol by volume," it refers to a mixture of 40 volume units of ethanol and enough water to give it a final volume of 100 volume units, as opposed to "40 volume units of ethanol." Ethanol is made up of 60 units of water. The term "mass percentage," also known as "wt%," is another method to express the composition of a mixture using a dimensionless quantity. Here is what the mass percentage means:

$$\varphi_i = \frac{m_i}{\sum_j m_j} \tag{2.24}$$

By using the factor m_{bf}, it is possible to convert a nanofluid's volume fraction into its mass fraction and taking into consideration the relationship between volume, mass, and density:

$$\frac{m_{np}/\rho_{np}}{(m_{np}/\rho_{np})+(m_{bf}/\rho_{bf})} = \frac{(m_{np}/m_{bf})/\rho_{np}}{((m_{np}/m_{bf})/\rho_{np})+(m_{bf}/m_{bf})/\rho_{bf}}$$

(2.25)

$$\varphi = \frac{\phi/\rho_{np}}{\frac{\phi}{\rho_{(np)}}+1/\rho_{bf}} \quad \text{[vol.\%]} \tag{2.26}$$

$$(\text{The weight percentage of nanoparticles}) = [\frac{\text{Weight of nanoparticles}}{\text{Weight of base fluid}}]x\ 100\%$$

(2.27)

$$\phi = [\frac{\varphi}{1-\varphi} \chi\ \frac{\rho_{np}}{\rho_{bf}}]\ \text{[weight.\%]} \tag{2.28}$$

Nanoparticle and base fluid are indicated here by the letters np and bf, respectively. In order to acquire a nanofluid's specific volume fraction, it is required to calculate the mass of NPs for a specific volume of base liquid, such as 100 ml (Naik *et al.*, 2013).

$$\frac{V_{np}}{(V_{np}/V_{bf})} = \frac{m_{np}/\rho_{np}}{((m_{np}/\rho_{np})+100} \tag{2.29}$$

The required mass of a nanoparticle (m_{np}) will then be determined for each specific number. Another way is to use mol%, which stands for mole fraction or percentage by moles. However, mass and volume portions are more typical.

2.6.3. Carbon-Based Nanoparticles

Iijima was the first to find carbon nanotubes. (Abdelrahman *et al*., 1979). He explained it by referring to "a new type of finite carbon structure consisting of needle-like tubes" in a letter he wrote to Nature in 1991. He employed the arc discharge evaporation technique, in which the electrode's negative end was used to produce a "needle."

Carbon nanotubes are described as "cylinder-shaped coiled graphene sheets of sp2-bonded carbon atoms," with the exception that their diameters are so tiny as to exhibit the effects of one-dimensional periodicity (1D) (Cambaz *et al*., 2008).

According to (Zhang *et al*., 2008), carbon nanotubes become electroactive when electron-rich interaction forms outside of them. The electron clouds change from a homogenous distribution in graphite to an asymmetric distribution around cylindrical nanotubes, causing this to happen. As a result, when electron withdrawing/electron donor molecules (like NO_2 or CH_4) interact with semiconducting carbon nanotubes, the abundance of electrons/holes in the nanotube's "core" changes, altering the conductivity of the carbon nanotubes as a whole (Lu *et al*., 2004).

The primary justification for using carbon nanotubes as nano monitors are this. Carbon nanotubes have a larger surface area-to-volume ratio, increasing their adsorption capacity. This causes a notable modification of the electrical properties when the target nano molecules are present (Cambaz *et al*., 2008 ; Lu et al., 2004; Schedin et al., 2007). This enables the detection of some chemicals at lower ppm levels and at room temperature.CNT chemical resistors are desirable options as methane sensors due to their low power consumption. In general, (CNT- BASED) sensors are perfect for outdoor leak detection applications due to their large methane response, low power needs, cheap cost (thanks to precision batch manufacturing

methods), and low-temperature response Bucky spheres (quasi-0D), CNTs (1D), and graphite (3D) can all be thought of as carbon nanomaterials that can be constructed from graphene (Schedin *et al*., 2007). Figure 2.5 illustrates the carbon nanotube (CNT) structure as a rotating graphite sheet.

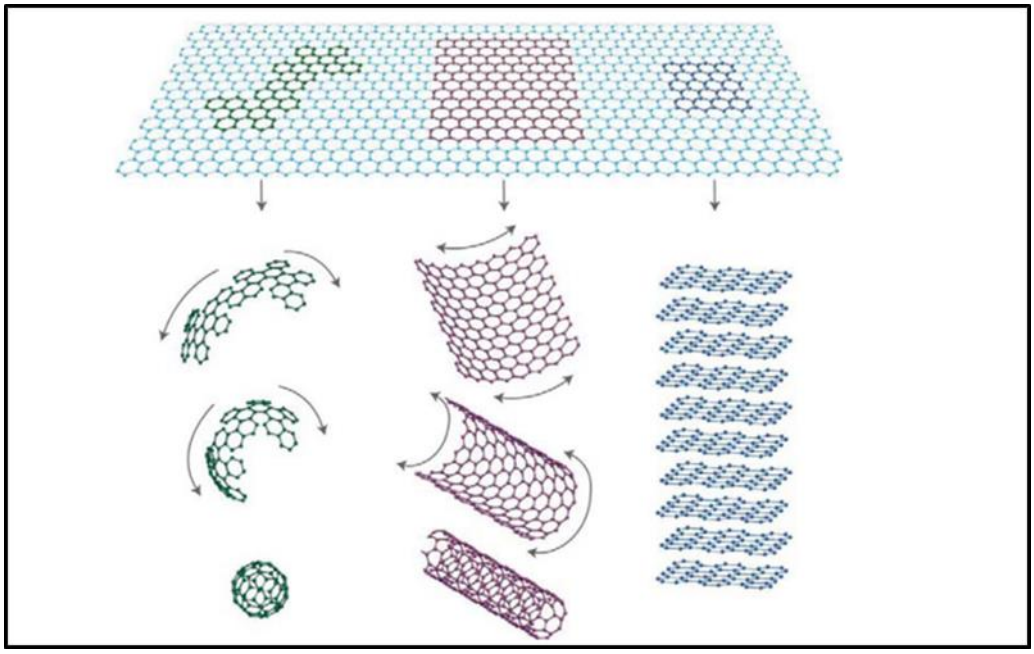

Figure 2.5. The fundamental component of bucky balls (on the left), nanotubes (in the middle), and graphite (on the right) is graphene (Schedin *et al.*, 2007).

2.6.3.1. Multi Walled Carbon Nanotubes (MWCNTS)

Carbon tubes are carbon solids with a cylindrical structure (Tsai *et al*., 2010). It was discovered for the first time in 1991 by a scientist (Sumio Iijima) (Liu *et al*., 2009). The variety of its use for multiple purposes, it was used in the working fluid to raise the thermal conductivity in the flat solar panels, and it possesses high rigidity and inertia, and the carbon tubes were considered a good conductor of heat (ballistic conductivity) (Marconnet *et al*., 2013). It exists in two cases, one of which is single-walled and the second is multi-walled. Most single-walled carbon tubes have a small diameter approaching nanometers, in the form of wrapping a single-atom thin layer of graphene down to the cylindrical shape; multi-walled carbon tubes consist of multiple layers of folded from graphene (Levshov.2013). The use of carbon tubes has

increased recently by researchers in their research and experiments due to their good qualities.

2.6.3.2. Titanium Oxide (TiO_2)

Due to its unique properties, titanium dioxide (TiO_2) is often used in research and experiments as it is available and cheap, i.e. low cost. In addition, it has high stability and is non-toxic. In addition, incorporating TiO_2 with carbon nanotubes as a catalyst as a photocatalyst is considered a useful compound because it removes organic pollutants (Cao *et al*., 2013). There is titanium dioxide, which has three crystal forms. These structures are anatase, rutile, and brookite.

On the same materials that have greater physical dimensions, nanomaterials behave differently. Compared to the same material's bigger size, the extent of chemical reactions in nanomaterials of various types is more distinct, primarily because chemical reactions of any material can occur on a material's surface. Due to this, most photocatalytic nanomaterials exhibit high reaction efficacy (Khan *et al*., 2015). Due to its large bandgap energy, titanium is regarded as the gold standard material for photocatalytic nanomaterials in industries (Berger *et al*., 2012). Carbon nanotubes (CNTs) and other nanomaterials, such as titanium, have been tried in hybrid formations over the past ten years to see if they could increase the effectiveness of removing various pollutants from water and air In order to create a hybrid material for water treatment that contains titanium, the Sol-Gel process was explored ((Alem *et al*., 2009; Kamanina *et al*., 2022; Sarkar *et al*., 2018). Titanium and CNT-containing catalytic nanomaterials demonstrated a highly efficient ability to remove contaminants from fresh water in our preliminary research. Regardless of whether the nanomaterial is in elemental or composite form, the removal rates of different types of photocatalytic nanomaterials have been called into doubt. This is particularly true when composite materials are exposed to brackish or saltwater environments.

2.6.3.3. Aluminum Oxide (AL_2O_3)

Aluminum dioxide Al_2O_3 is a chemical compound used by researchers in their research and experiments for its good properties, as it is odorless and non-toxic, matches well with the hematite group, has high hardness, high corrosion resistance, and good thermal conductivity (Khan & Hossain,. 2022). Due to its high thermal stability, it is considered an oxidant in high-temperature reactions. It is one of the minerals available in the market and is cheap. Aluminum's ability is due to its thin, non-permeable, corrosion-resistant surface layer, One of the chemical properties of aluminum oxide is that it does not react with water unless there is a strong base (Satish *et al*., 2018). It has two different patterns in the crystalline structure, which are the alpha (α) and gamma (λ) patterns, and thus there is a difference in its physical and chemical properties (Tavakoli *et al*., 2013). It was discovered for the first time in a year by the scientist Hans Christian Oersted (Poinern *et al.*, 2011). The combination of aluminum oxide and nanofluid a composite working fluid made of multi-walled carbon tubes. The experiment was carried out using zeta voltage, and the durability of the nano-oil and the dynamic viscosity and thermal conductivity of the nano-liquid used in it were studied. The nano-liquid showed Newtonian behavior, and the dynamic viscosity increased with the increasing concentrations of solids. The study's results showed the possibility of increasing the efficiency in the case of the hybrid nanofluid of solids instead of the base fluid for both laminar and turbulent flow systems except for solids with concentrations of 1 and 1.5% (Asadi *et al.*, 2018).

2.6.4. Functionalization of Carbon Nanotubes

As previously mentioned, carbon nanotubes are coveted for various applications due to their unique properties. However, the activation of carbon nanotubes was necessary to activate the effect of the thermal properties of nanomaterials. This may entail joining functional groups or polymer chains or changing the surface components to make the nanotubes soluble in different media.

Following are the two major categories of activation techniques. According to (Wu *et al*., 1998), the first step in processing MWCNTs is to fill their empty inner cavity with different molecules or nanoparticles (NPs), as depicted in Figure 2.6. Endo-structure activation and intrinsic activation are terms used to describe this.

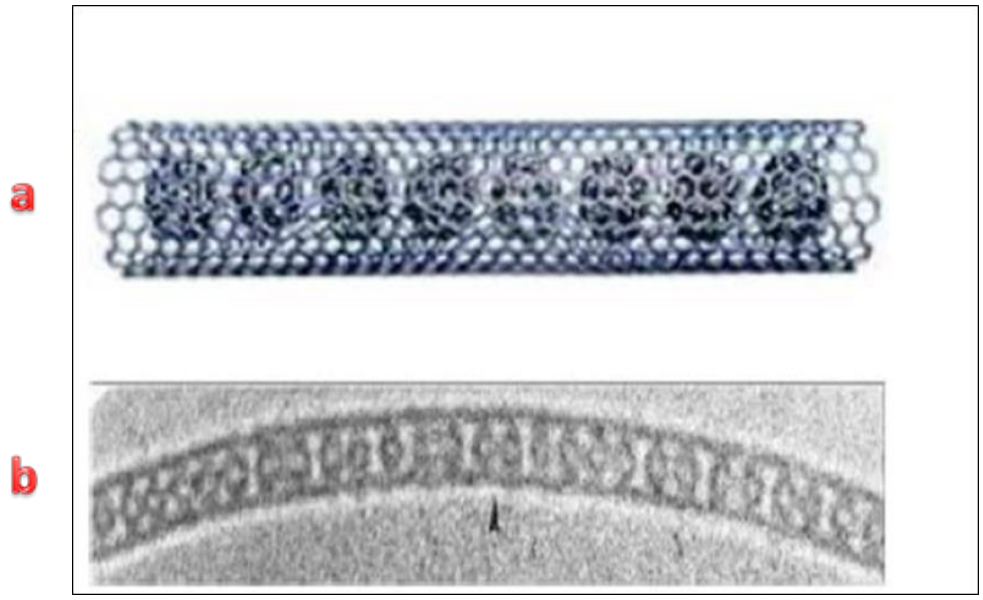

Figure 2.6. Diagrams of SWCNTs filled with C 60 fullerenes and a HRTEM picture of those materials are shown in (a) and (b), respectively (Xu & Wang, 2008).

The energy released during the formation of a non-covalent bond is lower than that of a covalent connection. However, the quantity of these bonds can increase and take over in supramolecular structures like carbon nanotubes and graphene. Thermodynamics governs the non-covalent contact and depends on van der Waals forces or -stacking. The key benefit of this kind of functionality is the ability to link various groups without interfering with the electronic operation of graphene sheets wrapped in carbon nanotubes (Vaisman *et al.*, 2006).

According to (Wang 2009), an appropriate technique for dispersing individual nanotubes in aqueous or organic solvents is to classify the creation of non-covalent aggregates with surfactants. (Long *et al.*, 2012). To dissolve carbon nanotubes in aqueous media, the surfactant used (Yu *et al.*, 2007) is an amphiphilic molecule in

which the hydrophobic parts are guided towards the surface of the carbon nanotubes, while the polar part interacts with the solvent molecules.

In order to perform a non-covalent function, (Moore *et al.,* 1995) confirmed the potent stacking interactions of beta- of polynuclear aromatic compounds on the side walls of carbon nanotubes, such as the planar pyrene fraction, and investigated the various aqueous dispersion of carbon nanotubes using anionic, cationic, and non-ionic surfactants. Due to the increased static stability, they demonstrate that the hydrophilic groups' size affects the surfactants' ability to spread individual carbon nanotubes (Fragneaud *et al.,* 2008) .as shown in Fig 2.7.

2.6.4.1. Covalent Functionalization

It is possible to distinguish between two major types of chemical activation of MWCNTs through covalent binding, namely end and "defect group" chemistry and side wall functionality.

- Final and defective sides Chemistry

Functionality is created through "end and defect" chemistry, which involves physically gluing functional groups to structural flaws in carbon nanotubes. In this instance, perfect graphite sheets rolled into nanocylinders are considered to be carbon nanotubes. All carbon nanotubes have flaws and can be twisted or folded. Typically, 1-3% of a nanotube's carbon atoms are found in defect locations (Niu *et al.,* 2009).

The end caps can be made of highly twisted, fullerene-like hemispheres, which are much more reactive than the side walls of the nanotubes. Defect sites like pentagon-heptagonal pairs known as Stone-Wells defects, sp3 hybridized defects, and gaps in the nanotube network can be found on the side walls themselves. (Yuan & Liew, 2009).

The so-called Stone Wells defect, which causes a small amount of curvature deformation in nanotubes, is the most prevalent sort of defect. For addition reactions,

these areas have better carbon-carbon double bonds. (Yuan & Liew, 2009). Fig. (2.7) shows several typical flaws.

Instead of the usual six bands around the carbon, there are five or seven, which helps to bend the tube Fig.(2.7). The symbol B (R = H and OH) is used to identify the sp3 hybridized defects. Oxidative conditions, which maintain the COOH groups at the hole's edge, can have an impact on the carbon framework (Fig. 2.7 "C","D"). depicts an SWCNT's open end with COOH groups at the termination. There is also the possibility of other terminal groups, like -OH, -H, and =O. Most frequently, strong acids used in the purification phase cause oxidative damage to the nanotube framework and these inherent defects. The oxygenated functional groups that these acids leave behind are filled by carboxylic acid, ketone, alcohol, and ester (Yang *et al.*, 2010). The introduced oxidized carboxyl groups serve as important sites for additional modifications in organic solvents, such as intermolecular coupling through the formation of amide and ester bonds.

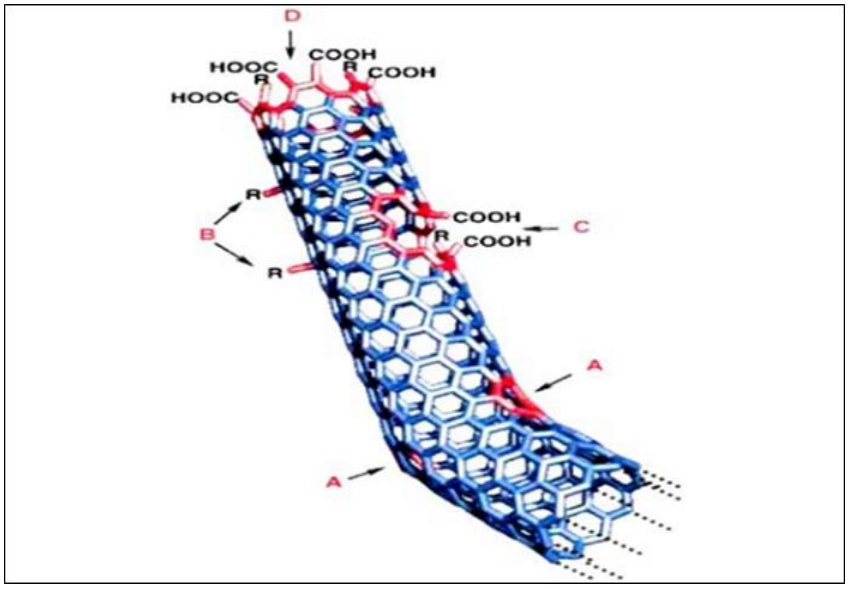

Figure 2.7. Typical defects in SWCNTs J after the functionalization process (Yuan & Liew, 2009).

Graphene particles have improved electrical transmission, superior mechanical strength, and thermal conductivity. Due to its exceptional thermophysical properties, graphene is a prime candidate for use in these applications. nanofluidic events

((Cham *et al.*, 2021)). In addition, the fabrication of graphene nanoparticles is a relatively easy and cost-effective task. Little difference in the properties of graphene has been reported due to different methods used to fabricate single or multilayer graphene, such as graphene oxide layer exfoliation, chemical vapor deposition, and mechanical cleavage (Yang *et al.*, 2015).

An experimental study found that single-layer graphene has greater thermal conductivity and heat transfer properties than CNT. Graphene nanosheets (GNPs) are two-dimensional honeycombs with more than ten layers. One major issue that needs to be addressed is graphene's stable distribution or dispersion. Therefore, it may be possible to produce stable nanofluids based on graphene by using the acid treatment and amine functionalization activation technique, appropriate ultrasonication, or adding a surfactant (Sridhar *et al.*, 210). The schematic layout of the priming procedure and the creation of CF-GNPs nanofluids is shown in Figure 2.8.

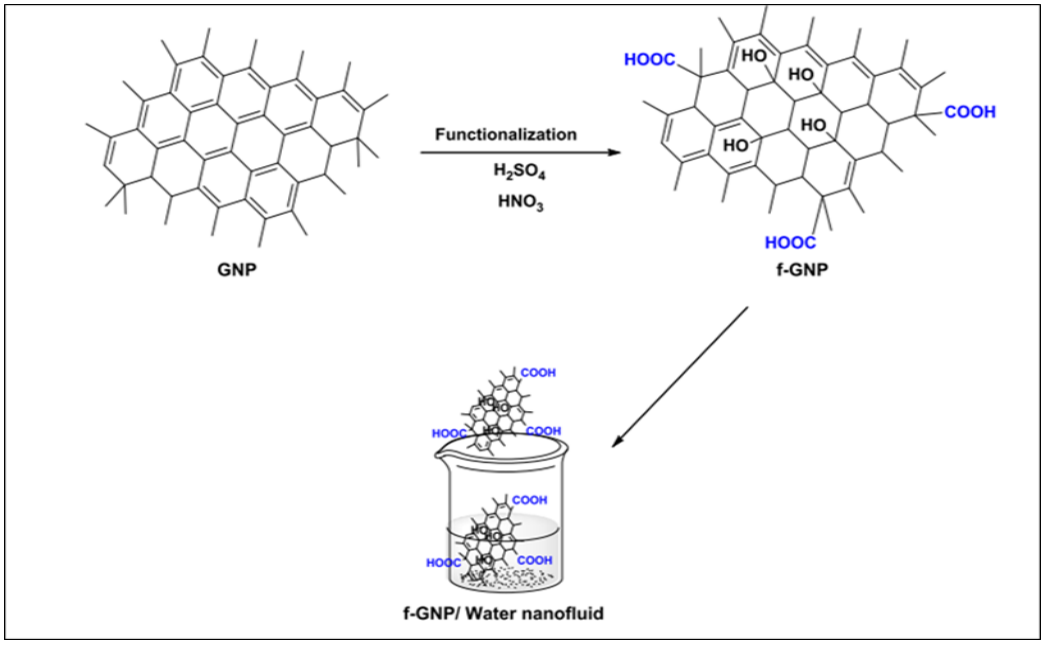

Figure 2.8. Schematic of functionalization and preparation process nanofluids (Benka 2005).

2.7. THERMOPHYSICAL PROPERTIES OF NANOFLUID

Nanofluids are solid-liquid suspensions first depicted by Maxwell (Sekhar & Sharma, 2015) in 1881. However, some prevailing technical limitations prevented researchers from investigating the validity of Maxwell's theory until Choi in 1995 (Choi 1995) conducted experiments To characterize nanoparticle suspension, which was named “nanofluid” for the first time (Gupta *et al.,* 2017). The characteristics of the basic fluid, nanomaterials, and surfactant shape the thermophysical characteristics of the nanofluid. Density (kg/m), specific heat (J/kg K), thermal conductivity (W/m K), and dynamic viscosity (kg/m s) are the nanofluid's primary thermophysical characteristics. Several models have been put forth to evaluate these traits. The theoretical models and experimental results are in good agreement for estimating nanofluids' density and heat capacity. (Bergmann *et al.*, 2013). Therefore, in practice, theoretical models are used with certainty. The most crucial variables are particle size, form, material, nanofluidic volume fraction, pH, and temperature.

2.7.1. Nanofluid Heat Conductivity

Thermal conductivity is the ability of a material to transfer thermal energy. (active vibrations). It is defined as the process of direct energy transfer between things through free electron diffusion and atomic lattice vibrations, whereas it occurs between liquids and gases through direct molecule contact. A basic characteristic of physical materials known as thermal conductivity is active energy per unit surface and per unit temperature gradient. The thermal conductivity of a material is eventually determined by its physical properties and current state. In design issues, a material's thermal transmission is an essential property that must be taken into account. Over the past few decades, careful attention has been paid to its measurements and properties.

In comparison to other proposed nanofluid delivery models, the Xuan model demonstrated good agreement with the experimental results (Farajollahi *et al*.,2010):

$$k_{nf} = k_{bf}\left[\frac{k_{np}+2k_{bf}-2\varphi(k_{bf}-k_{np})}{k_{np}+2k_{bf}+\varphi(k_{bf}-k_{np})}\right] \quad (2.30)$$

The thermal conductivity of hybrid nanofluid can be estimated by modifying the Maxwell model (Takabi & Shokouhmand, 2015) and is given by:

$$k_{nf} = k_{bf}\left[\frac{\left[\frac{k_{(np1}\varphi_{np1)}+k_{np2}\varphi_{np2}}{\varphi_h}+2k_{bf}+2\left(k_{(np1}\varphi_{np1)}+k_{(np2}\varphi_{np2)}\right)-2\varphi_h k_{bf}\right]}{\left[\frac{k_{(np1}\varphi_{np1)}+k_{np2}\varphi_{np2}}{\varphi_h}+2k_{bf}-\left(k_{(np1}\varphi_{np1)}+k_{(np2}\varphi_{np2)}\right)+\varphi_h k_{bf}\right]}\right] \quad (2.31)$$

2.7.1.1. Nanofluid Thermal Conductivity Testing Techniques

Because they have greater thermal conductivity than the standard working fluid, nanofluids have garnered much interest. Measuring nanofluids' thermophysical characteristics has been difficult because various techniques and methods have produced inconsistent findings. Therefore, picking the appropriate strategy to minimise measurement mistakes and uncertainty will be crucial. The following methods will be examined as briefly discuss superconductivity and measurement methods from the literature nanofluids (Oh *et al.*, 2008).

2.7.1.2. Improvement of Nanofluid's Thermal Conductivity

One of the most crucial elements influencing heat transmission and the thermal performance of the working fluid is thermal conductivity. For this matter many experiments have been done in this aspect. The best method, the transient hot wire method, was obtained to be more suitable compared to other techniques. Since nanofluids are frequently electrically and thermally conductive, it is challenging to employ various techniques directly. Consequently, techniques for temperature variation and constant state parallelism have been created. (Lee *et al.*, 2013) determine the thermal conductivities of four oxide nanofluids (CuO/water, CuO/ethylene glycol, $A1_2O_3$/ethylene glycol, and $A1_2O_3$/water) at room temperature using the transient hot-wire method. Nanoparticle volume sections ranging in size from 1.0 to 5.0% were used. They discovered that increasing the basic liquid,

ethylene glycol, significantly increased the thermal conductivity of the A12O3 and CuO dispersions in water. At a volume fraction of CuO of 4.0, a 20% increase in thermal conductivity was noted. Additionally, they observed that the improvement in thermal conductivity of up to 12% at 3.5 vol% of copper was less significant when water was deemed as the main fluid, and an increase in thermal conductivity of up to 10% at 4.0 vol% of Al_2O_3 will happen.

The work of Choi and coworkers at the Argonne National Laboratory (ANL) is responsible for the biggest increase in the thermal conductivity of nanofluids that has been documented in the study. (Choi *et al.,* 2001). They discovered a massive 160% increase in thermal conductivity in a nanofluid of multi-walled carbon nanotubes (MWCNTs) suspended in motor oil, with an average diameter of about 25 nm and an average length of about 50 m. This was the case even with the volume fraction of nanoparticles at only 1% of the nanotubes. The transient hot wire technique was employed by (Choi *et al.*, 2001) to measure thermal conductivity. In the water, a suspension of multi walled carbon nanotubes with an inner diameter of about 25 nm was tested for thermal conductivity by (Assael *et al*., 2004). using SDS as a surfactant or sodium dodecyl sulfate. Thermal conductivity was measured using the temporary heated wire method. According to their research, the highest thermal conductivity increase was achieved at 0.6 vol% MWCNTs/water suspension with SDS, which was 38%.

At room temperature, the thermal conductivity of multi- or double-walled carbon nanotubes floating in the water was measured by (Assael *et al.* 2005). Dispersants included Hexadecyl Trimethyl Ammonium Bromide (CTAB) and Nanosperse AQ. They found that double-walled carbon nanotubes improved thermal conductivity by 7.6% at 1.0% volume fraction in water with a dispersant, while MWCNTs improved thermal conductivity by 34% at 0.6% volume fraction in water with (CTAB) and have an average diameter of about 130 nm and a length of about 40 m (CTAB).

Published studies have verified that many variables, including the type of base fluid, temperature, acidity, particle material, volume fraction, size, and shape of the

particles, affect the thermal conductivity of nanofluids. In this section, we quickly discuss the effects of these important parameters.

2.7.2. Viscosity of Nanofluids

A fluid's viscosity can be considered a measurement of its reluctance to flow. The attraction between the watery molecules causes this resistance. The liquid flows only when sufficient energy is applied to counteract the attraction between the molecules. The term "viscosity" was first used formally by Newton (1642–1727). (Rohrig 2004). This part describes the effects of parametric variables and the theoretical models used to forecast nanofluids' viscosity.

The manner in which a nanofluid flows in the flat solar panel collector is affected by the dynamic viscosity of the working fluid. By taking into account the Brownian motion (Batchelor 1977). proposed a reciprocal relationship to estimate the dynamic viscosity of a nanofluid, as shown below:

$$\mu_{nf} = [(1 + 2.5\ X\ \varphi + \ 6.2\ X\ \varphi^2)\ X\ \ \mu_{bf}\ ]$$

(2.32)

For hybrid nanofluids (φ) is replaced with(φ_h).

$$\mu_{nf} = [(1 + 2.5\ X\ \varphi_h + \ 6.2\ X\ \ \varphi_h^2)\ X\ \mu_{bf}] \qquad (2.33)$$

2.7.3. Density of Nanofluids

It has been demonstrated that density measurements and the flow of two-phase mixtures of micrometer-sized particles coincide. (Karadimitriou *et al.,* 2012; Hwang *et al.,* 2008). Powder
with nanoscale size has the following formula, according to (Pak & Cho 1998; Kanti *et al.,* 2020):

$$\rho_{nf} = [(1-\varphi)\rho_{bf} + \varphi^{\chi}\rho_{nf}] \quad (2.34)$$

Where bf and nf are the basic fluid's and solid NPs' respective mass densities. By extending the mixture principle, equation (2.35), which has a good agreement with the experimental findings given by (Takabi & Shokouhmand, 2015), can be used to measure the density of hybrid nanofluid:

$$\rho_{hnf} = \varphi_{np1}{}^{\chi}\rho_{np1} + \varphi_{np2}{}^{\chi}\rho_{np2} + \left(1-\varphi_{np1}-\varphi_{np2}\right)^{\chi}\rho_{bf} \quad (2.35)$$

In this case, (φ_h) is supplied by and represents the total volume fraction of individual nanoparticles suspended in a hybrid nanofluid.

$$\varphi_{(h)} = \varphi_{(np1)} + \varphi_{(np2)} \quad (2.36)$$

Pak & Cho calculated the densities of TiO2 and Al_2O_3 nanofluids at 25 °C and 4.5% nanoparticle volume concentration to verify the correctness of equation (2.3). (Vajjha *et al.,* 2009) measured the density of three nanofluids—zinc oxide, antimony oxide, tin oxide, and aluminum oxide NPs—in a (60:40) EG / w base fluid using an Anton Paar digital densimeter. Then, These numbers were contrasted with the Pak & Chu theory equation.

Excellent agreement exists between the theory equation for the Al_2O_3 nanofluid and its experimental values. The Pak and Cho equation can be used to calculate the densities of all nanofluids because they also looked into the densities of SiO and CuO nanofluids and discovered that they were very similar. Since nanofluids are liquids, their density is linearly correlated with their particle volumetric concentration and can be minimally influenced by temperature. The density of nanofluids at various temps has not yet been adequately studied. Additionally, it should be mentioned that platelets and cylindrical nanoparticles (CNT) densitometry research is lacking (GNP).

2.7.4. Nanofluids Specific Thermal Capacity

Nanofluid-specific heat capacity has been determined using a variety of differential scanning calorimeter (DSC) models. Some of these DSCs were constructed on location to measure the temperature capacity of nanofluids. The specific heat capacity of nanofluids can be determined using some correlation and mixing theory formulae (O'Hanley *et al.,* 2012). The first connection of a nanofluid's specific heat capacity was published by Buck and Chu.

$$C_{nf} = [(1 - \varphi_v)^{x} C_w + \varphi_v + C_{np}] \tag{2.37}$$

C stands for specific thermal capacity, w is water, np is NPs, and φ is the volume fraction of NPs.

(Farajollahi *te al*.,2010; Jayachandra Babu., *et al* 2017;) subsequently changed that equation into:

$$(\rho Cp)_{(nf)} = [(1 - \varphi)(\rho Cp)_{(bf)} + \varphi^{x}(\rho Cp)_{(np)}] \tag{2.38}$$

According to (Takabi & Shokouhmand, 2015), equations (2.41) and (2.42) can be used to determine the heat capacity of hybrid nanofluids.

$$C_{p,hnf} = [\frac{(1 - \varphi_h)x(\rho Cp)_{bf} + \varphi_{np1}\, x\, \rho_{np1}\, x\, C_{p,np1} + \varphi_{np2}\, x\, \rho_{np2}{}^{x} C_{p,np2}}{\rho_{hnf}}] \tag{2.39}$$

The volume proportion of nanoparticles and the specific heat capacity of nanofluids have been linked in numerous studies. Some studies suggest a negative relationship between the drop in fraction size and the specific heat of nanofluid. According to the researchers' findings, the specific heat of the nanofluid dropped to 25% as the volume fraction of Al_2O_3 nanoparticles in water increased. (Luo *et al.*, 2008). In ethylene glycol, four different nanofluidic dispersions of Al_2O_3, TiO_2, and Al were studied for their specific heat at varying volumetric nanoparticle concentrations

(Namburu *et al*., 2007). Moreover, found that in every instance, increasing the volume fraction causes a decrease in the specific heat of the nanofluidics.

Additionally, according to (Karami *et al.,* 2014) showed that as the weight of nanoparticles increases, the specific heat of graphene nanoparticles decreases. A different group of researchers found exactly the opposite result; For example, (Fathi *et al.,* 2012) found that the specific heat of nanofluids decreased as the concentration of nanoparticles decreased.

2.7.5. Addition of Surfactant

A technique for preventing the nanoparticles from settling includes a surfactant. By converting the surface from hydrophobic to hydrophilic, the surfactant improves the diffusion and stability of the NPs. It is necessary to add enough surfactant to create the right quantity of coating in order to overcome electrostatic repulsion (Jiang *et al.*, 2003). It should be noted that the viscosity of the nanofluids rises with the addition of materials, and this is a problem because the viscosity is directly proportional to the addition of surfactants. The bonds formed between the NPs and the surfactants can weaken when the temperature of the surfactants exceeds 60 °C, which may have a detrimental impact on the stability of the NPs in the nanofluid (Wang & Mujumdar, 2008).

In addition to salt and oleic acid (Hwang *et al.,* 2008), Tween 80, triton X-100, and gum arabic, some popular surfactants include sodium dodecyl sulfate (SDS), sodium dodecyl benzene sulfonate (SDBS), polyvinylpyrrolidone (PVP), sodium dodecyl sulfate (SDS), and sodium dodecy (GA). Selecting the proper surfactant with the correct concentration is crucial. However, no set method for doing this or that has been documented in the books.

2.8. METHODS FOR STABİLİTY ASSESSMENT

There are six ways to assess the dispersion state of a nanofluid, all of which have been widely studied in the evaluation of nanofluid stability:

2.8.1. Spectrophotometer, UV-vis

Investigating nanofluids with UV-Vis spectrometers is possible because it is a common technique for examining solids and liquids. It is easy to use, and the results are easy to assess (Mukesh Kumar 2017). UV-Vis was used to evaluate the durability of the suspensions in nanofluids. The viscosity of test samples, which is necessary for this technique to function because it depends on light scattered at different wavelengths, is a limitation / of absorbent elements (Yu & Xie , 2012). Nanofluids can be identified by contrasting the concentrations of the suspensions with the sedimentation duration. Beer-Lambert's rule, which states that absorption is directly proportional to the concentration of NPs in nanofluids, forms the foundation of this technique. (Alicia *et al.,* 2016).

Colloid stability can be assessed qualitatively using UV-vis spectrophotometric research. Equation illustrates how the Beer-Lambert law can be used to determine the light absorption ratio index. (2.40).

$$A = [-\log x \left(\frac{I}{I_i}\right)] = \varepsilon bc \tag{2.40}$$

Equation (2.40) shows that, for a particular molar optical path and absorptivity, the absorbency is proportional to the weight percentage of the suspended particles (Said *et al.*, 2014).

2.8.2. Potential Zeta Rating

A technique frequently used by researchers to measure the stability of nanofluids is the zeta-stress test. Its working theory is based on the electrophoresis rule, which states that when the zeta potential displays high (absolute) values, the electrostatic repulsion inside the NPs rises, resulting in stable nanofluids (Lee *et al.,* 2006). Particles with low surface charge tend to aggregate. A suspension is usually considered a stable nanofluid if its measured zeta potential value is more accurate than 30 mV (positive or negative) (see Table 2.4). The pH is the most significant

factor in determining a suspension's zeta potential number. The value of the zeta potential varies along with a solution's pH. The impact of pH on nanofluids' zeta potential and durability was investigated by (kumar *et al.,* 2018).

Table 2.4. Zeta potential value and stability.

Zeta potential [mv]	**Colloidal behavior with respect to stability**
From (0 to ±5)	Scarring or rapid clotting
From (10 to ±30)	Light equilibrium and low stability
From (30 to ±40)	stable
From (40 to ±60)	good safety, potential for reliability
More than (±61)	exceptional steadiness

2.9. SUMMARY AND CONCLUSİONS

The outcomes show that, as previously mentioned, nanofluids can be used to improve the thermal efficiency of flat plate solar collectors. Consideration of the effects of creating novel nanomaterials with a high thermal conductivity as working fluids within the flat plate solar collector requires more research. Various nanofluids, such as HTFs, have been used in solar collector applications. It was less interested in other materials like metal oxides, Gr, GNPs, and SWCNTs because most of the papers he found focused on using MWCNTs and Al_2O_3. The experimental work's reported findings demonstrated that using aqueous dispersions of MWNTs and GNPs, which have relatively low mass fractions of carbon nanomaterials, improved the FPSC efficiency more effectively. In comparison, using higher mass fractions of non-carbon nanomaterials allowed for modest increases in FPSC energy efficiency. Therefore, it can be concluded that FPSCs work effectively when carbon-based nanoparticles are suspended in DW at low ratios. With a lower weight concentration of nanofluids, along with small increases in viscosity, pressure drop, and pumping force, the price, dispersion stability, and pumping power will all be higher.

Additionally, stable nanofluidic dispersions that can endure for a long period require covalent and/or non-covalent functionalization. The detrimental effects of surfactants, particularly the non-covalent functionalization, on the thermophysical

properties of both the base and the nanofluid have been considered in earlier studies. Using nanomaterials with covalent functionalities is advised to make highly stable nanofluids with improved thermal performance. (Sarsam *et al.,* 2020). Covalent functionalization is a commonly used technique for causing hydrophilic behavior in previously hydrophobic nanoparticles. Experimental research on covalent and non-covalent activation processes was done in this work. Additionally, consideration has been given to how various factors may affect the thermophysical characteristics of newly created nanofluids and the thermal performance of FPSCs.

PART 3

RESEARCH METHODOLOGY

This research aims to ascertain the effects of using aqueous colloidal dispersions of multi-walled carbon nanotubes and metal oxides as working fluids on the fluid flow, physical properties, heat transfer properties, and thermal performance of FPSC. The goal of this chapter is also to fully describe the methodology used to carry out the study's objectives and satisfy its requirements. These data include measurements of the thermophysical properties of the nanomaterials used, information on the nanomaterials themselves, and numerical solutions created with the ANSYS software. (View fig 3.1).

3.1. RAW MATERIALS AND NANOFLUID PROCESSING

The presentation of materials used in preparing nanofluids for this study will be discussed below:

Where purchased multi-walled carbon nanotubes from XG Sciences in Lansing, Michigan, USA. MWCNTs have a specific surface area of 230 m/g, are 5-15 nm in diameter, and are 5 m long. It is 95–98% pure. This high degree of purity uses it directly without needing purification a second time. Sulfuric acid 95–97% (H_2SO_4) and analytical reagent grade nitric acid 65% (HNO_3) were purchased from Sigma-Aldrich as running medium.

The following describes the elements used to create the nanofluids for this study:

Multi-walled carbon nanotubes were purchased from XG Technologies in Lansing, Michigan, USA. The MWCNTs have an area of 230 m/g, a diameter of 5–15 nm, and a length of 5 μm. 95-98% pure. Due to its high level of hygiene, we can use it right

away without having to scrub it again. As a running medium, H_2SO_4 (sulfuric acid 95–97%) and HNO_3 (nitric acid with analytical reagent grade 65%) were purchased from Sigma-Aldrich. Raw materials of GNPs with a purity of 98%, a maximum particle diameter of 2 μm and a specific surface area of 750 sq/g purchased from XG Sciences, Lansing, MI, USA, were used in this study.

Solid, whitish powder of more than 98% pure spherical titanium oxide (TiO_2) has a diameter of 10–25 nm. Furthermore, due to their high purity, all the chemicals used, as previously stated, were used without further purification. We used four available surfactants from Sigma-Aldrich in Selangor, Malaysia: Cetrimonium bromide (CTAB), sorbitan mono (Tween 80), sodium dodecyl sulfate (SDS), and triton X-100 (Tx-100).

3.1.1. Functionalization and Preparation of Mwcnts

At present, there is a problem that MWCNTs are hydrophobic and cannot be dispersed in any polar solvent, such as distilled water. The researchers found suitable methods for the compatibility of MWCNTs with water, which is done by acid treatment. The MWCNTs were transferred to H_2SO_4, where they underwent an acid treatment procedure that involved dispersing them in a solution of H_2SO_4 (98%) and HNO_3 (67%) at a ratio of (1:3) (strong acidic medium), all while the solution was being shaken. One gram of MWCNTs was combined with 250 cc of an acid solution to mix. Then, an ice bath was used, and nitric acid droplets were added to the mixture tray. Considering its choice as an acidic treatment, the mixing ratio of sulfur to nitric acid (3:1) was chosen (Verma *et al.,* 2017). After 30 minutes of continuous stirring at room temperature, the solution underwent three hours of ultrasonic sonication to settle the dispersion. The sample combination was re-flowed for 30 minutes at room temperature with constant stirring after 3 hours of probe sonication. The MWCNTs were then centrifuged at 6000 rpm for 15 minutes to eliminate the excess acid, and then they were cleaned several times with distilled water before being dried for 24 hours at 80 °C. As shown in Table 3.1, rich samples of (0.02, 0.05, 0.08, and 0.1 wt%) were determined. Fig. 3.2 showed a graphical representation of how CF-MWCNTs nanofluids were primed and prepared. The necessary mass of each

nanomaterial is determined using equations (2.1) to (2.7) from Chapter 2. Figure 3.3 shows samples created from CF-MWCNT nanofluids.

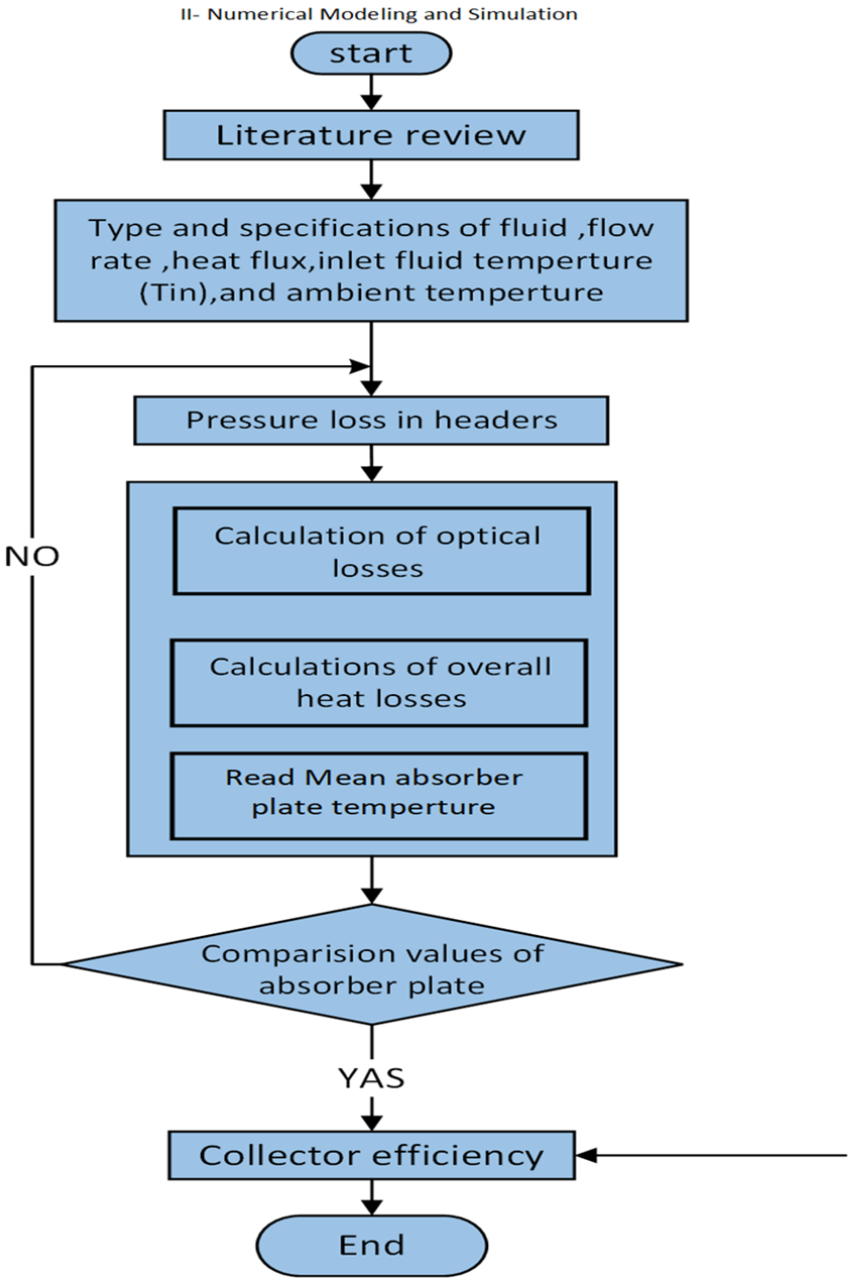

Figure 3.1. Diagram of the study process.

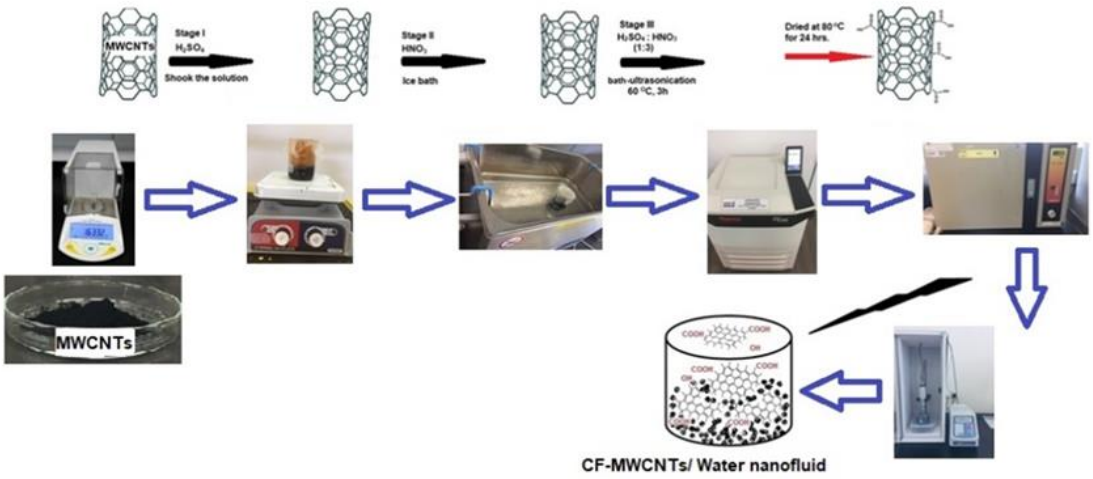

Figure 3.2. Schematic of functionalization and preparation process nanofluid (Hussein *et al.*, 2020).

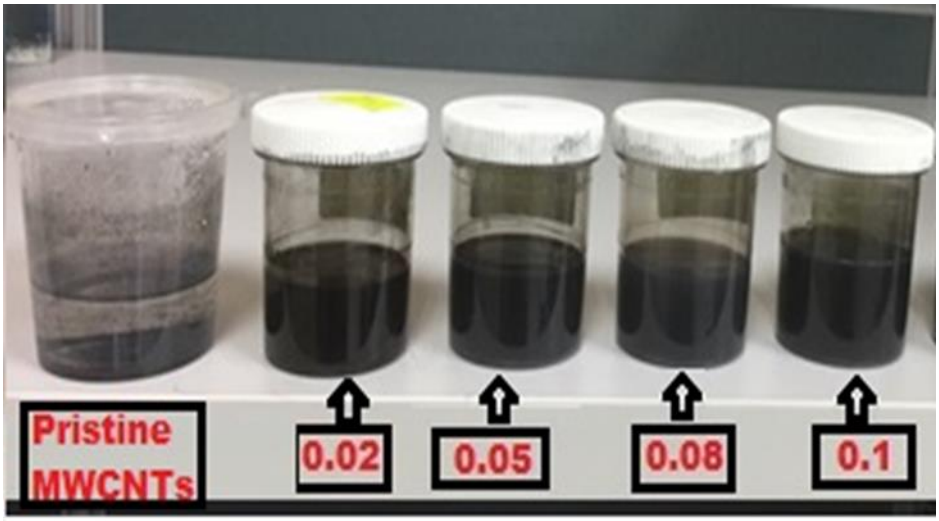

Figure 3.3. CF-MWCNTs nanofluid samples in a picture (Hussein *et al.*, 2020).

Table 3.1. Required mass to achieve optimal CF-MWCNTs of nanofluid concentrations.

No.	mass	weight concentration
1	(0.012 -gram %)	(0.02 wt%)
2	(0.03- gram %)	(0.05 wt%)
3	(0.048 -gram %)	(0.08 wt%)
4	(0.06- gram %)	(0.1 wt%)

3.1.2. Preparation of NCF-MWCNTS

The study of using an ultrasound probe sonicator (Sonics Vibra-Cell, VC 750, Sonics & Materials, Inc., USA) with an output power (750 W) and a frequency (20 kHz) power source to disperse MWCNTs in distilled water. Notably, the MWCNT supplier suggested using a sonication probe and surfactants or functionalization to disperse the materials in water. NCF-MWCNTs have thus been produced using a variety of additive detergents, including SDS, CTAB, Tween80, and Triton X-100. Four distinct ultrasound durations have been used: 15, 30, 60, and 90 minutes. For sample processing, the MWCNT weight concentrations ranged between 0.02, 0.05, 0.08, and 0.1 wt%. Figure 3.4 and Table 3.2 both display sample combinations. The weight concentration ratio of NCF-MWCNTs (1:1) and 60 min fixed MWCNTs were held in reserve during sample processing. Ice is used to maintain the temperature at the proper level all the time. Within 60 minutes, the power source's ultrasonic procedure added the dispersant to its already-consolidated role. The necessary mass of each nanomaterial is determined using equations (2.1) to (2.7) from Chapter 2. fig 3.5 shows samples made from NCF-MWCNTs nanofluids.

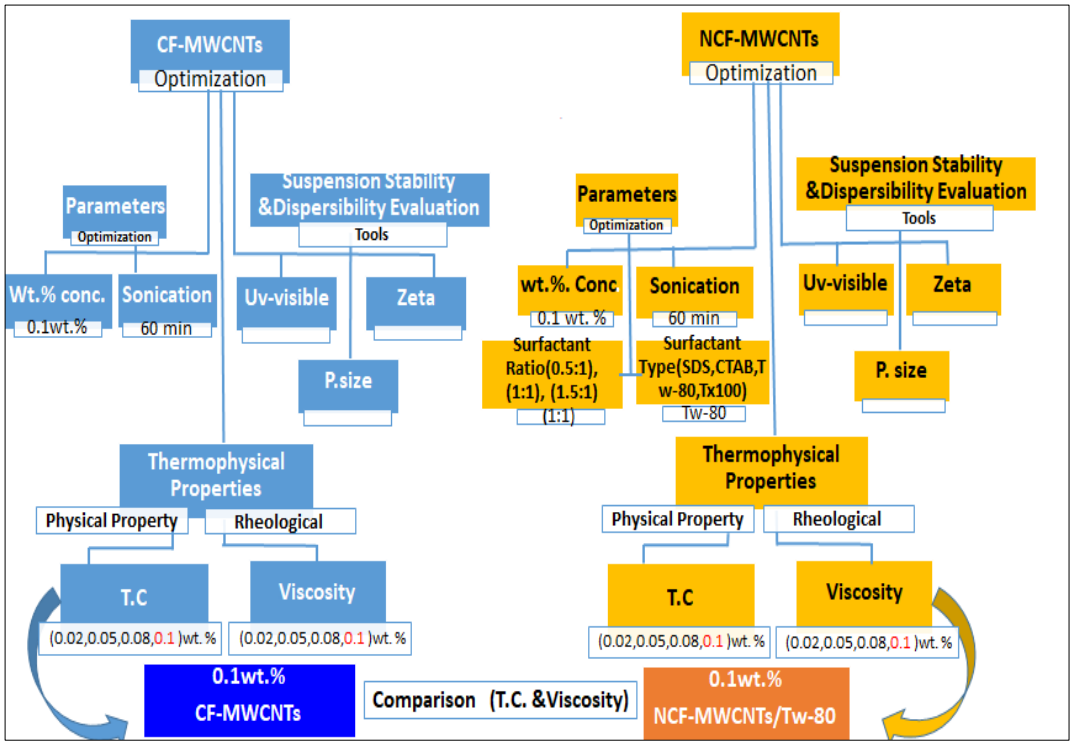

Figure 3.4. Flowchart for Nanofluids Preparation and Optimization.

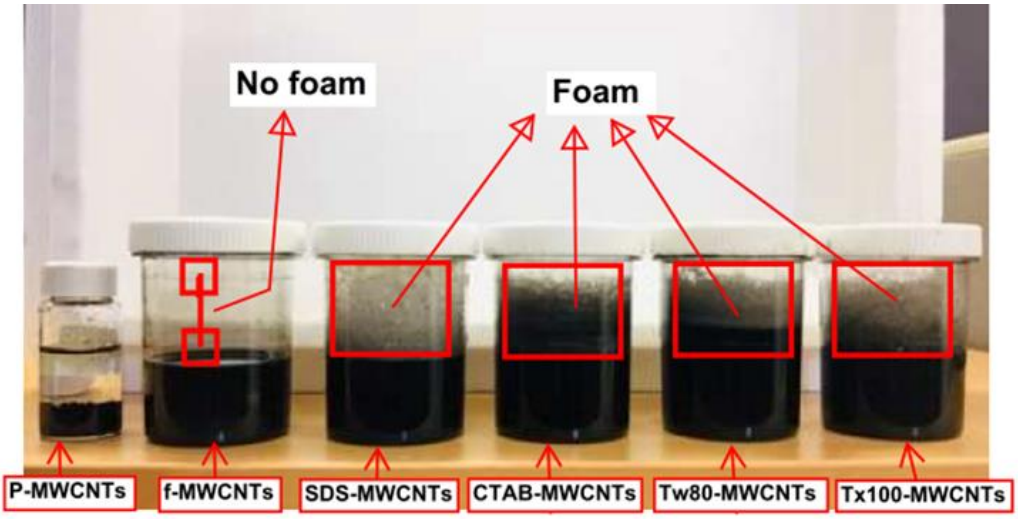

Figure 3.5. NCF-MWCNTs nanofluid samples photographed (Hussein *et al.*, 2020)

Table 3.2. Information about the samples created for this study at various concentrations after creation(Hussein *et al.*, 2020).

Sample no.	**Ultrasonication time**	**Surfactant type**	**Surfactant-MWCNTs ratio**	**Weight concentration**
1	(30 min)	(P- MWCNTs)	-	0.02 wt%
2	(60 min)	(P-MWCNTs)	-	0.02 wt%
3	(90 min)	(P- MWCNTs)	-	0.02 wt%
4	(15 min)	(SDS)	1:1	0.02 wt%
5	(30 min)	(SDS)	1:1	0.02 wt%
6	(60 min)	(SDS)	1:1	0.02 wt%
7	(60 min)	(CF- MWCNTs)	-	0.02 wt%
8	(60 min)	(CF- MWCNTs)	-	0.05 wt%
9	(60 min)	(CF- MWCNTs)	-	0.08 wt%
10	(60 min)	(CF- MWCNTs)	-	0.1 wt%
11	(60 min)	(SDS)	0.5:1	0.02 wt%
12	(60 min)	(SDS)	1:1	0.02 wt%
13	(60 min)	(SDS)	1.5:1	0.02 wt%
14	(60 min)	(SDS)	1:1	0.02 wt%
15	(60 min)	(SDS)	1:1	0.05 wt%
16	(60 min)	(SDS)	1:1	0.08 wt%
17	(60 min)	(SDS)	1:1	0.1 wt%
18	(60 min)	(CTAB)	1:1	0.02 wt%
19	(60 min)	(CTAB)	1:1	0.05 wt%
20	(60 min)	(CTAB)	1:1	0.08 wt%
21	(60 min)	(CTAB)	1:1	0.1 wt%

3.2. CHARACTERİZATİON OF THE PREPARATİON OF NANOFLUİDS

Due to the influence of thermal conductivity and the transmission of nanofluid on the shape, structure and morpholi, it has become necessary to identify them. The ideal description of Nanopowder is one of the important basics in enhancing the understanding of nanoparticles. Therefore, the description will be fully explained in the following sections.

3.2.1. High-Resolution Transmission Electron Microscopy (HR-TEM)

The purpose of using a high-accuracy electronic microscope (HR-TEM) is to know the shape and dimensions of the single nano identify whether the samples have agglomerated or are composed of single nanoparticles. Moreover, knowing the sampling cluster or not, the electronic radiation in the electronic microscope (HR-TEM), which can photograph nanomaterial standards by radiation, with the importance and accuracy that HR-TEM characterizes until it has some defects as the electronic microscope (HR-TEM) is that samples are from the nanoparticles that are to be examined must be dried before the examination. It is not easy to obtain pictures in the colloidal state with absolute accuracy due to the nanoparticles clustering together when they are dried, which affects their shape and size. This makes it time-consuming to use dynamic light scattering to analyze the samples, and it is ineffective. To solve this problem, FEMM was employed, which was used in the initial photography. This method is commonly used in the emissions field JEM-2100F.

3.2.2. Field Emission Scanning Electron Microscopy (FESEM)

The measurements were made in the transitional microscope of field emissions (FE-TEM) on the electronic emissions HR-TEM Field Emission Scanning Electron Microscopy (FE-SEM).For the purpose of photographing the nanoparticles sample with very high accuracy for this, the electronic microscope for field emissions (FE-SEM) is used. During the process of examination by electronic field emissions (FE-SEM), electronic radiation is focused on the sample spot, and via radiation is

transferred Green energy to the sample spot. The initial electrons are called the e - electrons, the sample electrons, the way to attract these rejected electrons that are called secondary electrons, these electrons are collected by a biased detector or network in a positive way, and then it turns them into a signal.

3.2.3. Fourier Transform İnfrared Spectroscopy (FT-IR)

Dry materials that focus on potassium bromide (KBR) have a very low concentration, which is used to form a very soft powder to convert FT-Yir, which is analyzed using the infrared spectrum. After that, a strong and thin peel is used to compress the powder and make it suitable for analysis. This process is important in determining the functions on the surfaces of hybrid and non –hybrid samples from other samples. Samples have been analyzed as an infrared transformation (Perkin Elmer-Spectrum100 FT-Yer) in wave ranges of 4000-400 cm^{-1}.

3.2.4. Raman Spectroscopy

To find out the rotation, vibrating situations and other low frequencies that occur to the sample, the Raman spectroscopy is used. It can be defined as Raman's prose or elastic prose is a unilateral light that is usually a laser within the infrared or closer to UV rays. The principle of work comes into contact with the excitement and vibrations in the system. This leads to a change in its capacity to the top or down. This condition leads to the opposite of the vibrations that occur to the sample in the system, that the reumer of the infrared spectrum is similarly, but there is more knowledge and information related to the samples and is more complementary, using the existing lens. It passes through a unilateral color, and there is a compatibility along the laser line between the wavelength and scattered radiation, which is called the flexible rayleight prose, while the light resulting from the laser remains collected through the scope pass filter on a detector. In this work, using the Renishaw invia raman microscope, the Raman spectra are collected with laser excitement at 514 nm.

3.2.5. Energy dispersive (X-ray) spectroscopy (EDX) and (X-Ray) diffraction (XRD)

SEM Field Emissions are intended to know the chemical structures of spectrum analyzes of the treated functional X-ray. There are several key advantages to using EDX analysis instead of XPS analysis. Firstly, EDX is highly portable due to its compact size, making it easy to use in various settings. Secondly, EDX allows for spectral analysis of X-ray emissions from samples. This is particularly useful when analyzing larger samples with spot sizes over 250 microns. The German-made Bruker AXS Model D8 Advance and XRD are used to perform this type of analysis. The peaks we obtained from the different minerals were matched to study the stages contained in the CF-MWCNTs and the NON-CF-MWCNTs. XRD was used to look into the formation of any karabide in the interface and the existence of nanoparticles. Using CUK (= 1.542) for the Siemens D-500X-ray, which operates at 40 how and 20 meters at a rate of 1.2 degrees/min, XRD is recorded with various patterns of the samples. An average temperature of room temperature was used for the exercise.

3.3. THERMOPHYSİCAL PROPERTİES MEASUREMENT

3.3.1. Thermal Conductivity

Decagon Devices KD2 (KD2 Pro, Decagon Devices, Inc., USA) was utilized in the experimental research. Whose thermal conductivity of nanofluids can be measured. It was used to measure the thermal conductivity of nanofluids at room temperature. The rest of the sub-sections are separated from each other through a hot copper wire, which operates on KD2. In addition, the temperatures range between 0-60 degrees Celsius, which is characterized by an accuracy of up to 5%. However, it turned out through experience that KD2 is considered very accurate when it is prepared and installed picture perfect, placed vertically and inside a 25 °C water bath. There are some barriers to numbers and some problems with external boundary effects and convection.

3.3.2. Rheometer

To obtain an ideal and good liquid in the performance of the thermal transmission, it has become important to know the viscosity of the nano, similar to the rest of the second simple nanopolitan fluid. RPMS is used to measure the viscosity of the nanopolitan fluid and know whether it is Newton or not. In general, the temperature determines the liquid viscosity that depends on it in general, regarding the behavior of the biological fluid and is known to use was measured using the Anton Paar rheometer Physica MCR 92 or which is called the moisture scale. The correlation for the dynamic viscosity of distilled water was used to test the values reported by the water testing in order to confirm the viability of the viscometer and the experimental methodologies (Wen *et al.*, 2009):

$$\mu = e^{(1.12646-0.039638*T)/(1-0.00729769*T)}/10^3 \quad (3.1)$$

Where, (T) temperature in Kelvin, and (μ) viscosity in mPa,s.

3.3.3. Differential Scanning Calorimetry

Differential scanning calorimetry (DSC) is used to determine nanofluids' heat capacity. The temperature gradient acquired for a given sample and fryer during heating is measured and considered as a function of the temperature. In the measurement stage, the frying pan and the sample are kept at the same temperatures. The heat capacity of the frying pan is a reference provided by the manufacturers. The gradient that occurs as a result of the heat flow allows us to know the heat capacity of the samples used. There is more or less heat flow to the sample container in relation to the return heat, which is done when moving from one phase to another. using DSC curves. DSC phase transition temperatures are calculated to demonstrate this in this work (LINSIS DSC1000-Error ± 0.25-1 °C). The heating rate was set at 5 °C/min, and the measurements were carried out under a purified nitrogen atmosphere.

3.3.4. Density Meter

Through experimental measurements of density, samples of nanofluids with volumetric behavior were obtained as a function of temperature and the weight fraction of nanoparticles. A Stabinger Viscometer (DMA 4500M, Anton Paar GmbH) was used to measure the density of the prepared nanofluid experimentally. Three measurements were recorded for each sample and temperature, and a density measurement accuracy of 4-10 g/cm3 was obtained. The density of distilled water was measured to ensure the probe's validity and the instrument's accuracy.

3.4. SİMULATİON STUDY

Chapter three deals with the details of mathematical performance modelling of a nanofluid-based FPSC in energy points of view. The pressure loss in FPSC header pipes is also important and should not be overlooked. The user graphical interface capability of using ANSYS-Fluent facilitates the performance modelling of a nanofluid-based FPSC. To produce homogenous feedstock of nanofluid, a combination of nanoscale dispersion of functionalized CF-MWCNTs in distilled water. MWCNTs were functionalized using concentrated acids (H2SO4/HNO3) with the assist of heating and sonication process. The nanofluid characterization must be performed in stable conditions. Outdoor tests should be adapted from the existing standards, i.e. ASHRAE method. The indoor experiments for characterizing the nanoparticles, two-step preparation of the nanofluids and then, their characterization are presented in this chapter along with the relevant apparatuses. The flowchart of the entire research work is presented as well.

3.4.1. Flat Plate Solar Collector

3.4.1.1. Flat-Plate Solar Collector Section

FPSC to maintain the test device, was provided with an aluminum casing and waterproof insulation materials consisting of mineral rock wool, as illustrated in Figure (3.6). An EPDM rubber substance encircles the complex and has a transparent

glass cover that covers every area of the complex. Table 3.3 provides information on the FPSC's technical specs.

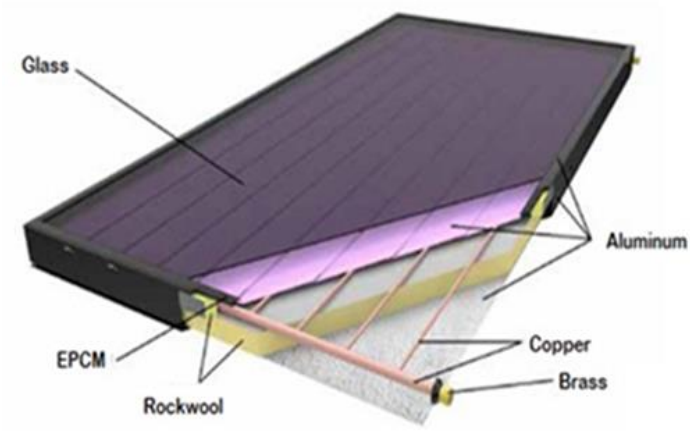

Figure 3.6. a glimpse of the various FPSC components seen during the test.

3.4.1.2. Theoretical Analysis of FPSC

In this study, a mathematical model is used to simulate the thermal performance in a flat solar panel collector using nanofluids, as the nanofluids were based on the HW model presented by (Duffie & Beckman, 2013), with some minor modifications. In order to simplify the problems that we are likely to encounter, some modifications were proposed based on certain assumptions, as follows:

- During the operation period, the flat plate solar collector was in a stable state.
- The flow through the rising pipes of the collector was uniform.
- Heat flow through the one-dimensional back insulation area.
- Temperatures around the ascending tube wall are uniform.
- Along the (y-axis) in the absorption plate, temperature gradients were dealt with, as shown in (Fig. 3.8), and along the (X-axis), the flow direction as shown in (Fig. 3.8) separately.
- The nanofluids used in the study are well dispersed and have excellent colloidal stability.
- The used nanofluid was considered a single-phase nanofluid.

At the medium temperature/spout to the temperature of the common basin, heat occurs from the top, bottom and edge of the flat solar collector of the absorber plate. Using all the above assumptions, the ambient temperature (Ta) was taken. To simulate FPSC based on nanofluids, ANSYS solution was developed to solve the mathematical model. The flowchart for solving this is presented in Fig. 3.7.

Table 3.3. Technical requirements for the FPSC.

SL. NO	Detaıls Of Parameters	Specıfıcatıon	UNİT
1-	Dimensıons	[198.8 × 104.1 × 9]	CM
2-	Casıng Materıal	[Electrostatically Painted (Black)]	...
3-	Weıght	[37200]	G
4-	Sealıng Material	[Electrostatically Painted [Black) Aluminium Case]	...
5-	Gross Area	[20700]	CM^2
6-	Aperture Area	[19200]	CM^2
7-	Absorber Area	[18900]	CM^2
8-	Absorber Material	[Almeco Tınox Hıghly Selective Aluminium]	...
9-	Absorptance (%)	[95]	...
10-	Emıttance (%)	[3]	...
11-	Weldıng Method	[Laser Welding]	...
12-	Heat Carrıer Carrıer Volume	[1.07]	LİTERS
13-	Number Of Rıser Tubes	[7]	...
14-	Tube Pıtch	[12]	CM
15-	Glass Materıal	[Low Iron Tempered Glass]	...
16-	Transmıttance Of Glass	[91%]	...
17-	Thıckness Of Glass	[0.4]	CM
18-	Insulatıon Materıal	[Rockwool]	...
19-	Thıckness Of Wool	[5]	CM
20-	Base Sheetıng	[Embossed Aluminium Sheet]	...
21-	Max. Operatıng pressure	[10 Bar]	...
22-	Max. Collectors ın series	[8]	...
23-	Stagnatıon Temperature At 930 W/M And 30˚C	[203]	˚C

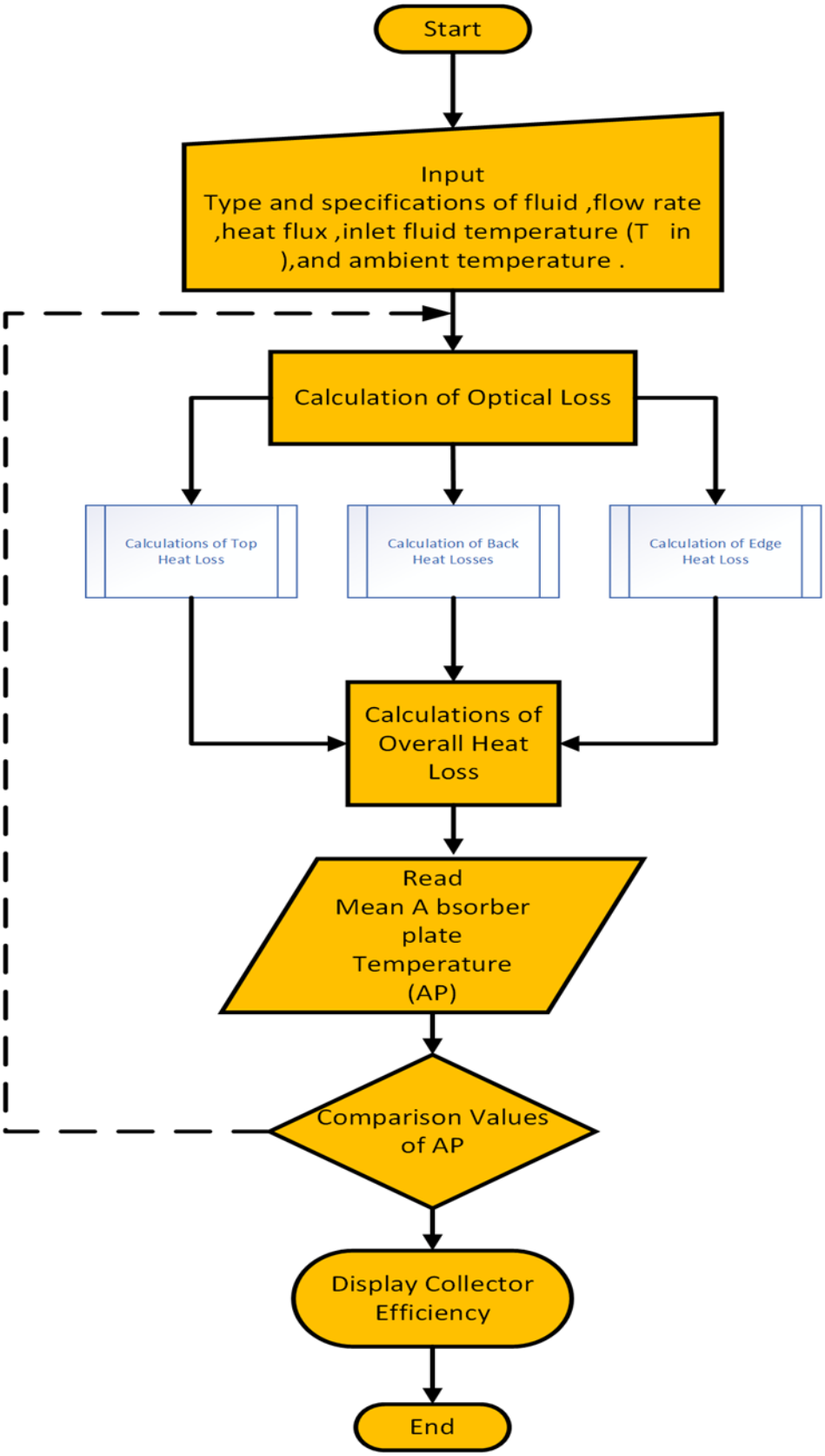

Figure 3.7. Flowchart for the FPSC's numerical answer

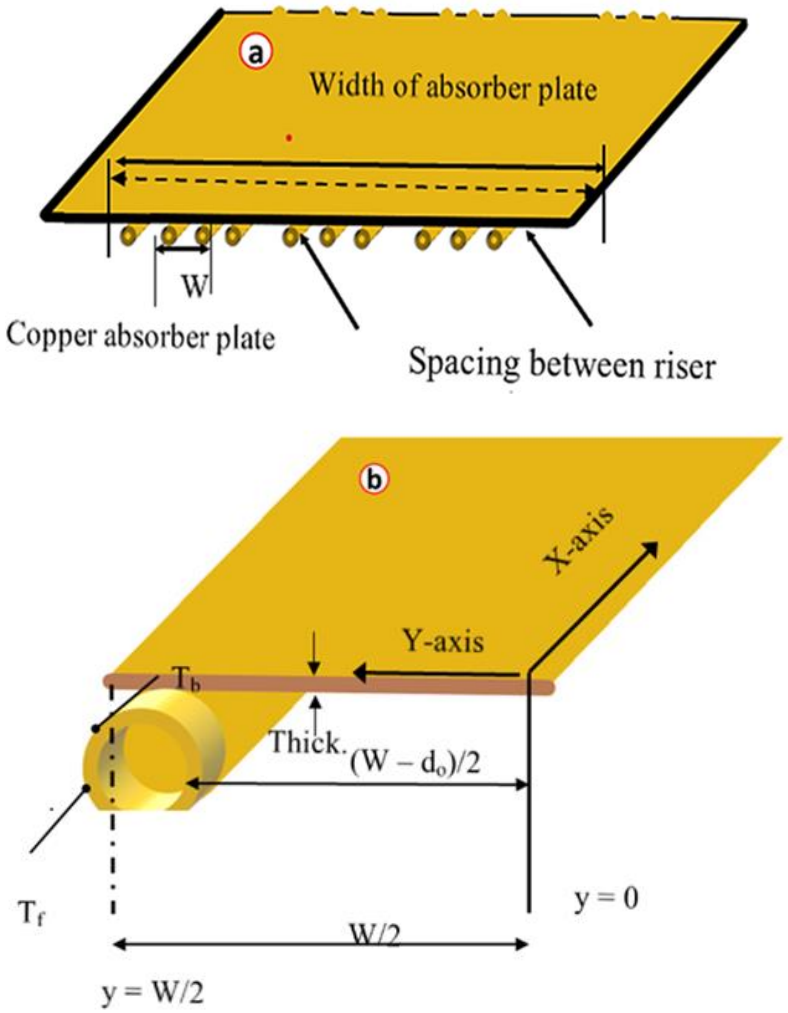

Figure 3.8. The mathematical model; (a) the components of a flat plate solar collector; (b) the fin and tube section taken into account in the mathematical model.

3.4.1.3. Energetic Efficiency

The active efficiency of the solar collector is determined (Hwang *et al.*, 2010):

$$\eta_i = \frac{Q_u}{Ac\,.\,G_t} \tag{3.1}$$

Here, the collection and the solar radiation regions on the collector, respectively, are thought of as Ac and Gt.In Eq. (3.1),

Q_u = (the useful heat gain)

A_c . G_t : (available solar energy)

One of the following relationships is a typical approach for the goal of estimating useful heat gain:

$$Q_u = m \cdot x\ C_p\ x(T_{out} - T_{in}) \tag{3.2}$$

$$= A_c x\ [(S - U_L)\ x\ (T_{pm} - T_a)] \tag{3.3}$$

Where

$S = \eta_o\ x\ G_t$ = the effective radiation on the collector,
η_o = optical efficiency, which is determined based on the transmittance-absorbance product as $\eta_o = (\tau\alpha)_{avg}$.

The cover glass and the absorbent plate absorber are related to the transmittance associated with them. Considering the difficulty in measuring the absorbent plate Tpm's average temperature, it is possible to substitute it into the equation. (3.3) with the liquid entry temperature by adding the FR (heat removal factor):

$$Q_u = A_c x\ F_R x[S - U_L\ x(T_{in} - T_a)] \tag{3.4}$$

$$= A_c x G_t x[F_R x(\tau\alpha)_{avg} - F_R x U_L x(\frac{T_{in} - T_a}{G_t}) \tag{3.5}$$

After those calculations, the active efficiency of the solar collector can be rewritten as

$$\eta_{eng} = F_R x(\tau\alpha)_{avg} - F_R x U_L x(\frac{T_{in} - T_a}{G_t}) \tag{3.6}$$

An essential practical parameter, the collector's FR heat removal factor is comparable to the conventional heat exchanger's EF efficiency factor. As a result, its research

demonstrates how much heat the collector can actually capture in comparison to the highest potential useful energy gain:

$$F_R = [\frac{Q_u}{A_c x G_T x(\tau_g \alpha_{ap}) - A_c x U_L x(T_{in} - T_a)} = \frac{\dot{m} x C_p x(T_{out} - T_{in})}{S x A_c - A_c x U_L x(T_{in} - T_a)}] \quad (3.7)$$

The heat removal factor and the collector design criteria are connected through the input of the collector efficiency factor F':

$$F_R = \frac{\dot{m} x C_p}{A_c x U_L} [1 - \exp x \left(-\frac{U_L F' x A_c}{\dot{m} x C_p}\right)] \quad (3.8)$$

$$F' = \frac{1/U_L}{W x [\frac{1}{U_L x(D + (W - D) x F]} + \frac{1}{C_b} + \frac{1}{\pi x D_i x h_{fi}}]} \quad (3.9)$$

where the fin efficiency is denoted by F, and the riser tubes' outer diameter, interior diameter, and spacing are denoted by D, Di, and W, respectively (Fig. 3.8). Cb, the riser tubes, and the absorption plate have been integrated to improve the conductivity between the components and produce a high number of bond conductivity. As a result, the 1/Cb word is rarely used today. (Suslick 1989). The bond standard, which includes the bond's conductivity, kb, length, b, and average thickness, is essential in welded or glued designs. It can be determined using the formula Cb = kbb/ γ. The heat loss coefficient, UL, determines how well the collector stops heat. One of the most important practical parameters is given in Eq. (3.6) loss from the edges, back, and upper insulation. The following represents a rough estimate of the collector's total heat loss:

$$U_L = [U_t + U_e + U_b] \quad (3.10)$$

The top of the collector accounts for the majority of the overall heat loss, which is calculated as follows (Hwang *et al.*, 2012; Suslick 1989):

$$U_t = \left| \frac{N}{\frac{cc}{T_{pm}}\left[\frac{(T_{(pm)}-T_a)}{N-\tau}\right]^{ee}} + \frac{1}{h_{wind}} \right|^{-1} + \frac{\sigma(T_{pm}-T_a)*(T_{pm}^2+T_a^2)}{\frac{1}{\varepsilon_{ap}+0.00591Nh_{wind}}+\frac{2N+\tau-1+0.133\varepsilon_{ap}}{\varepsilon_g}-N} \quad (3.11)$$

Where :

τ =[(1-0.089xh_{wind}+0.1166x$h^2_{wind}\varepsilon_p$)(1+0.078661xN)]

C C =[520 × (1-0.000051x φ^2)]

e e =[0.430 × (1-100/T_{pm})]

T_{pm} =[Absorber plate mean temperature]

The Stefan-Boltzmann constant, the number of glasses, the glass emittance, the emittance of the absorber plate, and the wind heat transfer coefficient are listed in that order: NG, GP, and KW. The wind heat transfer coefficient is calculated as follows for a particular number of the wind speed, Vw, and riser length, L (Suslick 1989):

$$h_w = \frac{8.6V_w^{0.6}}{L^{0.4}} \quad (3.12)$$

Once the average temperature of the absorption plate (Tap) has been established (Figure 3.8). Fourier's law states that the bottom heat loss coefficient (Ub) can be used to describe the conduction heat loss from the absorber plate to its surroundings as follows:

$$Q_b = [k_{ins(b)} x\, A_C x \frac{(T_{(ap)} - T_a)}{thk_{(ins(b))}} = U_b x A_C x (T_{(ap)} - T_a)] \quad (3.13)$$

$$U_b = [\frac{k_{(ins(b))}}{th\ x\ k_{ins(b)}}]$$

$$= (T.C\ of\ insulation\ at\ bottom) / (Thickness\ of\ insulation\ at\ bottom) \quad (3.14)$$

T.C = $Thermal\ conductivity$

Similar to this, the FPSC's edge heat leakage to the environment is as follows:

$$Q_e = k_{ins(e)} x\ A_e x \frac{(T_{ap} - T_a)}{thk_{ins(e)}} \tag{3.15}$$

The collector area (Ac) was used as the reference point for all heat loss factors, so equation (3.13) was changed to read as follows:

$$Q_e = [\frac{k_{(ins(e))} x A_e}{A_C} A_C x \frac{(T_{(ap)} - T_a)}{thk_{(ins(e))}} = U_e x A_C x (T_{(ap)} - T_a)] \tag{3.16}$$

$$U_e = [\frac{k_{ins(e)} A_e}{thk_{ins(e)} A_C}] = \frac{[T.C\ of\ insulation\ at\ edge] \times [Edge\ Area]}{[Thickness\ of\ insulation\ at\ bottom] \times [Collector\ Area]} \tag{3.17}$$

T.C=$Thermal\ conductivity$

The heat gain term qu = Qu /Ac is contrasted to the expression UL (Tin - Ta), which is referred to as the collector, heat loss term. Using Eq. (3.18), the average temperature of the absorber plate is calculated according to the heat clearance factor and heat loss coefficient:

$$T_{pm} = T_{in} + \frac{Q_u}{A_c F_R U_L}(1 - F_R) \tag{3.18}$$

A crucial measure that should be assessed based on the thermophysical characteristics of a specific nanofluid flowing in an FPSC is the convection internal heat transfer coefficient, (h*fi*) according to Eq. (3.9).

3.4.1.4. Physical Modeling of FPSC

Using the commercial package ANSYS-Fluent 18.1 computationally, the simulation was performed for a three-dimensional flat-panel solar collector with an inclination angle of 10° operating under mixed laminar convection heat transfer, as shown in Fig. 3.9 (a). In Table 3. 3, an engineering detail of the system has been made. The computational domain, which is under study, contains four regions to induce the best

control of its networks. The structure lattice has been calculated, and it is denser near the tube wall and is displayed at fig 3.9 (b).

1. Fluid flow in and out:At the inlet section of the riser is the flow of laminar water-based nanoparticles with initial temperature and velocity T-inlet and U-inlet, and at the outlet section, it is the pressure outlet boundary state.
2. Pump:The copper tube is installed under the absorbent plate (copper).
3. Welded joint:Soldering made of copper is considered as part of this simulation on the calculation related to the absorber plate.
4. Absorption plate: The joint was covered with a thin copper plate that was absorbent. The side and bottom edges of the absorbent plate were supposed to have a constant boundary state, while the top surface experiences a constant heat flux.

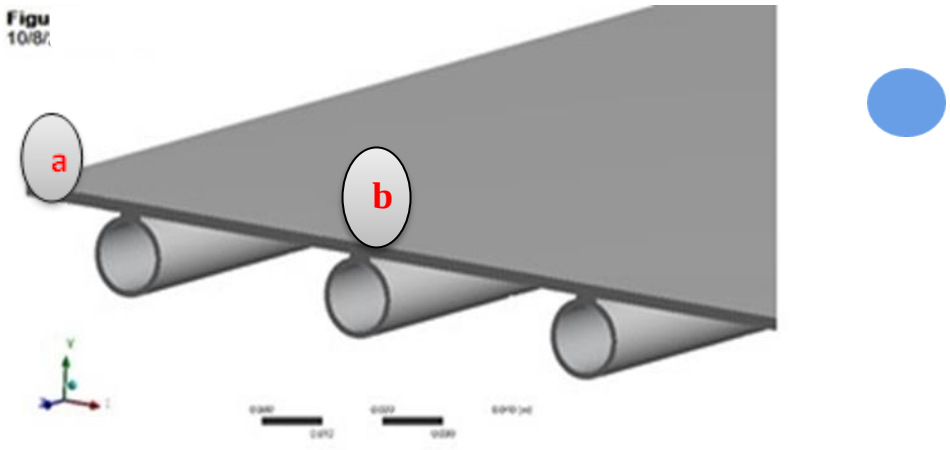

Figure 3.9. (a) The tube-on-sheet flat plate solar collector's schematic illustration

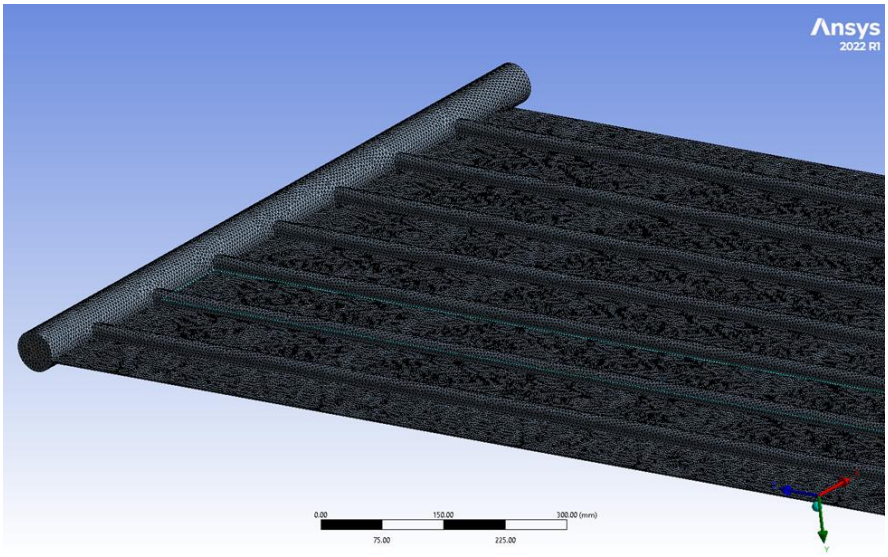

Figure 3.9. (b) Grid Layout of the Flat Plate Solar Collector Tube-on-Sheet Problem.

The three-dimensional flat solar panel collector from this study, which operates under conjugate mixed layer convection heat transfer, has a 10-degree inclination angle and comprises a thin copper absorbing plate type plate, a copper tube, and a welding component that joins the tube to the absorber plate. It is observed that the used fluids—water-based nanofluids with a weight concentration of 0.1% show a uniform inlet temperature and velocity profile as they travel through the riser in the inlet area section. Several of the methods outlined in the preceding sections have been used to experimentally determine the structural characteristics of metal oxide and carbon nanoparticles. The movement is Newtonian, fluffy, three-dimensional, steadily and slowly. The side walls of the absorbent plate were given non-slip conditions and thermal limits, while the top surface of the absorbent plate was exposed to a uniform and constant heat flow. Both the normal (y-axis) and current (z-axis) directions of gravitational pull are provided. Therefore, it was anticipated that the pure basic phase of the fluid and the nanoparticles would be in thermal balance with zero relative velocity and that the effects of heat transfer rate, compressibility, and radiation would be minimal. The formulae (continuity, momentum, energy, X, Y, and Z), where y was the normal direction, x was the direction of extension, and z was the direction of current, are all subject to the constant conservation of 3D Cartesian coordinates., as follows:

Continuity:

$$\frac{\partial}{\partial x_i} x(\rho u_i) = 0 \tag{3.19}$$

Momentum:

$$\frac{\partial}{\partial x_j} x(\rho u_i u_j) = \frac{\partial p}{\partial x_i} + \frac{\partial}{\partial x_j}\left(v\left(\frac{\partial u_i}{\partial x_j} + \frac{\partial u_j}{\partial x_i}\right) - \acute{u}_i \acute{u}_j\right) \tag{3.20}$$

Energy:

$$\frac{\partial \rho x C_p u_j T}{\partial x_j} = \frac{\partial}{\partial x_j}\left(k\frac{\partial T}{\partial x_j} - \rho C_p \overline{u_j T}\right) + S_t \tag{3.21}$$

Where, $i = 1,2,3, u_i = (u, v, w)$ are vectors of velocity.

The necessary border conditions for the tube-on-sheet flat plate solar collector are explained in the paragraphs that follow;

Inlet tube sectio
$u = v = 0, w = U_{inlet}, T = T_{inlet}$n: (3.22)

Upper absorber plate surface: $u = v = w = 0, q_w^{"} = I(\lambda \, x \, k) - h \, X \, (T_{col} - T_{amb})$ (3.23)

Bottom surface of absorber plate: $u = v = w = 0, \frac{\partial T}{\partial y} = 0$ (3.24)

Left and right lateral walls of the absorber plate: (3.25)

$$u = v = w = 0, \frac{\partial T}{\partial x} = 0$$

Outlet tube section: $$[(\frac{\partial u}{\partial z}) = (\frac{\partial v}{\partial z}) = (\frac{\partial w}{\partial z}) = 0, \frac{\partial T}{\partial z} = 0] \quad (3.26)$$

Solid-liquid interfaces: $$[k(\frac{\partial T}{\partial x}) = k_s(\frac{\partial T_s}{\partial x})] \quad (3.27)$$

When the solar radiation shines its beam (intensity = I) on the glass cover of the FPSC, a part of it that is not absorbed is reflected in the surrounding areas. After reflecting part of the unabsorbed radiation, the glass cover absorbs the other parts. The remaining adsorbent portion was transferred to the absorbing plate through the cover glass. Through convection and radiation, which results in a partial loss of heat in the nearby areas, the solar radiation (intensity = I) transmitted to the flat solar panel collector raises its temperature to higher levels than the surrounding areas. An inclined tube-on-plate flat-plate solar collector was computationally simulated in this study using ANSYS-Fluent 18.1. The nonlinear equations causing the issue have been resolved using the finite volume technique (FVM). A second-order headwind diagram was used to predict the load and propagation conditions, and the SIMPLEC algorithm approach (composed of SIMPLE) was used to take advantage of the compression velocity coupling. The computational domain was split into several small regions to enhance the coupling quality and enable greater control over the network sizes. Except for the energy equation, where the residual number is less than 10-8, the iterative process is a convergent solution process until the residuals of the momentum and continuity equations are less than 10-4. When only pure water was used in the riser tube of the flat plate solar collector, four separate networks were monitored to arrive at a dependable solution independent of the engineering networks. The top absorption plate's surface was assigned a constant heat flux of 930 W/m2, and the inlet water's temperature was kept within a range of (20, 30, 40, and 60 °C) while the Reynolds number (Re) was regarded as laminar. Table 3.4 summarises and tabulates the findings and deviations from the network independence study. This research used a fine grid with 311,101 cells for all simulations.

Table 3.4. Results and variations from the test for grid independence.

Number of Cells	$\overline{Nu}$	**% Diff** $\overline{Nu}$	T_{Outlet}	**Diff** T_{Outlet}
[159, 966] = [coarse]	[8.090]	[8.188]	[28.63]	[17.2 e-3]
[219,760] = [intermediate]	[6.384]	[2.302]	[28.65]	[7.6 e-3]
[311,101] = [fine]	[6.211]	[0.0724]	[28.65]	[2.8 e-3]
[428,988] = [very fine]	[6.289]	-	[28.64]	-

3.4.2. Heat Transfer Criteria

The Nusselt number depends on the Reynolds number and the collector's heat transfer coefficient, which in turn depends on the Reynolds number and the Prandtl number, which defines the flow regime:

$$h_{fi} = \frac{Nu\, k_{nf}}{D_i} \tag{3.28}$$

The optimal model for estimating the Nusselt number could be developed once the flow regime of the nanofluid inside the risers was identified.

The following symbols are used Reynolds and Prandtl's numbers:

$$Re_{nf} = \frac{\rho_{nf}\, V D_i}{\mu_{nf}} = \frac{4\dot{m}_{riser}}{\pi D_i \mu_{nf}} \tag{3.29}$$

$$Pr_{nf} = \frac{\mu_{(nf)X}\, c_{(p,nf)}}{k_{(nf)}} \tag{3.30}$$

The above equations showed that nanoparticles play an important role by changing the thermo-physical properties of the fluid flow, thus affecting the values of the non-dimensional heat transfer coefficients.

Thermal boundary conditions will determine the heat transfer performance for laminar flows of Re < 23 00 inside the riser tubes. For short circular tubes in which hydrodynamic and thermal boundary layers develop, the heat transfer coefficient is

higher near the inlet. As a result, it is common practice to determine the local Nusselt number with constant heat flux using the Heaton correlation (Hwang *et al.*, 2010).

$$Nu = Nu_{(\infty)} + \frac{a\ X\ (Re\,\mathrm{x}\mathrm{Pr}\,xD_h/L)^m}{1+b(Rex\,\mathrm{Pr}\,xD_h/L)^n} = Nu_{\infty} + \frac{a(\mathrm{Pex}\,D_h/\,L)^m}{1+b(\mathrm{Pe}\,xD_h\,/\,L)^n} \tag{3.31}$$

In Eq. 3.31, Dh and L stand for the hydraulic diameter and tube length, respectively, while Pe is the Peclet number.

3.5. UNCERTAİNTY ANALYSİS

According to ASME recommendations, experimental measurements have some errors, and the true measurement cannot be fully obtained (Xu *et al.*, 2013). These errors may result from unintentional or intentional mistakes, systematic errors, and data volatility brought on by using inappropriate instruments. The uncertainty in the measurement data is estimated to determine the variation in the experimental parameters and to guarantee measurement precision. In the FPSC performance experiment using nanofluidics, the flow rate, temperature, and solar radiation measurement errors are the main causes of uncertainty, according to Eq. (3.1). The uncertainty analysis equation, according to (Ramires *et al.*, 1995), has the basic form:

$$U_y^2 = \sum_{i=1}^{n} U_{xi}^2 \tag{3.33}$$

Where Uxi is the root sum square (RSS) of the scatter and measuring uncertainty of each measured parameter, and Uy is the overall uncertainty of the calculated parameter. As a result, the RSS technique yields the following combined uncertainty for the evaluation of collector efficiency, U (Nguyen 2007):

$$U_{\eta_i} = [\sqrt{(\frac{\Delta \dot{m}}{\dot{m}})^2 + (\frac{\Delta(T_{out}-T_{in})}{T_{out}-T_{in}})^2 + (\frac{\Delta G_t}{G_t})^2}] \tag{3.34}$$

It is believed that the mistakes in Cp and Ac are insignificant. The measurement of the nanofluids' thermophysical properties employs an analogous relationship.

3.6. SUMMARY AND CONCLUSİONS

The third chapter covers the specifics of the mathematical performance and computational modeling from the energy viewpoints of the flat-panel solar collector based on nanofluids. It's crucial to take into account the pressure reduction in the flat plate collector pipes. Using a graphical user interface with ANSYS-Fluent makes it easier to model FPSC performance using nanofluids. An aqueous solution containing a nanoscale dispersion of functionalized CF-MWCNTs can create a uniform starting material from a nanofluid. With the aid of heating and sonication, strong acids (H_2SO_4/HNO_3) were used to functionalize MWCNTs. Stable circumstances must be used for the nanofluidic characterization. Existing standards, such as the ASHRAE technique, must be modified for external tests. The two-step preparation of nanofluids and internal tests to identify nanoparticles. This chapter introduces linked devices and follows with characterization. Additionally, a flowchart of the complete research project is provided.

PART 4

RESULTS AND DISCUSSION

The analysis of the microscopic, physical, and thermal characteristics of artificial CF-MWCNTs is presented in this part, along with a comprehensive discussion. Moreover, providing information on the produced nanofluids' characterization.

Using characterisation, Fourier Transform Infrared (FTIR), Fourier Transform Infrared (XRD), Raman spectroscopy, and FESEM techniques, the effects of residual chemical activation processes on microstructure analysis were examined. Under various temperatures and concentrations of nano additives, the viscosity and thermal conductivity trends of CF-MWCNTs have been closely observed. The efficacy of the flat plate solar collector and the measured thermophysical characteristics of nanofluids were compared with earlier experimental results for validation reasons; Besides, a CFD (FLUENT) code has Convective heat transfer and fluid flow simulation software has been created.

4.1. MATERİALS CHARACTERİZATİON

4.1.1. Characterization of P -MWCNTs and CF-MWCNTs

4.1.1.1. Characterization of Functionalized MWCNTs using FTIR

The results of the FTIR spectroscopy study on samples of natural MWCNTs and CF-MWCNTs are shown in Fig. 4.1. The locations of the absorption peaks at 2850, 1650, 1383, and 1100 cm-1, which in CF-MWCNTs were separated by C-H bonds, C=O bonds, CO bonds, and CO-C bonds, were also shown in Figure 4.1. The links show how the acid-treated molecules adhered to the MWCNT's edges and surface. The direct esterification process on these two bonds, C=O and C-O, was very strong.

CF-MWCNTs displayed a wide absorption peak between 4,000 and 3,000 cm-1, which can be linked to the functionalization-related -OH bond signature. (Amiri et al., 2015). The peaks in the distinctive spectra of the purified MWCNTs demonstrate the effectiveness of the CF process.

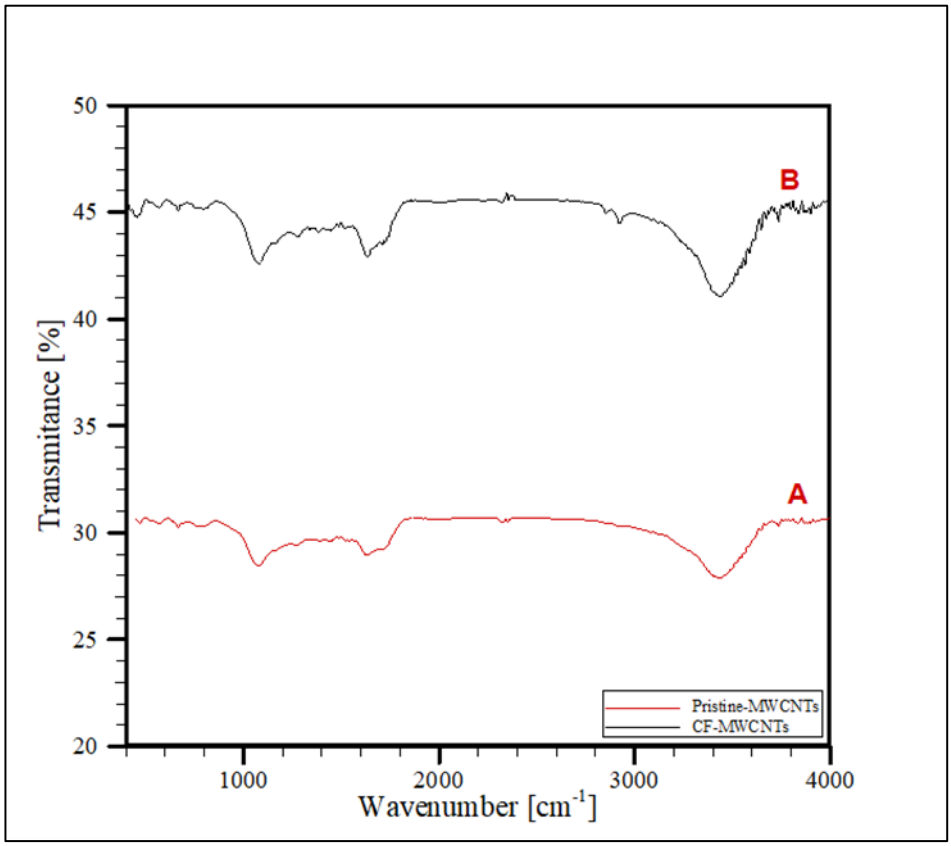

Figure 4.1. MWCNT FT-IR spectra: (A) as received MWCNTs, (B) after a 3-hour ultrasonication solution(Hussein *et al.*, 2020).

4.1.1.2. Raman Spectroscopy-Based Characterization of Functionalized MWCNTs

The ID/IG ratio of the (3) h-treated MWCNTs was higher than that of P-MWCNTs. After the procedure of preparation, Raman spectroscopy was used to analyze the structural properties of covalent chemical bonding (CF) in MWCNTs. The (G) band in the spectrum typically indicates the presence of sp2 carbon, whereas the (D) band denotes an out-of-equilibrium chemical makeup. (Yadav & Cho, 2013) displays the two-dimensional Raman spectra of CF-MWCNTs and P-MWCNTs Figure (4.2). P-

MWCNTs and CF-MWCNTs have ID/IG rates of 0.624 and 0.855, respectively. Similarly, covalent activation caused new covalent bonds to develop on the carbon sheets CF-MWCNTs.

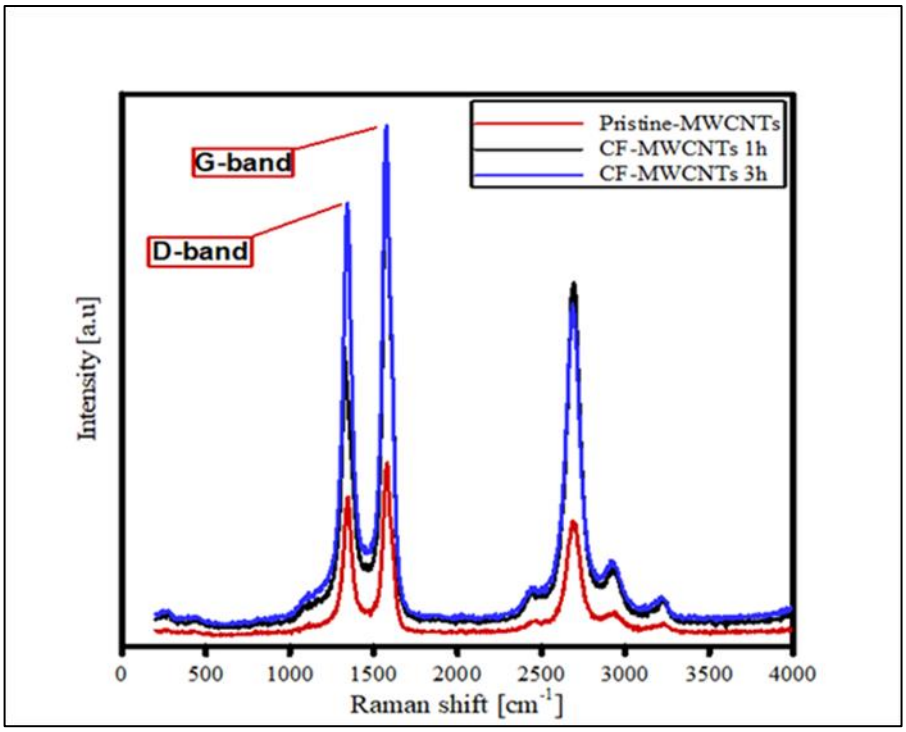

Figure 4.2. P-MWCNT and CF-MWCNT after-treatment Raman spectroscopy (Hussein *et al.*, 2020).

4.1.1.3. Characterization of Functionalized MWCNTs Using XRD

The pure and oxidized states of the nanomaterial were examined using an X-ray powder diffraction (XRD) research procedure. The diffraction characteristic of a sample of chemically treated MWCNTs). According to the ideal structure of MWCNTs, there are two distinct peaks in the pattern at 2-theta 25° and at 44.4°, which correlate to the (002) and (004) crystal planes, respectively. The XRD findings show that CF-MWCNTs do not affect the crystal structure of MWCNTs. This result is compatible with research by (Yarmand *et al.*, 2016), is shown in Figure (4.3).

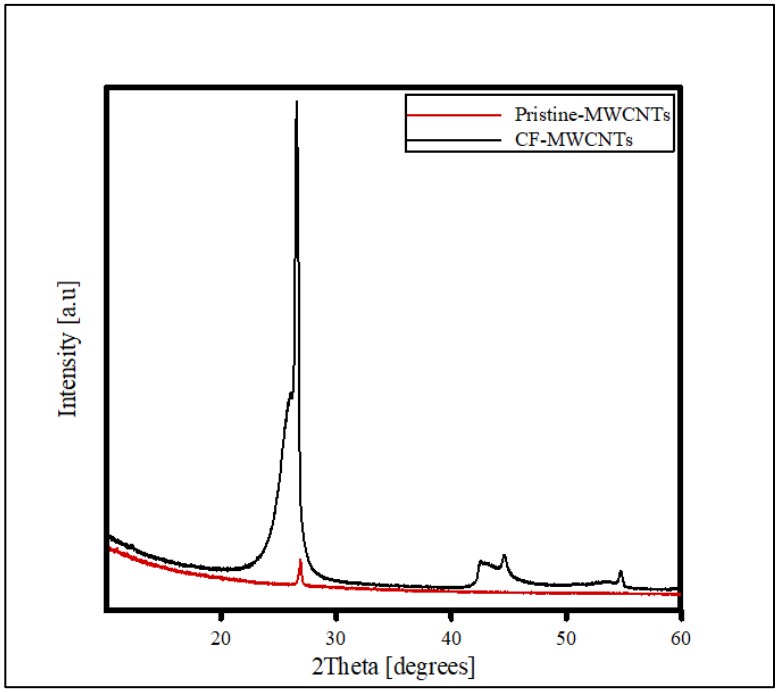

Figure 4.3. P-MWCNTs and CF-MWCNTs' XRD patterns(Hussein *et al.*, 2020).

4.1.1.4. Functionalization Processes' Effects on the Microstructure Of Mwcnts

FESEM Observations

The impact of the chemical activation procedure on the quality and microstructure of individual MWCNTs has been investigated using various characterization techniques, including FESEM. Research indicates that MWCNTs consistently have low phase integrity. (Hou *et al.*, 2008). This is because MWCNTs are typically produced using metal catalyst nanoparticles like iron and nickel. (Chng & Pumera, 2011). Since pure MWCNTs are primarily made of iron and nickel, it was highly anticipated that some impurities would be found in the materials once received. The results of the FESEM characterization are revealed. consists of two parts to image: acid-treated MWCNTs under sonication for 3 hours. However, no variation could be discerned with respect to the structures of the MWCNTs after 1 hour of ultrasonication; However, the sample that underwent the 3-hour ultrasound showed some obvious changes, show this in Fig. (4.4).

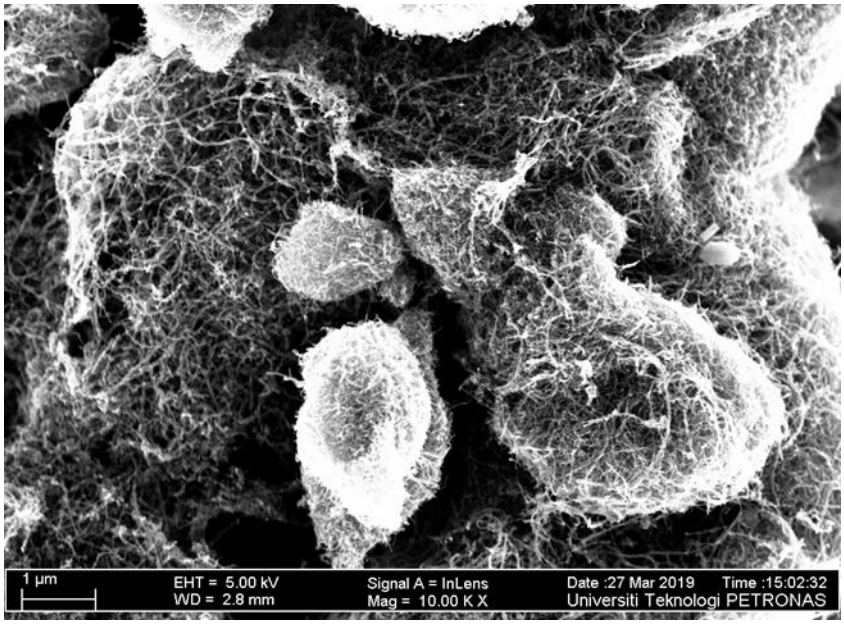

Figure 4.4. FESEM images of MWCNTs; sonicated for 3 hrs (Hussein *et al.,* 2020)

4.1.2. Characterization of Al_2O_3 and TiO_2

4.1.2.1. Morphology and XRD of Al_2O_3

Using FESEM imaging, the crystalline nature and surface morphology of Al_2O_3 nanoparticles. As observed through this microscopic image, the nanoparticles are almost hexagonal, with some structures having an aggregate shape. The presence of aggregated particles is problematic, and breaking up those agglomerates, therefore, will require the use of high shear strength by the two-step method of preparing the nanofluids. Qualitative EDX analyses revealed that (O) and (Al) were significantly present in the nanopowder.

To determine the level of oxidation and purity of the material, an XRD measurement was conducted, Al_2O_3 was verified to be present in the sample by two distinct peaks of 26.72 and 41.7, which is consistent with the results of (Kuang *et al.,* 2015). Fig.(4.5,), in Fig. (4.6). shows this .

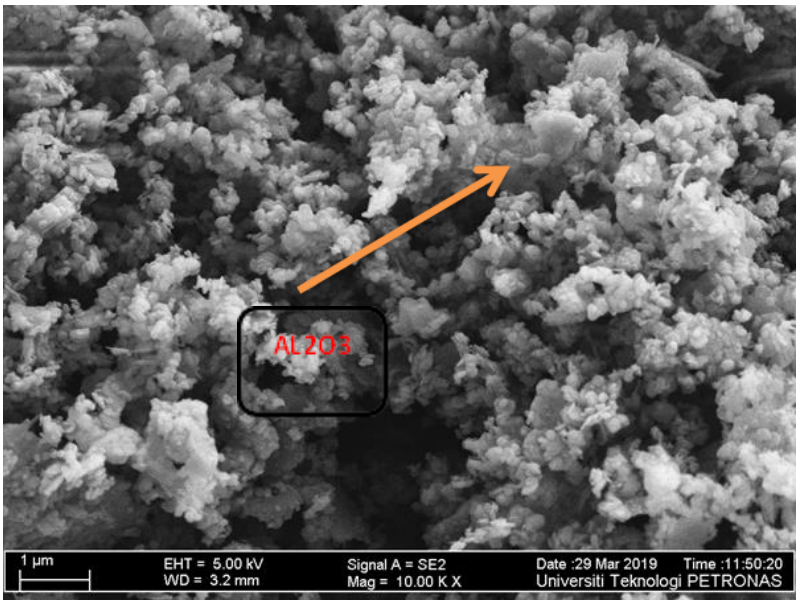

Figure 4.5. Test for Al_2O_3 nanopowder using FESEM

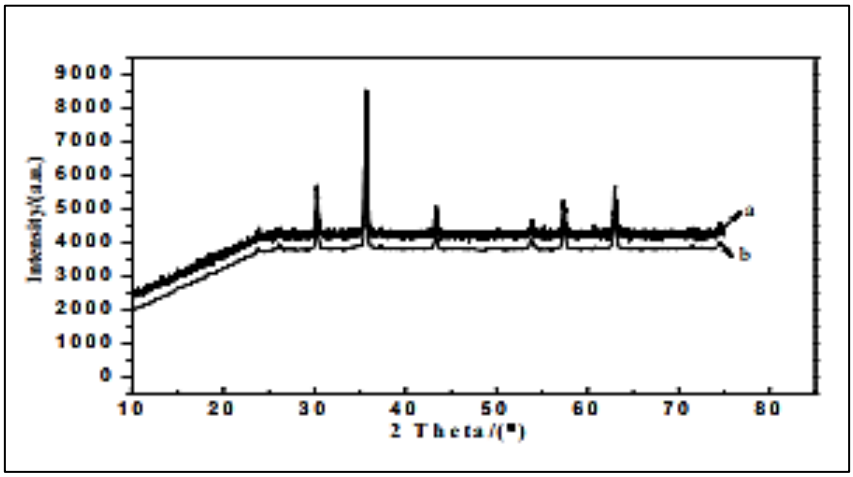

Figure 4.6. Results of an XRD measurement on an Al_2O_3 nanomaterial(Ting-ting *et al.*,2018).

4.1.2.2. XRD and Morphology of TiO_2 Nanopowder

The structural and morphological properties of the TiO_2-NPs are depicted. The particles are almost all (Ti), as seen from the FESEM microscopy pictures, with some aggregated shaped structures. The chemical compositions of the materials obtained through EDX. According to the research, the nanopowder contains the basic elements C, O, and Ti.

XRD patterns were used to examine the purity and oxidation behavior of the TiO_2 nanopowder samples. The existence of TiO_2 is confirmed by the presence of four strong peaks at 26.4, 38.4, 39.1, and 42.7, which is consistent with earlier observations (Madhesh *et al.*, 2014). The solid, crystalline, and well-ordered main orientation of titanium dioxide was revealed by the sharp, intense peaks.as show in Figures . (4.7), (4.8).

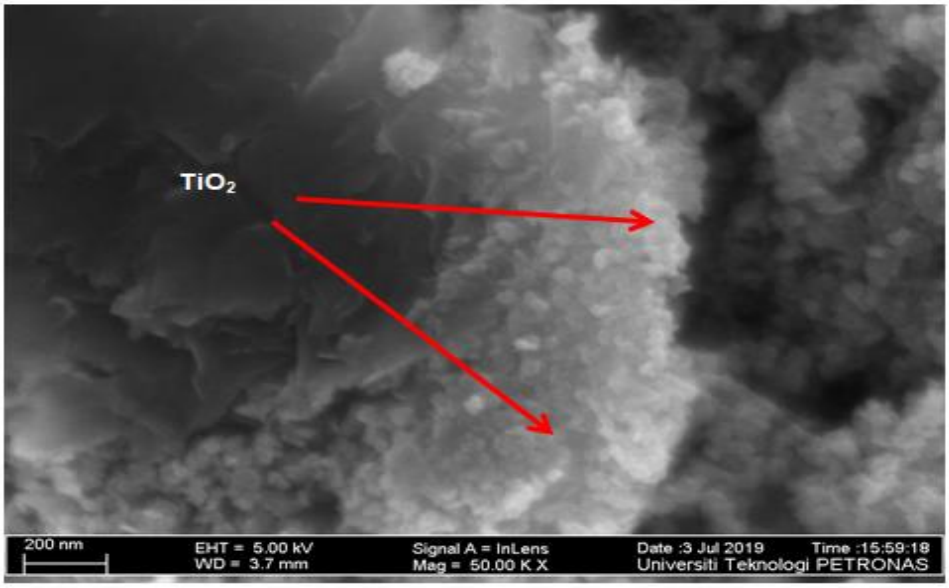

Figure 4.7. FESEM test for TiO_2 nanopowder.

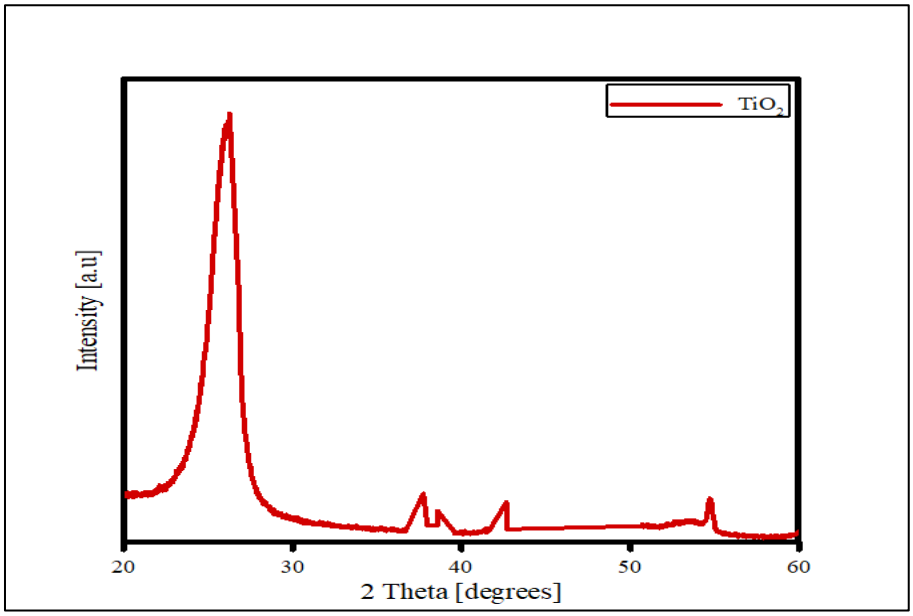

Figure 4.8. XRD test result for TiO_2 nanomaterial.

4.2. PERMANENT STABİLİTY

4.2.1. Chemically Modifying MWCNTs (CF-MWCNTs)

The UV-Vis absorbance spectra of water nanofluids containing different amounts of nanoparticles (0.02, 0.05, 0.08, and 0.1 wt%). The spectral area between 270 and 290 nm was discovered to contain a distinct absorption peak. When the C = C double bonds in MWCNTs undergo the $(\pi \rightarrow \pi^*)$ transition, a very sharp point appears at about 275 nm (Pan *et al.,* 2010). With the growing particle loading of nanofluids, it is seen that peak intensity primarily improves, which is in good accordance with the traditional Beer-Lambert law (Amiri 2015).

Regardless of the particle concentrations, which produced about 76, 79, 81 and 84% against the weight of the nanoparticle concentrations (0.02, 0.05, 0.08, and 0.1) by weight, CF-MWCNTs, respectively, the volume of sediment formed in the nanofluids after a period of thirty days was relatively small. The optimal conditions for MWCNTs/water nanofluids dispersion have been tested with numerous parameters, including the types of surfactants (CTAB, SDS and TritonX-100) and the probe sonication duration (15, 30 and 60). Figure 4.13 displays the results from an investigation into P-MWCNTs and NCF-MWCNTs distributed in distilled water with various molecular mass loadings (d-i). That was observed that all samples exhibit a decreasing tendency in the visible absorption of ultraviolet light, as depicted in Figure 4.9. sample recruitment (NCF-MWCNTs and CF-MWCNTs) is necessary to produce more steady MWCNTs nanofluids because P-MWCNTs cannot disperse to maintain the height under a specific range of ultrasound times. This research discovered that the sonication process probe works best when given 60 minutes to prepare nanofluids. According to Fig. 4.9, the Tw80 sample with stable MWCNTs demonstrated greater dispersion stability than the other samples when sonication was applied for 60 minutes over the same number of days (f). In contrast to other tested ratios, Figure 4.9 (e) demonstrates that 1:1 (MWCNTs: SDS) is the best mixing formula for a stable nanofluid suspension. For various weight concentrations, the quantitative UV-Vis pattern (Fig. 4.9(b)) provides a clear image of the long-term stability of CF-MWCNTs. The stability of CF-MWCNTs deteriorated over time, but

the effect on the proportion of nanofluidic materials was minimal. Contrarily, after 24 hours, CF-MWCNTs exhibit preferred dispersion and stability in distilled water (Fig. 4.9k).

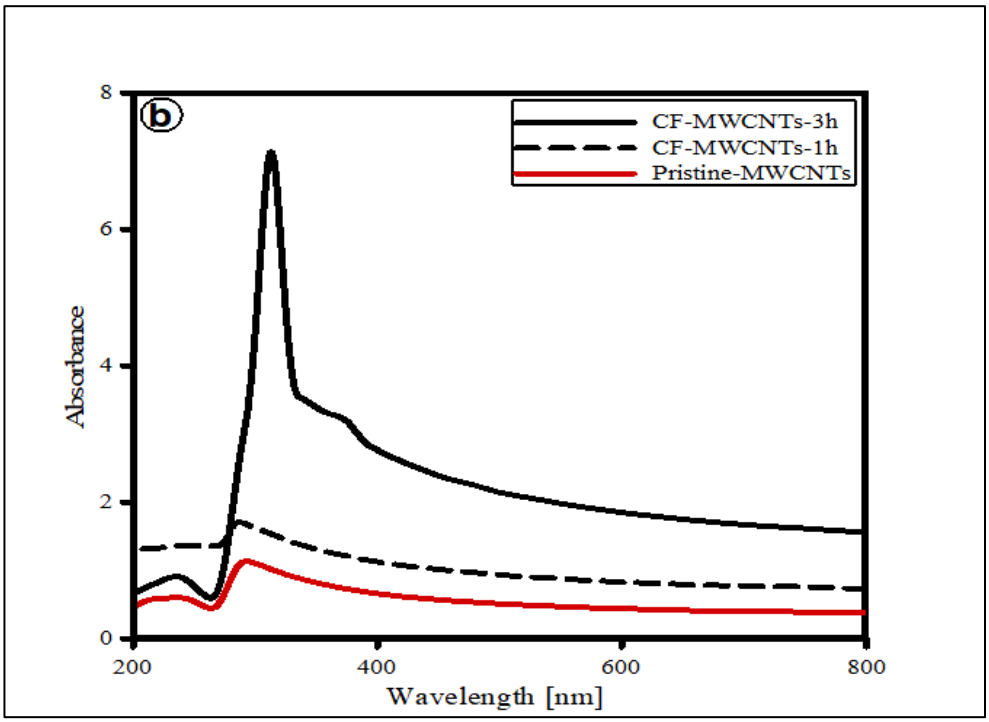

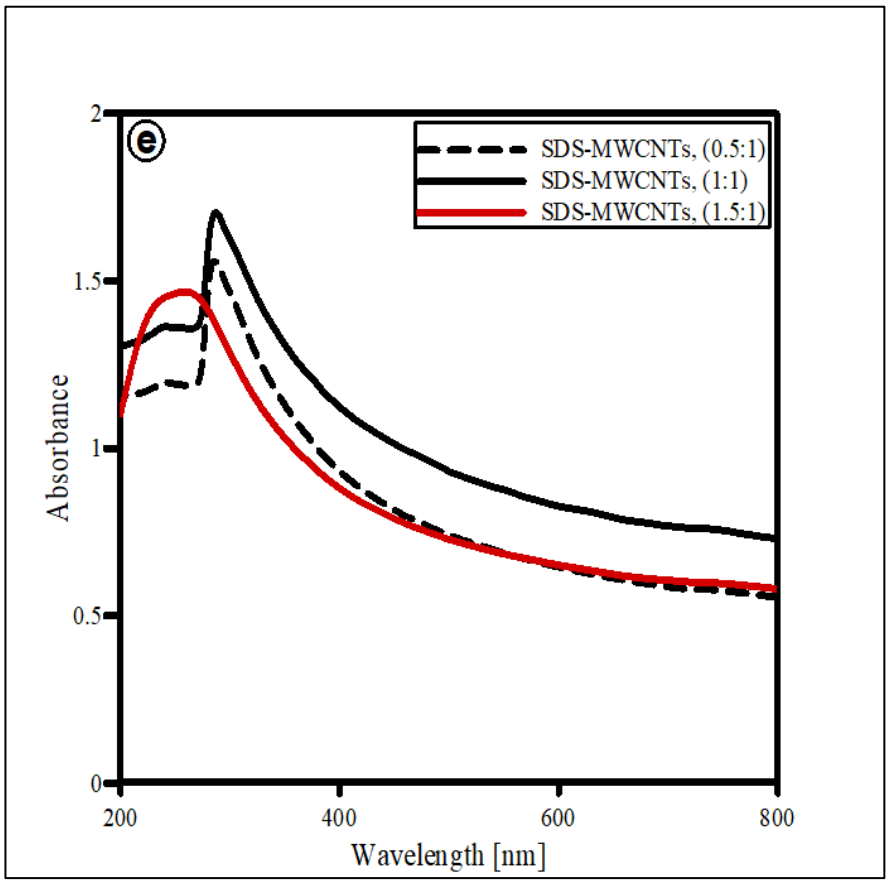

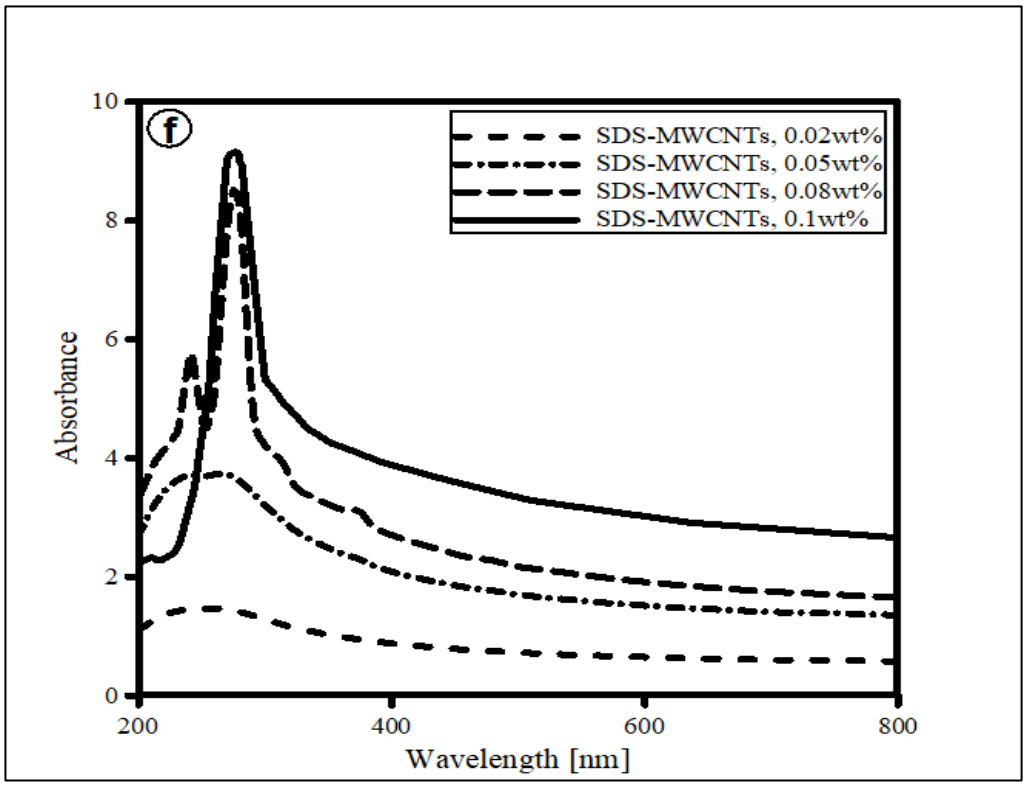
f
SDS-MWCNTs, 0.02wt%
SDS-MWCNTs, 0.05wt%
SDS-MWCNTs, 0.08wt%
SDS-MWCNTs, 0.1wt%
Absorbance
Wavelength [nm]
0
2
4
6
8
10
200
400
600
800

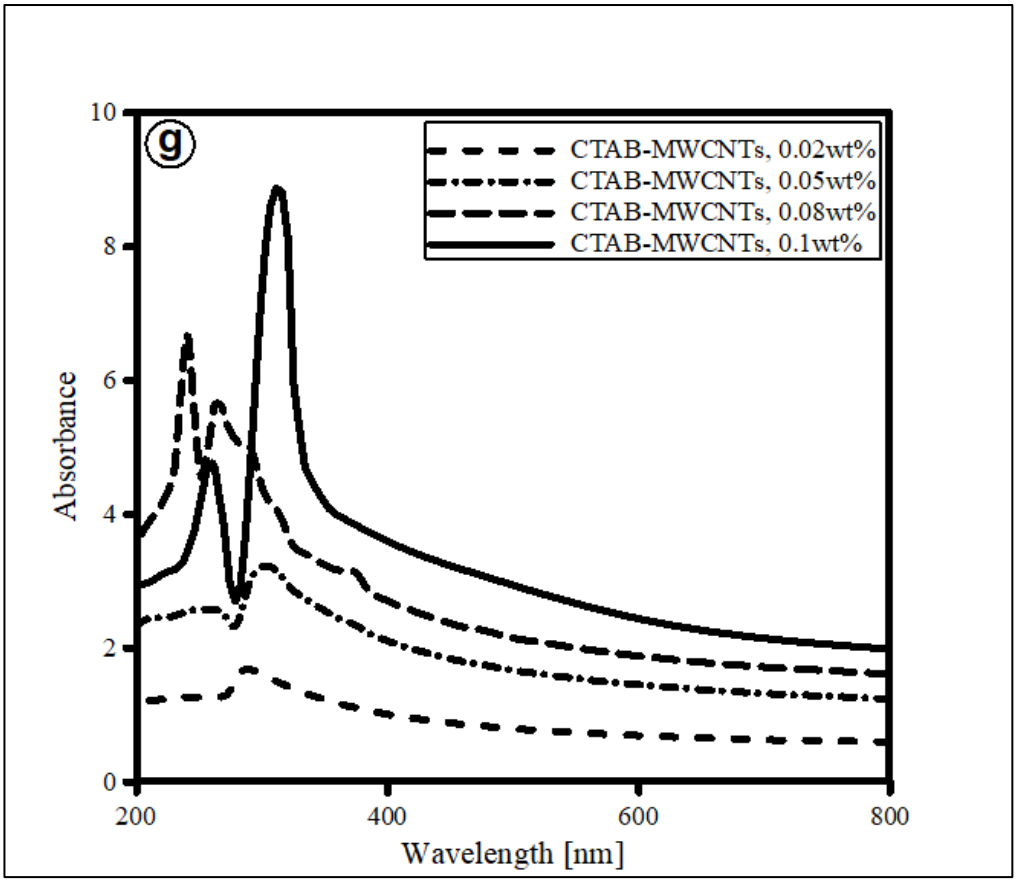
g
CTAB-MWCNTs, 0.02wt%
CTAB-MWCNTs, 0.05wt%
CTAB-MWCNTs, 0.08wt%
CTAB-MWCNTs, 0.1wt%
Absorbance
Wavelength [nm]
0
2
4
6
8
10
200
400
600
800

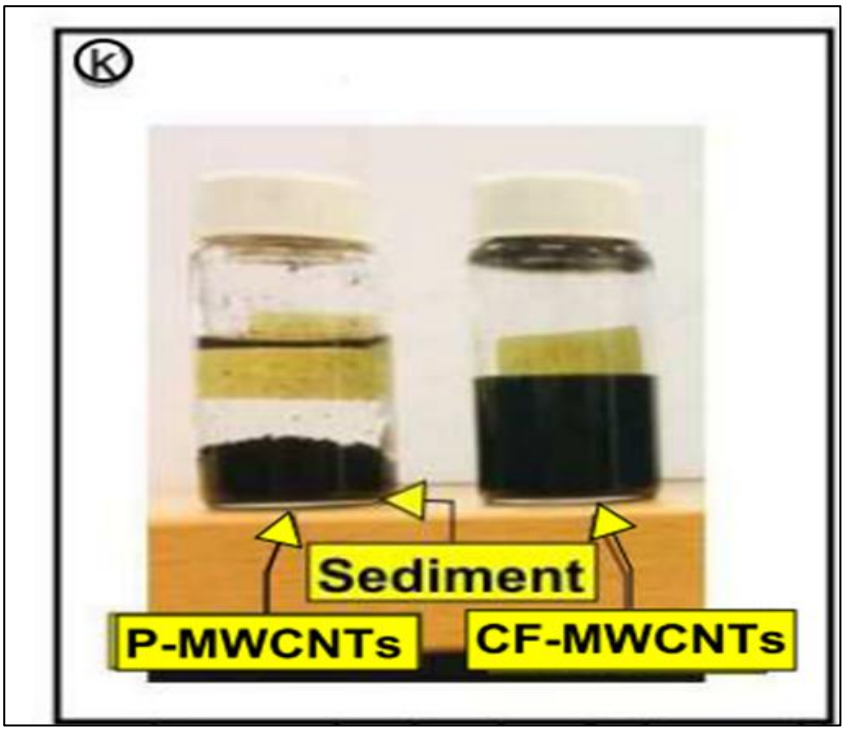

Figure 4.9. Differences between UV and (b) P-MWCNT nanofluids and CF-MWCNT nanofluids (e) SDS-MWCNT nanofluids, carried out at various sonication periods and surfactant ratios (f) MWCNT nanofluids, with Loading many particles and types of surfactants with a time of (60) minutes. Ultrasound instrument. (g) Over the course of thirty days, the relative particle accumulation of CF-MWCNTs. (k) Images of the P-MWCNTs & CF-MWCNTs after 24 hours of being dissolved in the working solution (distilled water).

4.2.2. Aluminium Oxide (Al_2O_3)

Displays the visible and ultraviolet absorption spectroscopy of Al_2O_3 nanofluids based on distilled water working fluid with multiple weight ratios (0.1% wt). A potent and distinct absorption peak was found in the wavelength region for all samples. 260–280 nm. It reached its maximum at 272 nm, which is attributed to Al_2O_3, as mentioned in the previous literature. An increase in particle concentration leads to an increase in the intensity of the peak, which obeys the Beer-Lambert law.

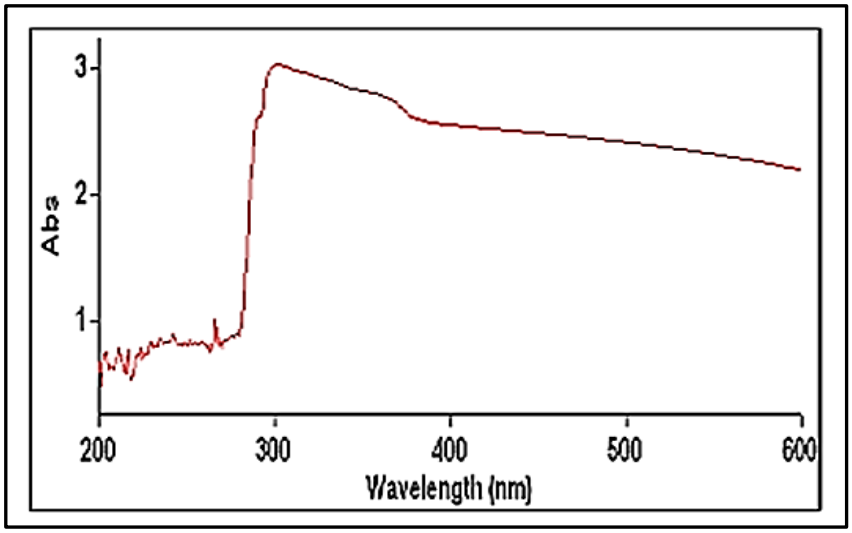

Figure 4.10. Different molecular amounts of Al_2O_3 nanofluids' UV-vis absorption spectra (Mukesh *et al.,* 2020).

4.2.3. Titanium Dioxide (TiO_2)

Based on the working fluid, displays the spectroscopy, visible and ultraviolet absorbance spectroscopy of TiO_2 nanofluids. (DW).At different mass-to-weight ratios (0.1 wt%) of nanoparticles. Two distinct peaks were recorded at two wavelengths 240 and 350 nm, and these values were consistent with prior literature. (Li *et al.,* 2018). Due to a rise in the concentration of nanoparticles that adhered to the Beer-Lambert law, the peak intensity increased ,this is illustrated in Figure 4.10.

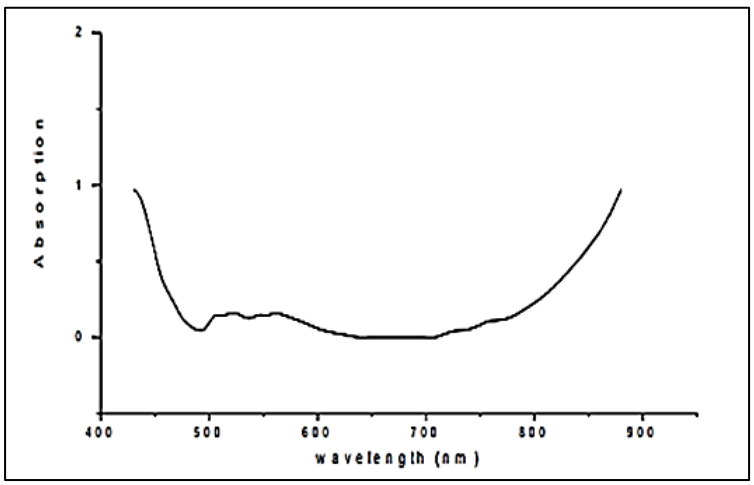

Figure 4.11. TiO_2 nanofluids' UV-vis absorbance spectra at various molecular concentrations (ALAGAPPAN *et al.,* 2015).

4.3. THERMAL AND RHEOLOGİCAL CHARACTERİSTİCS

4.3.1. Dynamic Viscosity

4.3.1.1. Viscosity and MWCNT Optimization

Viscosity readings using a rotating viscometer showed high NIST compliance. The viscosity values for CF-MWCNTs / DW as a function of weight concentration is shown in Figure 4.12(b) and were obtained at constant shear rates of 200/sec and between 20 and 60 °C. As a result of the large extensions of the internal fluid shear stress, the findings demonstrated that viscosity is directly proportional to concentrations and thus rises with an increase in the weight of the nanofluid concentration. (Nguyen 2007). Also, the viscosity is inversely proportional to the temperature, as the high temperature rapidly decreased the viscosity. This refers to the decrease in the bonding forces between particles. In comparison to the base fluid, the viscosity rose by about 27% at 0.1 wt% and 60 °C. Because of the influence of the surfactant-MWCNTs, as seen in Fig. 4.12(c), the NCF-MWCNTs nanofluid had a greater viscosity than the CF-MWCNTs nanofluids at 0.1 wt%. This is the primary justification for why nanofluids increase viscosity values when surfactants are present (SDS, CTAB, Tw-100, Tw-80).

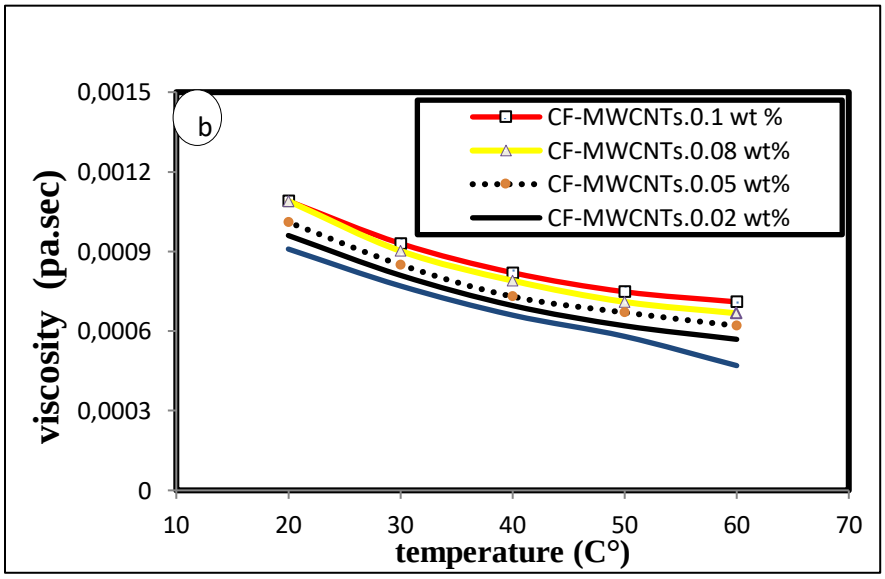

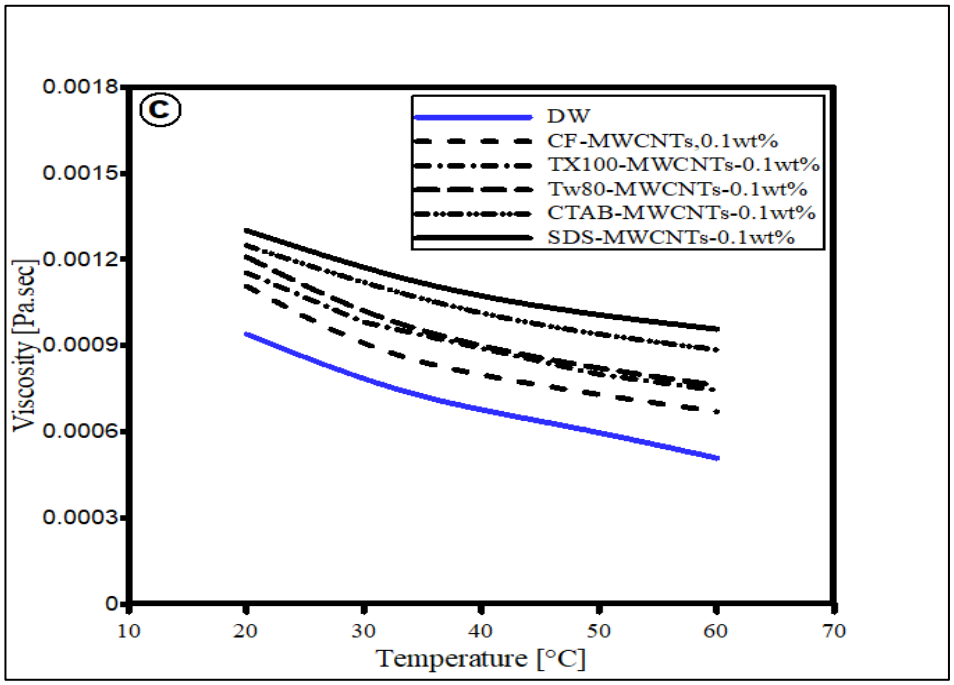

Figure 4.12. Viscosity versus temperature for (b,c) water nanofluids based on CF-MWCNTs and NCF-MWCNTs .

4.3.2. Thermal of Conductivity

4.3.2.1. MWCNTs Thermal Conductivity and Optimization

The thermal conductivity data for nanofluids (CF-MWCNTs and NCF-MWCNTs) at various temperatures and for various weight loadings of nanoparticles (0.02, 0.05, 0.08, and 0.1 wt%) are shown in Figure 4.13(a-c). To ensure the accuracy of the distilled water weight thermal conductivity measurements, the temperature range was 20–60 °C. The collected data and the National Institute of Technology and Standards (NIST) data are in good agreement . It was found that the average thermal conductivity mistake was ±1.172%, which is within the permitted measurement tolerances. As shown in Fig. 4.13(b-c), the heat conductivity of CF-MWCNTs nanofluid is greater than that of basic liquid (distilled water) and nanofluid NCF-MWCNTs.(b-c). If the CF-MWCNT ratios are optimized, water-based nanofluids will transfer heat more effectively. It is also attributed to the Brownian motion of the suspended particles caused by an increase in thermal conductivity owing to

temperature rise. (Jha *et al.*, 2008). Carbon nanostructures are affected by Brownian motion and chemotherapeutic activation, whereas

surface nanostructures are employed in nanofluids to transmit thermal energy. Additionally, decreasing the nearby liquid layer are MWCNTs. Due to their appropriate thermal conductivity at low-weight loading, MWCNTs nanofluids can be used for medium-temperature The uniform MWCNT dispersion/friction in water readily causes the agglomeration between NPs to dissociate at high temperatures. By reducing the effective heat transfer area, the formation of layers near the surface of MWCNTs nanostructures can be made better. Non-covalent groups precipitating around the nanotube interfaces and sticking to them allow for this.

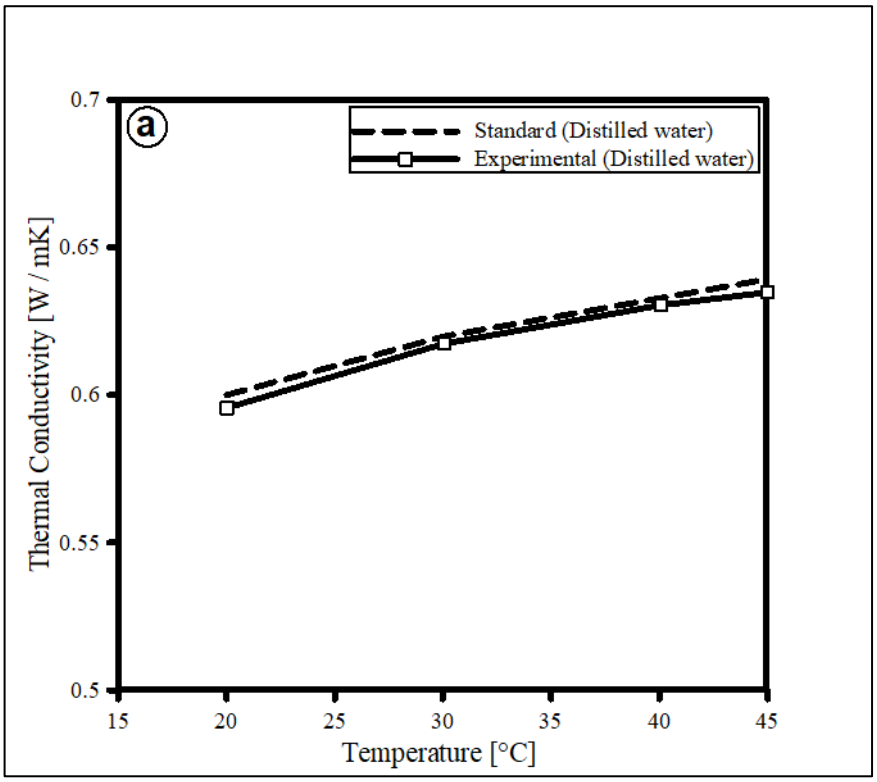

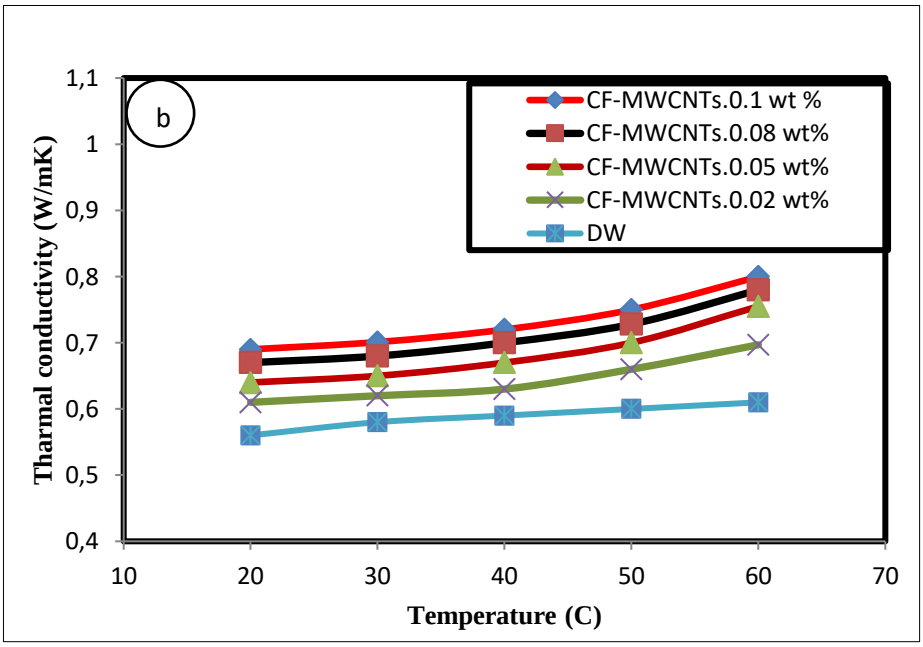

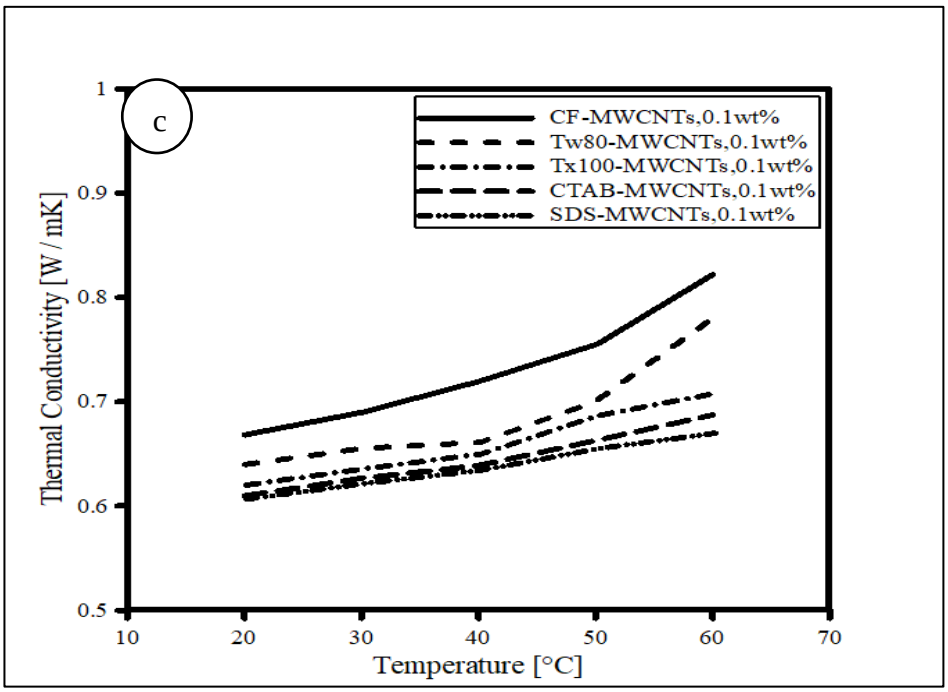

Figure 4.13. Thermal conductivity measurements; (a) Experimental data and NIST standard (Nguyen 2007), (b) CF-MWCNTs nanofluids for different weight loadings, (c) CF-MWCNTs and NCF-MWCNTs nanofluids with 0.1wt.

4.3.3. Density and Specific Heat Capacity, Section

4.3.3.1. Density and Optimization of CF-MWCNTs

Figure D1 shows that by (Arnold *et al*.,2002), the density meter had been calibrated with distilled water, and the recorded data had been compared to reference values. It was demonstrated that the instrument is appropriate for measuring the density of nanofluid by verifying the estimated margin of error of 2.3%.

Figure 4.14 displays the results of density tests performed on the basic liquid and CF-MWCNT/water suspensions at various temperatures. With a rise in liquid temperature, there is a sudden drop in the density of the CF-MWCNTs / DW nanofluids that the liquid's thermal expansion may cause. Further loading of the nanoparticles also results in a small rise in the density of the suspension. This rise in density may be related to the inherent density of CF-MWCNTs. As a result, the nanofluid's high-density value in relation to the base fluid was achieved. For loads of 0.1 wt% at 20 °C, the CF-MWCNTs-DW nanofluid's maximum density rise was approximately 0.08%. On the other hand, the population declines by about 0.6% when the temperature increases from 20-60 °C for the same particle concentration.

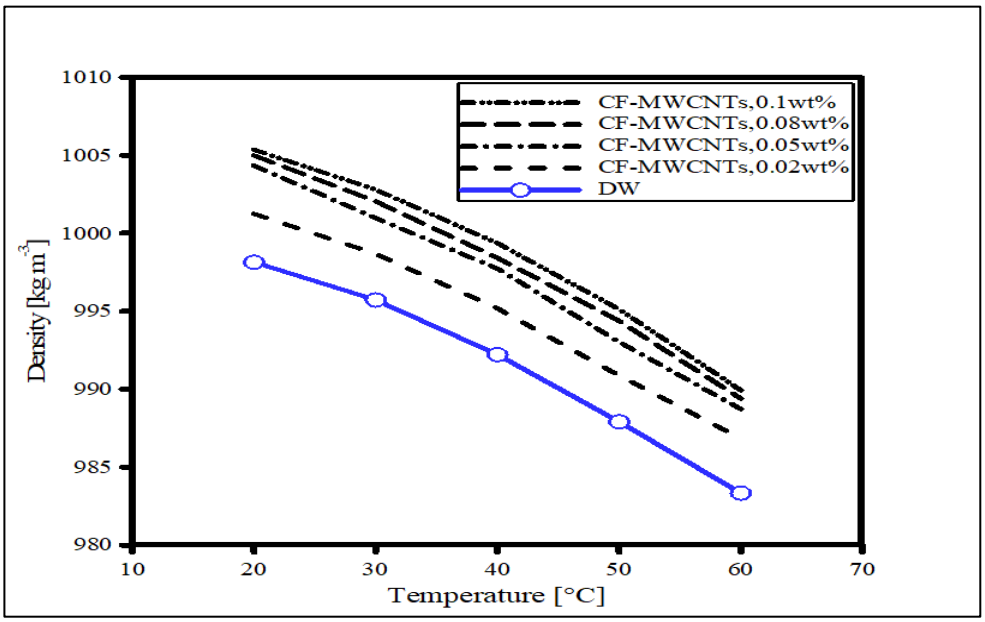

Figure 4.14. CF-MWCNTs/water and water densities at various weight percentages.

4.3.3.2. CF-MWCNTs' Specific Heat Capacity and Optimization

Comparison of the specific thermal readings of distilled water taken at various temperatures with the standard values gathered by (Arnold *et al.*,2002). It was concluded that DSC is accurate when determining the specific heat of nanofluidic samples after discovering a maximum discrepancy of 2.6%. The specific heat capacity of CF-MWCNTs nanofluids is shown in Figure (4.15) as a function of temperature and particle content. In comparison to the results for DW, all nanofluids displayed a reduced specific heat capacity. As the weight of the nanoparticles is raised, the specific heat capacity also rises. The nanofluid experienced a 4% and 11% heat increase, respectively, for nanoparticle concentrations of 0.05 and 0.1 wt%, respectively, and at 60 °C. In previous studies that had produced disparate results, researchers claimed that adding nanoparticles increased the specific heat capacity. The unique heat capacity component of both the base liquid and the nanoparticles boosted the heating capacity of the nanofluids in addition to the increase in the interfacial free energy of the liquid-solid interface caused by the varying loading of the nanoparticles. Surface free energy's positive effects on a material's thermal performance in nanocomposite materials are provided by the bigger surface area of the nanoparticles.

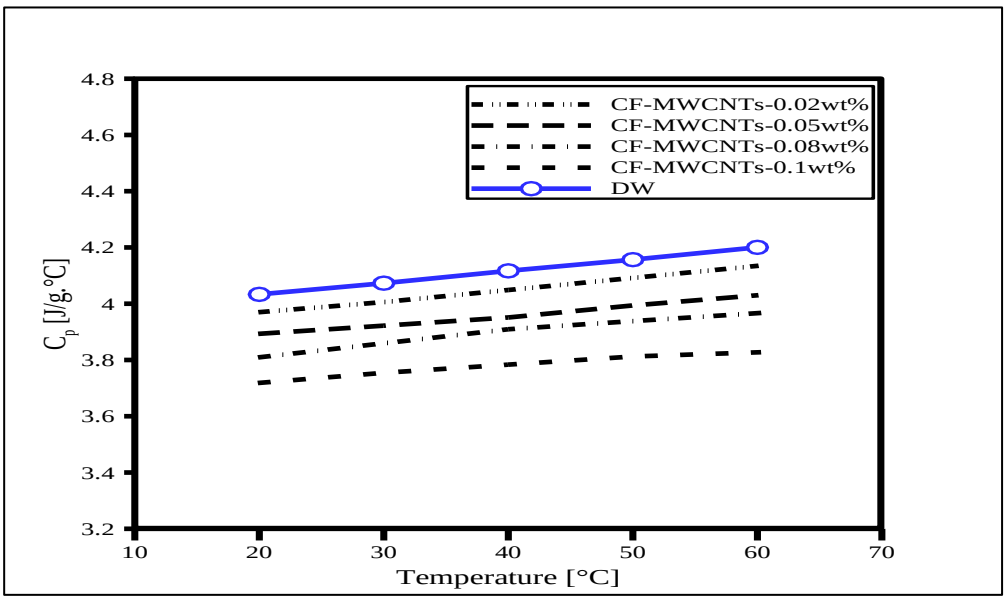

Figure 4.15. Specific heat of CF-MWCNTs nanofluid at different concentrations versus temperature

Table 4.1. Comparison between experimentally meaured thermal conductivities and the previous exp. works on water-based nanofluids.

Researcher	Particles type	Base Fluid	Particles Concentration	T.C Enhancement	Notes
Yarmand *et al*., 2016	GNPs 500	H_2O	0.1 wt %	15.87 %	Temperature effect
Mehrali *et al*., 2014	GNPs 750	H_2O	0.1 wt %	25 %	Temperature effect
Sarsam *et al*., 2016	TEA-GNPs, SSA of 300, 500 and 750	H_2O	0.1 wt %	11% (750), 9% (500), 7% (300)	Temperature effect
Arzani *et al*., 2016	MWCNT	H_2O	0.1 wt %	17.6 %	Temperature effect
Yarmand *et al*., 2016	GNP–Pt	H_2O	0.1 wt %	29.6 %	Temperature effect
Amiri *et al*., 2012	MWCNT-Ag	H_2O	0.1 wt %	34.3 %	Temperature effect
Chandrasekar *et al*., 2010	Al_2O_3/43 nm	H_2O	(0.33–5) vol%.	9.7% was observed for 3 vol%	Temperature effect
Saleh *et al*., 2014	TiO_2/33 nm	H_2O	(0–5) vol%.	5% for vol% of 5%	Temperature effect
Present study	MWCNTs,	H_2O	0.1 wt %	32.4% MWCNTs	Temperature effect

4.4. THERMAL PERFORMANCE OF FPSC AND NUMERİCAL METHOD EVALUATİON

Different working fluids were used in the numerical results to verify the modeling methodology and measured outcomes (distilled water and water-based nanofluids). The modeling and measurement results that were obtained for each instance were compared. Thermal Performance using water as the working fluid.

4.4.1. Thermal performance during water run

The test rig was put together at the University Teknologi PETRONAS (MALAYSIA) Solar Thermal Advanced Research Centre [STARC] solar facility, which is situated 32 meters above sea level at 101 degrees east longitude and 4.38 degrees north latitude. Operating under laminar conjugated mixed-convection heat transfer is a solar FPC angled at a 10° angle. Between March and September 2019, from 8 a.m. to 5 p.m. on sunny days with an average wind speed of 2 m/s, tests incorporating FPSC and DW were conducted. Thermo-Anemometer and Tenmars solar power meters were used to measure the sun radiation.

The test was carried out on a 3D FPSC model with a tilt angle of 10° numerically using several different hybrid nanofluids, different nanomaterials and different concentrations of nanoparticles. As mentioned above, the thermophysical properties of the hybrid nanofluids and H2O were collected from a literature review at the inlet temperature of 293 K (Sarsam *et al*., 2022; Vatani & Mohammed, 2013). The present model makes the following assumptions: flow invariance, Newtonian flow, de Sondergouin monophasic nanophase flow, and islamina flow, solar radiation. Meanwhile, the non-slip and temperature boundary conditions were applied in the present simulation cases. Moreover, gravity was activated at $-9.81\ m/s^2$ in the direction normal to the y-axis.

This study examined the variance in solar radiation, fluid temperatures at the collector's inlet and exit, and ambient air temperature for the scenario where rainwater serves as the working fluid (Gt). The figure displays average Gt, Ta, Ti,

and Tout measurements obtained in clear circumstances. The system's thermal performance was predicted under steady-state circumstances, ignoring the transient effect. Up until solar noon (about 13 hours), there is an increase in solar radiation;

After that, there is a decline. The temperature rose due to the rising outside temperature and the water in the climbing tubes absorbing radiation heat when both the solar energy, the fluid outlet temperature, and the ambient air temperature decreased.

The experimental findings with a maximum temperature of 66.2 °C and the numerical prediction of the outlet temperature profile with a maximum of 64 °C demonstrated good agreement.

Due to the oversimplified assumptions in heat transfer (Tout) computations, the model (Tout, Num) will overestimate the fluid's actual temperature at the collector's outlet as driving force . the temperature difference between the ambient air and the inlet of the collector, along with the useful heat energy (Qu) absorbed by the collector. Since the radiation falling on the collector greatly affects it, thermal energy moves like solar radiation. Although the maximum error of the model was only about 5.2%, it could not accurately match the numerical values from the experiments and the real values measured by the compound. show this in the fig (4.16), Fig. (4.17)

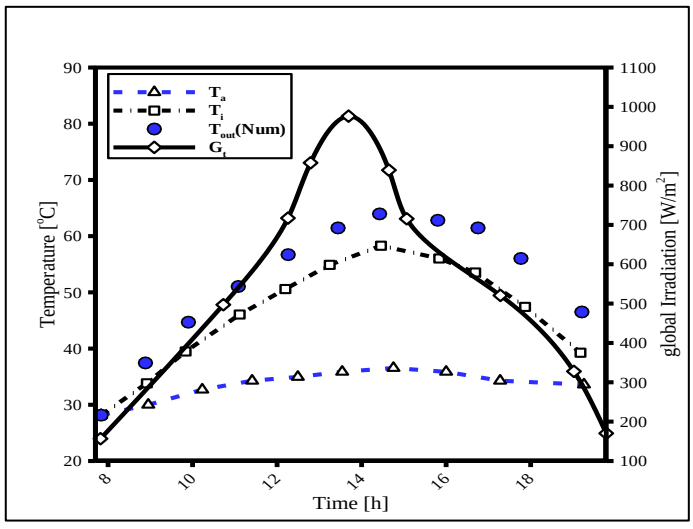

Figure 4.16. Collector temperatures and radiation graphics for DW.

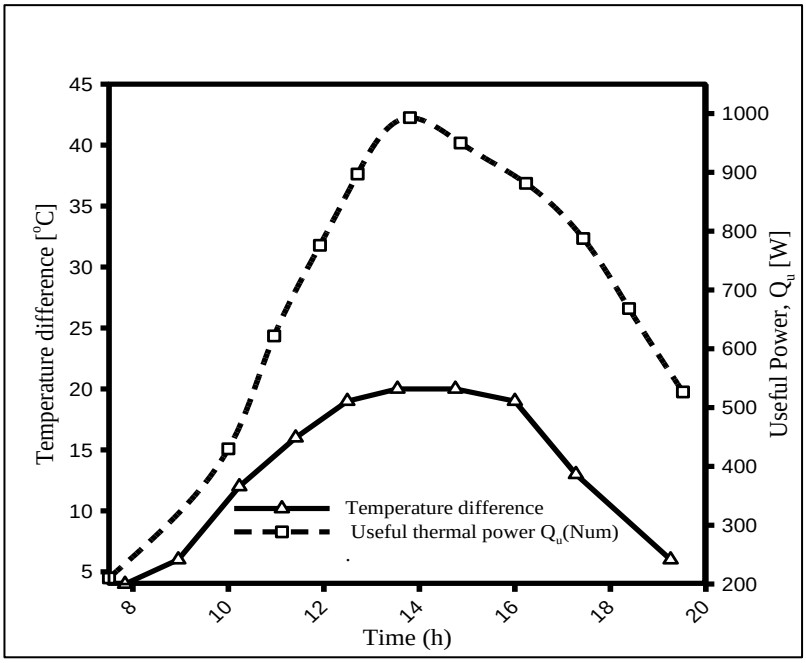

Figure 4.17. Comparison of the usable thermal power variations versus temperature differential from experimental and numerical data.

Using numerical data pertaining to the volume flow rate for different fluid inlet temperatures, the collector efficiency of the FPSC was evaluatedThe numerical results may be used for the study because of the findings' minimal maximum error of 4.6% , as seen in Figure (4.18).

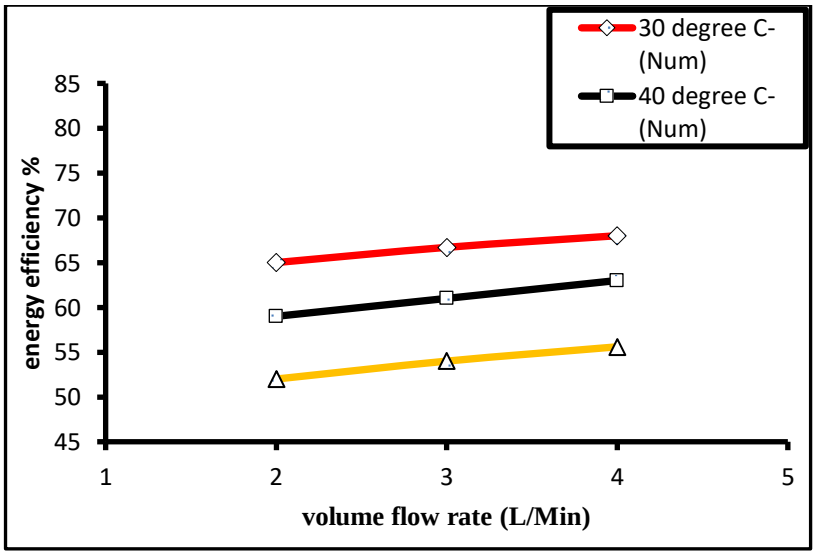

Figure 4.18. Calculated efficiency numbers for the FPSC versus volume flow rate at various inlet fluid temperatures.

Because it affects how well a flat plate solar collector performs and how much energy is used for pumping, the pressure drop across the collector must be carefully assessed. The observed pressure drop variation is displayed using a differential pressure transducer and at different volume flow rates.

Pressure drop values calculated numerically (pNum) were displayed side by side and contrasted with the manufacturer's data (pm_{fr}), corresponding in the same way as the digital data from the manufacturer. The model understates the pressure loss across the accumulator because it ignores some flow paths and connections where there is a pressure decline that cannot be precisely predicted by theory. However, the importance of using the numerical findings for the analysis is determined by how well the data agree with one another, as shown in Fig.(4.19).

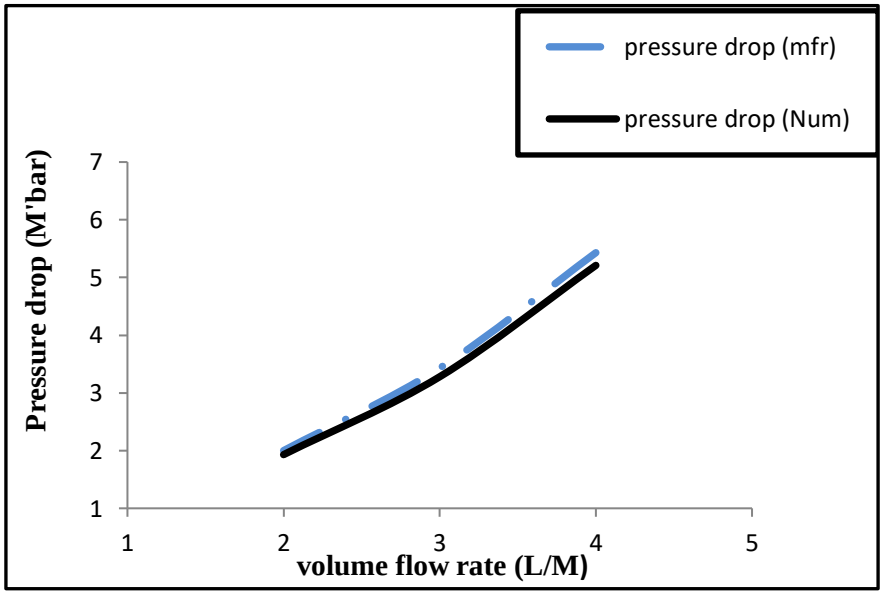

Figure 4.19. Manufacturer statistics on pressure drop and numerical comparisons with various volume rates.

4.4.2. Thermal Performance Using Nanofluids

Numerical analysis determined the impact of nanofluids (CF-MWCNTs) and purified water on the collector's effectiveness. To acquire data and characteristic curves in both the instances of water flow and nanofluids, the study was carried out

numerically over the course of several days with the solar atmosphere. To evaluate the outcomes, the pertinent scalar curves were also shown.

The volume flow rate for 0.1 wt% nanofluids at various inlet fluid temperatures, along with the estimated FPSC efficiency values obtained from numerical techniques. Like distilled water, efficiency rose with volume flow rate and fell with fluid intake temperature, is shown in Figure 4.20.

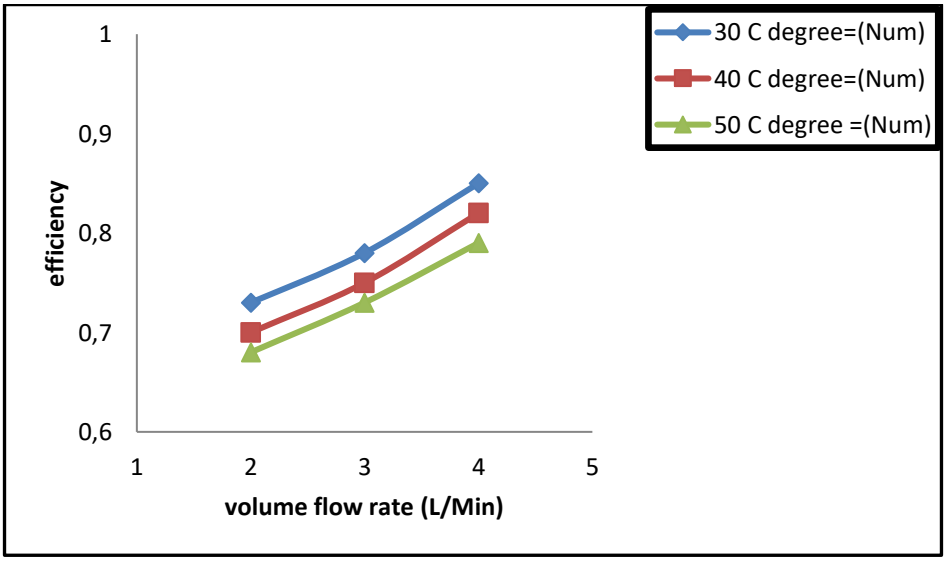

Figure 4.20. Calculated values of the energy efficiency of the FPSC as a function of volume flow rate for 0.1 weight percent of nanofluids at different inlet fluid temperatures

For different fluid nanoparticle weight loads, the numerical values of FPSC effectiveness versus volume flow rate. The effectiveness rises with higher weight percentages of nanofluids and falls with lower volume flow rates of the liquid at 30 °C and 930 W/m^2. Trends in nanofluids have a lot in common with purified water, as shown in Fig. (4.21)

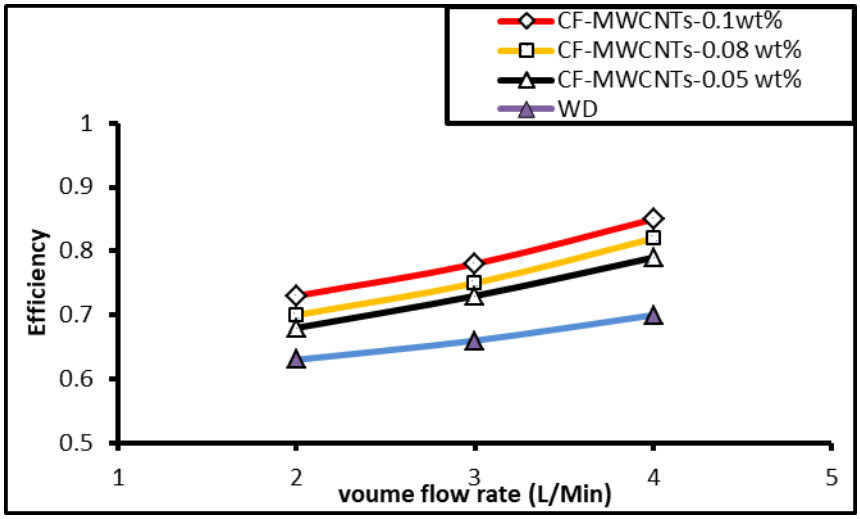

Figure 4.21. Calculated values of the energy efficiency of the FPSC for various weight concentrations of nanofluids at 30 oC and 930 W/m2.

4.4.2.1. Working Fluid with Nanofluid

Checks and calculations were performed on the solar collector using flow rates of 2, 3 and 4 LPM. Semi-constant experimental data were based on the efficiency of the collector against low temperature (Ti-Ta / Gt). Depending on the specific run setting for repeatability, this study considers only consistent experimental data. The collector variable efficiency of distilled water (DW) flow. The increased flow rate of nanofluids enhances the efficiency of FPSC. The neglected power component, FRUL, is reflected in the slope of the curve line in the data. It was discovered that there is a clear correlation between FR and fluid flow rate, with FR rising as the flow rate rises while FRUL stays constant. Therefore, by raising the flow rate of the absorbent fluid volume, FPSC efficiency can be improved. Table 4.2 lists the feature lines' junctions and slopes. The figure displays the FPSC's typical profile based on the ASHRAE standard for water as a working fluid, is shown in Fig. (4.22).

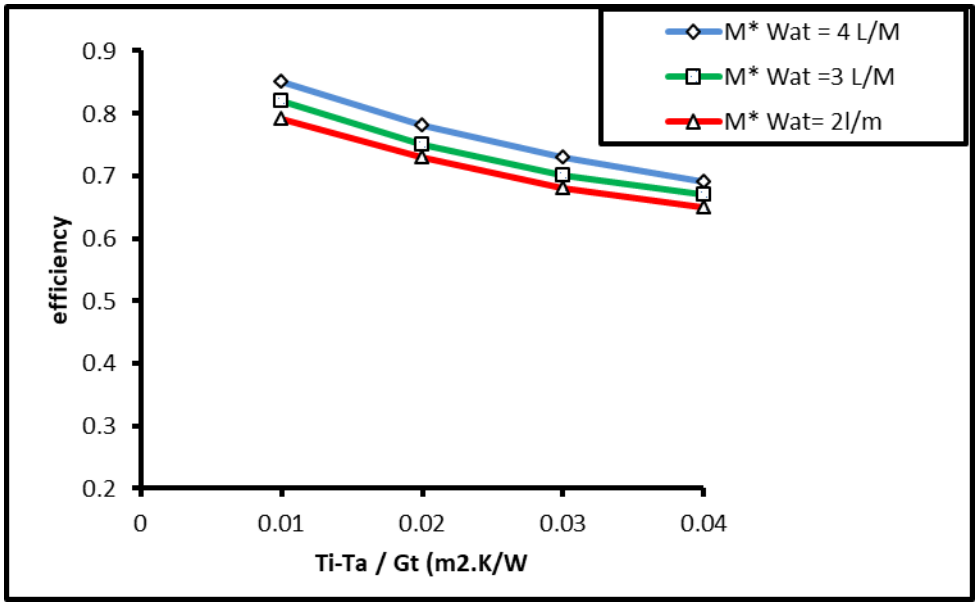

Figure 4.22. Variation in collector performance due to varying basic fluid volume flow rates

Table 4.2. Values for the base fluid at different volume flow rates for FRUL, FR, and R^2.

Working fluid (L/min)	**$F_R(\tau\alpha)$**	**$F_R U_L$**	**R^2**
Water @ 2 L/M (Num)	(0.6756)	(6.2805)	-
Water @ 3 L/M (Num)	(0.7159)	(6.8079)	-
Water @ 4 L/M (Num)	(0.7213)	(6.2416)	-

Figure 4.23 The graphics (a-b-c-d) show the relationship between low-temperature parameters and collector effectiveness for all nanofluids. The ruling relationship revealed by Eq, (3.6) determines the graphs' linearity. The effectiveness line is also shown in the numerical representation of a 4 LPM flow rate. It is correct that the intensity of the radiation also impacts the efficiency of the collector.

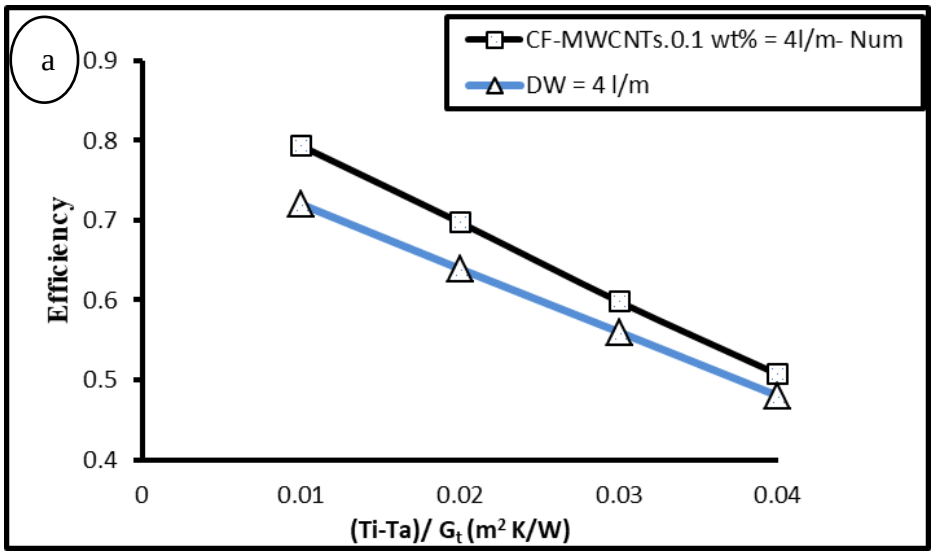
a
CF-MWCNTs.0.1 wt% = 4l/m- Num
DW = 4 l/m
Efficiency
0.9
0.8
0.7
0.6
0.5
0.4
0
0.01
0.02
0.03
0.04
(Ti-Ta)/ Gt (m2 K/W)

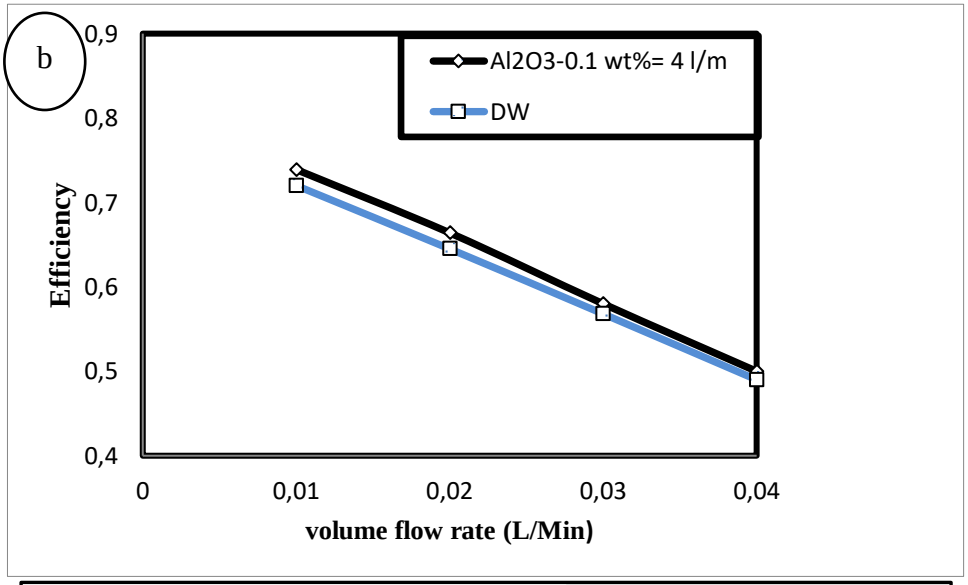
b
Al2O3-0.1 wt%= 4 l/m
DW
Efficiency
0,9
0,8
0,7
0,6
0,5
0,4
0
0,01
0,02
0,03
0,04
volume flow rate (L/Min)

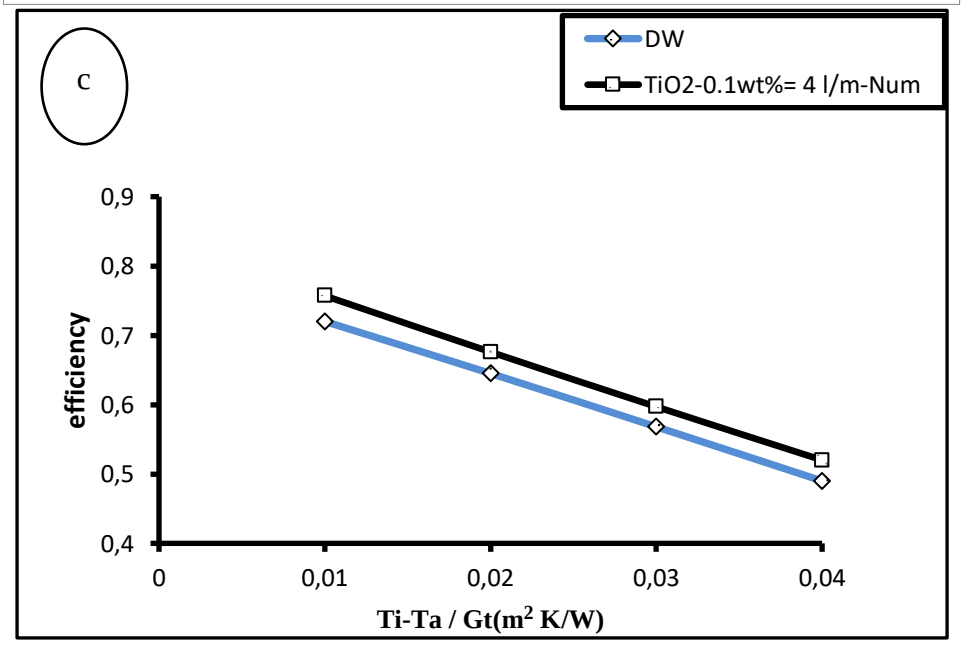
c
DW
TiO2-0.1wt%= 4 l/m-Num
efficiency
0,9
0,8
0,7
0,6
0,5
0,4
0
0,01
0,02
0,03
0,04
Ti-Ta / Gt(m2 K/W)

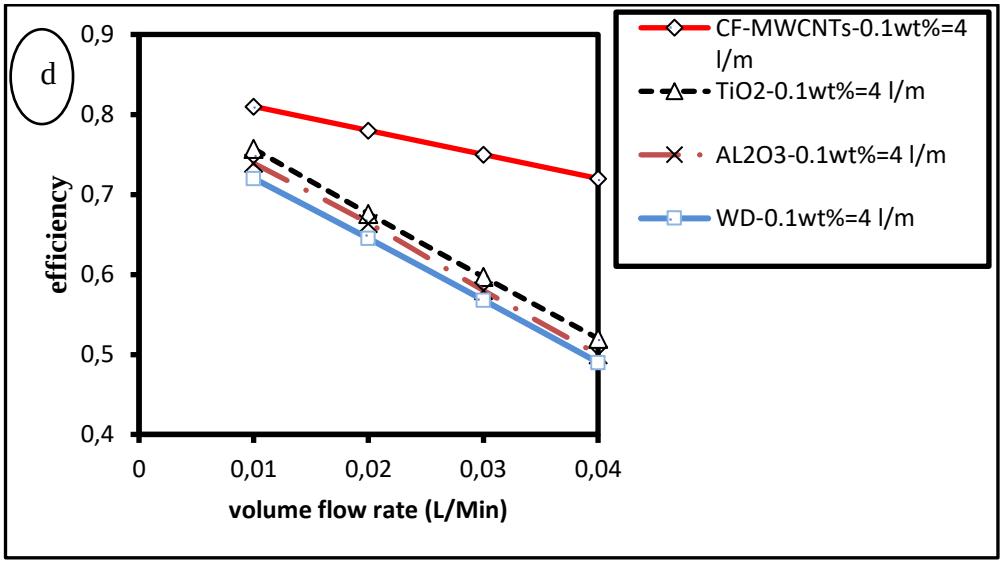

Figure 4.23. a) At 30°C, 930 W/m^2, and 0.1 weight percent (CF-MWCNTs/DW), the collector effectiveness is plotted against the reduced temperature parameter.b) At 30°C, 930 W/m^2, and 0.1 weight percent, collector effectiveness versus reduced temperature parameter (A_2lO_3/DW, c) At 30°C, 930 W/m^2, and 0.1 weight percent, collector effectiveness versus reduced temperature parameter (TiO_2/DW), d) Collector efficiency versus reduced temperature parameter at 30^{o}C and 930 W/m^2 and 0.1wt.%, (CF-MWCNTs, Al_2O_3, , TiO_2 and WD).

Figure 4.24 displays the thermal efficacy of CF-MWCNTs nanofluid at various flow rates and nanoparticle weight loadings. It makes sense that hybrid nanofluids have unique heat transfer properties because convection is one of the potential effects of energy transfer. A significant contributor to the improvement of thermal conductivity is the high thermal conductivity of the scattering and the ensuing Brownian motion of the particles. The efficiency is immediately correlated with the nanofluids' concentration and volumetric flow rate, as seen in the previous Figure 4.24. The highest solar collector efficiency was 82% at 4 litres per minute and 0.1 weight percent nanofluid.

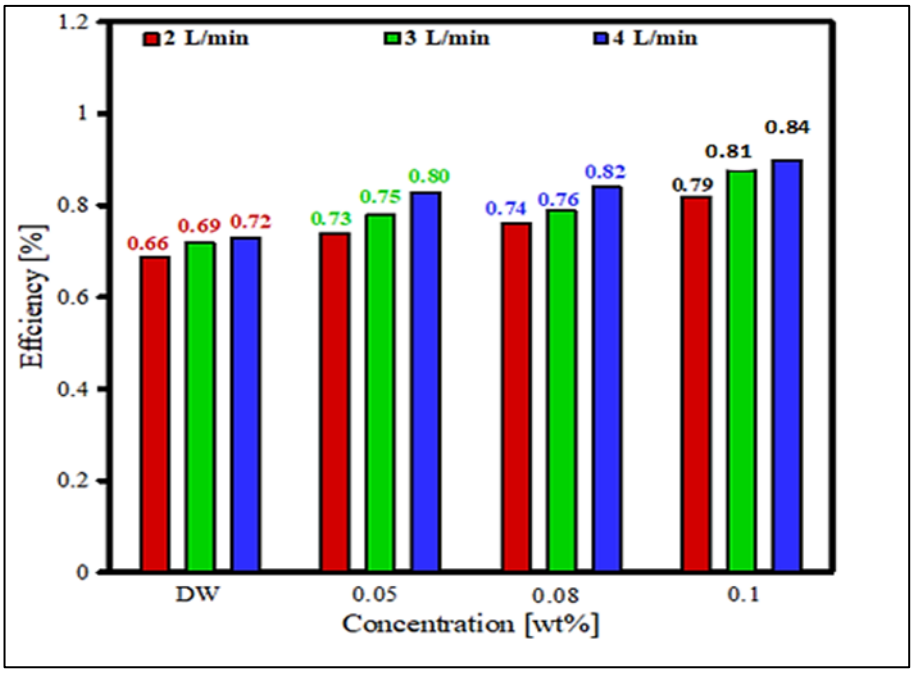

Figure 4.24. Thermal efficiency is influenced by volumetric flow rates and particle weight ratios.

The link between pressure drop and (CF-MWCNTs)/DW concentration is depicted in Figure 4.25. The pressure drop rises along with the weight percentage (wt%) of nanoparticles in the nanofluids inside the accumulator. The pressure drop numbers, however, are significant. Due to the small quantity of electricity needed to counteract this pressure drop, particularly for a concentration of low-weight nanoparticles of nanofluid, this figure is nonetheless regarded as negligible. It should be mentioned that the difference between pressure drop and pumping force for nanofluid with low weight concentration is very minimal.

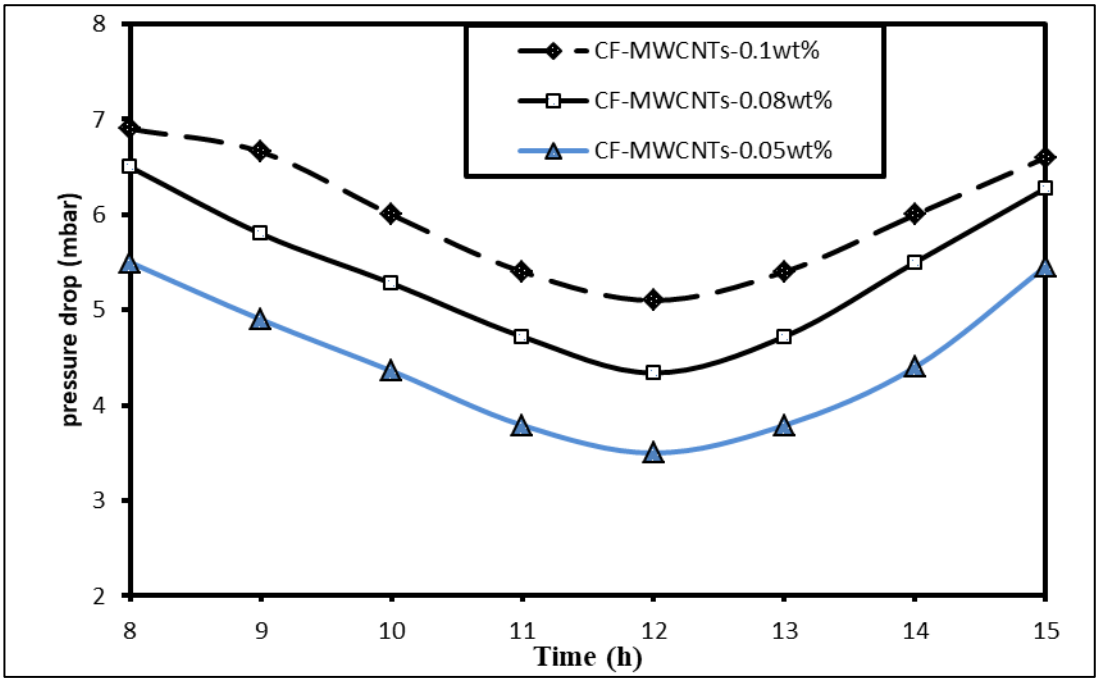

Figure 4.25. Effect of the concentrations of (CF-MWCNTs)/DW nanofluid on the pressure decrease inside the FPSC at 4 LPM.

The fluctuation of pressure drop and pumping force in a flat plate solar collector as a function of volume flow rate for various (CF-MWCNTs)/DW nanofluids is depicted in Figures (4.26) and (4.27). The volumetric flow rate rises linearly with the pressure drop value. For all nanofluids, the orientation of the increase is frequently the same. On the other hand, it was observed that the pressure drop is controlled by the second critical parameter, which is the density of the nanofluid. As was already stated, the density of the nanofluid rises in direct proportion to the concentration of nanoparticles. Because of this, friction process losses and density gradients are greater in nanoparticles with higher concentrations, but the pressure drop also rises. Distilled water (DW)/CF-MWCNTs cause a pressure decrease in comparison to various nanofluids. Viscosity is yet another element that influences pressure decrease. Despite being crucial for improving the high thermal transfer characteristics, these nanoclusters raise viscosity gradients. The flat plate solar collector's pressure decrease is caused by density gradients and frictional resistance effects. Figure 4.26 demonstrates that at high concentrations of nanoparticles by weight, the percentage of pressure drop rises with a rising volumetric flow rate. The maximum pressure drop for a nanofluid is 0.1 % wt percent, so the corresponding

pumping force is relatively large. When compared to water, the pumping power rises by 3.4, 5.8, and 6.2% for concentrations of 0.1 % wt percent nanofluid, correspondingly.

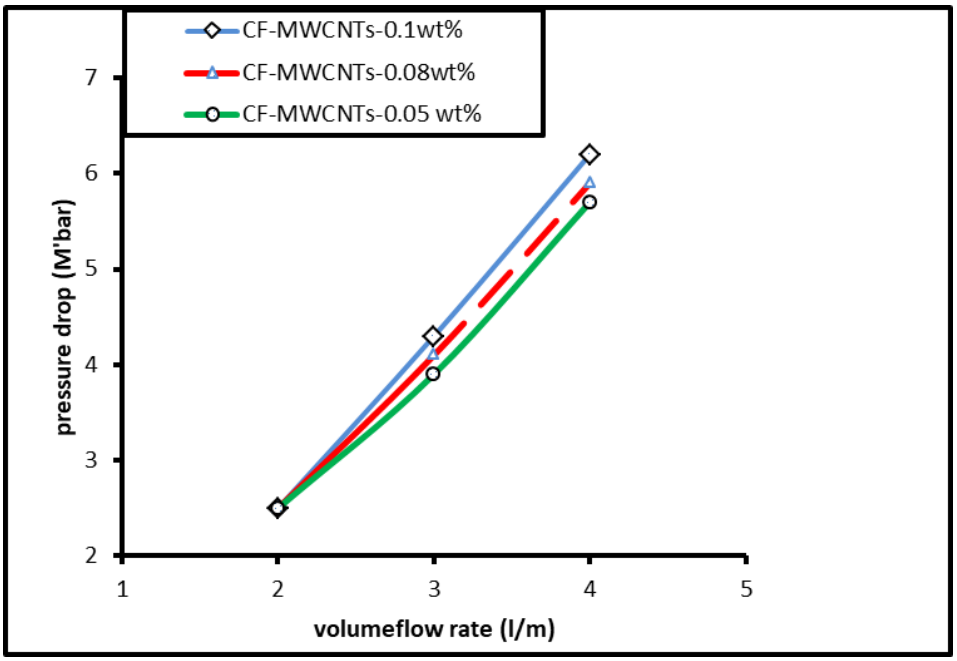

Figure 4.26. Volume flow rate verses pressure drop for FPSC using (CF-MWCNTs)/DW nanofluid at 30 oC and 930 W/m2.

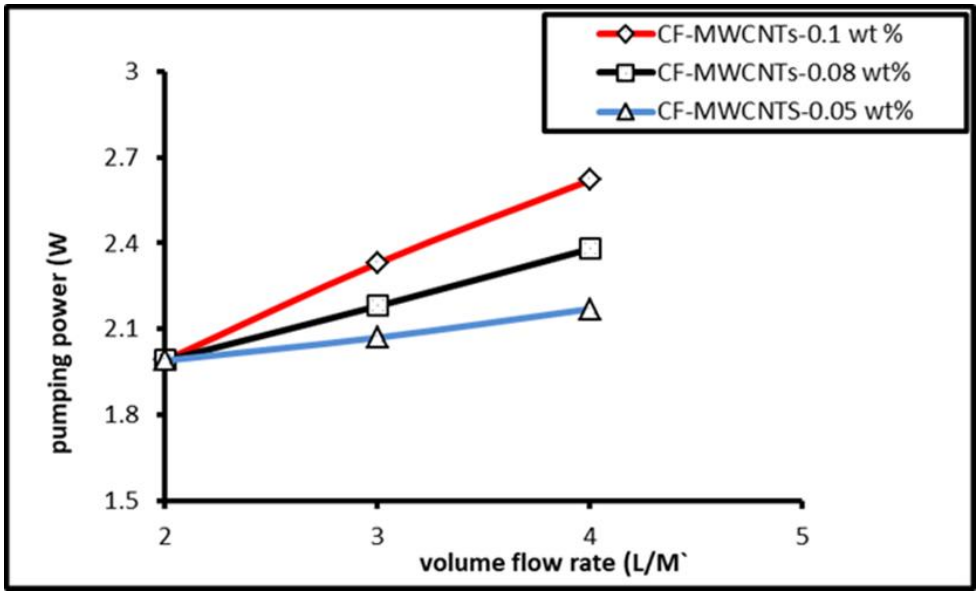

Figure 4.27. Pumping efficiency of FPSC with (CF-MWCNTs)/DW nanofluid at 30 oC and 930 W/m2 as a function of volume flow rate

The validity of the numerical analysis used to evaluate the thermal performance of a flat panel solar collector based on nanofluids was established by comparing the performance results. The increase in collector efficiency is due to a change in the flat solar collector's heat removal factor (FR) and heat loss factor (UL), which causes a shift in the Nusselt number and heat transfer coefficient. For various CF-MWCNTs/DW nanofluid concentrations (wt%) and volume flow rates under the specified conditions (inlet (T) of 30, 40, 50 and 60 °C, Gt of 930 W/m2), the changes were interpreted in Fig. 4.28 and 4.29.

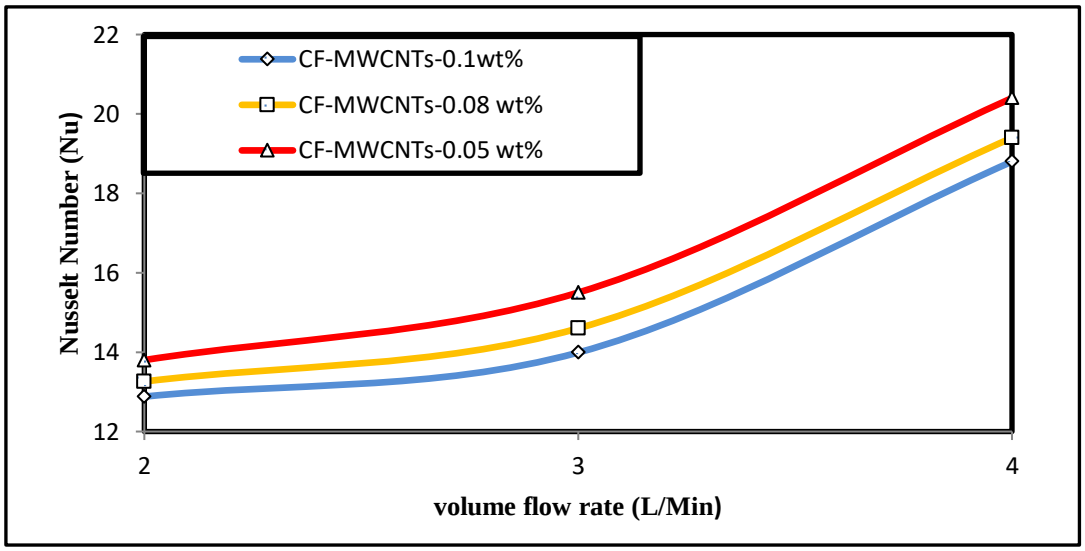

Figure 4.28. Nusselt number fluctuation at varying volume flow rates and weight concentrations

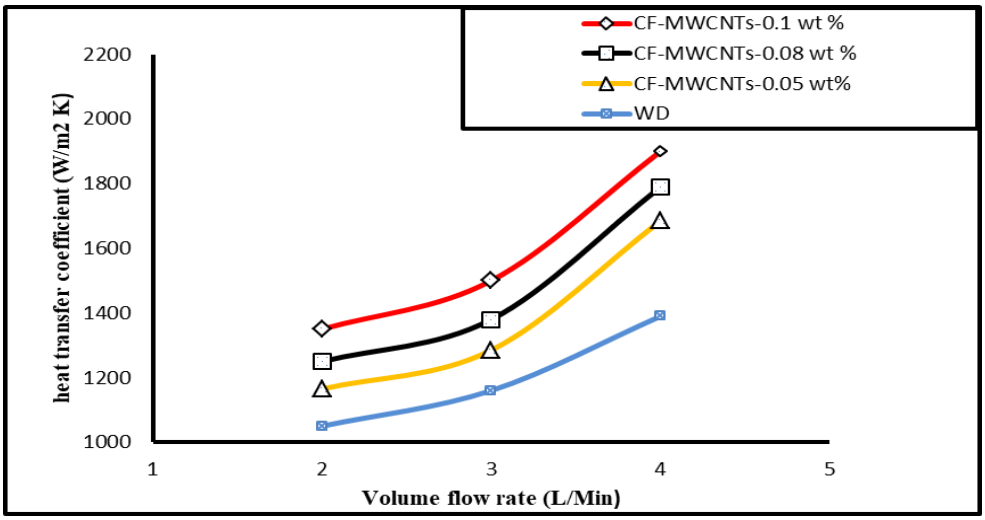

Figure 4.29. Variations in the heat transfer coefficient at varying weight concentrations and volume flow rates

4.5. SUMMARY

The numerical study research looked into how CF-MWCNTs/DW affected FPSC performance. Nanofluids requiring increased thermal conductivity of the nanofluid and the chemical activation process of MWCNTs have been used to create a uniform dispersion of MWCNTs. For the first time, acid treatment of virgin MWCNTs was used in this procedure to add carboxyl groups to the surfaces of the materials. Raman, XRD, FTIR, and EDX analyses demonstrate that (H_2SO_4 / HNO_3) treatment of MWCNTs can effectively modify and enhance the material's intrinsic properties without noticeably impairing the material's structural integrity. In fact, the chemical functionalization employed in this study effectively creates the necessary functional groups on the surface surfaces of MWCNTs while preserving their structural integrity. FESEM was used to conduct microscopic analysis on the nanofluid made with modified and unmodified MWCNTs. SDS surfactants demonstrated superior solid particle stabilization in DW as the base liquid. The ultrasonic agitation method used to activate the MWCNTs improved their excellent dispersion, which significantly enhanced the interfacial heat transfer between the nanofluid samples and the DW and was advantageous for increasing the nanofluid's thermal conductivity.

In order to quickly compare our optimized nanofluid with recent studies that have examined nano/micro-based fluids for comparable applications, I discovered that it would be essential to focus on the thermophysical and rheological properties of each. Examination of the thermophysical characteristics showed that fluids respond well to temperature and particle weight concentration increases. With a particle loading of 0.10 wt%, the nanofluid's thermal conductivity improved by 12% and 48% at 20 and 60 °C, respectively. Both CF-MWCNTs also had a higher specific heat capacity and were extremely sticky. In comparison to using the nanofluid with just one substance, FPSC performed better when using the nanofluid. When using 0.1 weight percent nanofluid, the system's thermal effeciency increased to 84 %, 16% higher than when using DW at a flow rate of 4 L/min. At 4 L/min and 0.1 wt% for the nanofluid, the greatest increases of (FR) and (FRUL) were 21.9% and 78.3%, respectively. The improvement of FR and FRUL for the base fluid at 4 L/min was 8% and 4%

compared to that recorded at 2 l/min. According to the comparative analysis, FPSC with nanofluid performs considerably better than single-particle nanofluid. In comparison to 0.02, 0.05, 0.08 and 0.1wt% nanofluids, the 0.1 wt% nanofluid operating FPSC system did better overall. Additionally, the numerical solutions suggested for a water-based nanofluid-powered collector using ANSYS software model the solar thermal efficiency with a respectable accuracy of 6.4%.

PART 5

CONCLUSIONS AND RECOMMENDATIONS

In this part, the main conclusions of the theoretical work are presented along with the author's observations and recommendations for further study.

5.1. CONCLUSİONS

This study of this research was to create high thermally conductive working fluids (DW) reinforced by carbon nanostructures (MWCNTs) of various concentrations in order to enhance the performance of solar heat collection systems. ANSYS-Fluent 18.1 was used to numerically verify the prepared nanofluids' properties using a real, conventional flat plate solar collector system (SWH/FPSC). It demonstrates that surface modification and dispersibility of the nano additives are crucial elements for more effectively absorbing the sun's heat source. The following inferences are drawn as a result:

1. In conclusion, chemically functionalized nanomaterials (CF-MWCNTs) in nanofluid samples demonstrated uniform dispersion with long-term stability (more than two months).
2. The emergence of peaks at 2850, 1650, 1383, and 1100 cm-1, which in CF-MWCNTs were separated by C-H bonds, C=O bonds, CO bonds, and CO-C bonds, respectively, served as confirmation of the functionalization.
3. To further understand the structure of MWCNTs, the morphology and surface degradation of functionalized samples were compared to unaltered samples.
4. The length of the sonication process had an effect on the absorption; the 0.1 weight percent of CF-MWCNTs exhibited stronger absorption than the other concentrations. Among other ratios, the (1:1) ratio in the non-covalent functionalization demonstrated a better absorption rate.

5. AN increase in the I_D/I_G ratio reveals that the number of sp^2 hybridized carbons changed to sp^3 hybridization carbons because of the covalent functionalization.
6. The morphology and surface deterioration of the functionalized samples were compared to the pristine to study the structure of MWCNTs.

7. Various microstructural analysis methods, such as FTIR, FESEM, Raman Spectroscopy, and XRD, are used to examine the surface morphology of carbon nanostructures before and after functionalization. Surface modification and chemical functionalization of nanomaterials. According to the results, functional groups were present after chemical functionalization, and it is thought that this caused the functionalized nanomaterials to disperse uniformly and steadily over an extended period of time in the reinforced working fluid. (DW). Effect of the type and quantity of nano additives on the thermophysical and rheological characteristics of the prepared nanofluids: 0.02, 0.05, 0.08, and 0.1% of various nano additives' types were assessed. The numerical results demonstrated that samples containing chemically functionalized carbon nanostructures (CF-MWCNTs) improved heat absorption efficiency by 23% when compared to water, while concentrations of 0.08, 0.05, and 0.01 registered 15.2%, 10.7%, and 8.6%, respectively. Thermal conductivity was measured as 56.1%, 26.4%, 20.6%, and 18.5% for 0.1-wt% at 60°C, respectively, in contrast to DW.
8. Four samples were examined in order to discuss the foaming test, and the CF-MWCNTs failed to produce the foam that is necessary for heat transfer applications in order to prevent blockages within piping systems.
9. The current investigation demonstrated a 30.3% increase in thermal conductivity at 0.1 weight percent. The viscosity of the nanofluid increases by roughly 22% at 0.1% weight concentration at 60 oC when compared to the viscosity of the base fluid.
10. Optimum point for thermal efficiency could be connecting for 0.1 wt.% nanofluid at 4 LPM.

5.2. SUGGESTİONS FOR FURTHER RESEARCH

It is important to note that this open-ended research project needs more analysis and optimization to cover a broader range of sophisticated applications. For that, the following suggestion may be taken into account:

1. Other nanoparticles, like SWCNT, SiO_2, or Fe_2O_3, could be added to the mix of nano additives.
2. The basic working fluid can alternate between engine oil, ethylene glycol, propylene glycol, and/or acetone to accommodate various uses.
3. Instead of using the outdoor system in the FPSC, use a flexible adhesive heater affixed to the top of the absorber plate. This heater emits a constant heat flow similar to solar radiation.

REFERENCES

Abdelrahman, M., Fumeaux, P., & Suter, P. (1979). Study of solid-gas-suspensions used for direct absorption of concentrated solar radiation. Solar Energy, 22(1), 45-48..

Abdisattar, A., Yeleuov, M., Daulbayev, C., Askaruly, K., Tolynbekov, A., Taurbekov, A., & Prikhodko, N. (2022). Recent advances and challenges of current collectors for supercapacitors. *Electrochemistry Communications*, 107373.

Ahmadi, A., Ganji, D. D., & Jafarkazemi, F. (2016). Analysis of utilizing Graphene nanoplatelets to enhance thermal performance of flat plate solar collectors. Energy conversion and management, 126, 1-11.

Ajeena, A. M., Vig, P., & Farkas, I. (2022). A comprehensive analysis of nanofluids and their practical applications for flat plate solar collectors: Fundamentals, thermophysical properties, stability, and difficulties. Energy Reports, 8, 4461-4490.

ALAGAPPAN, S., SUBRAMANİYAN, A., PRİYA, S. L., & ILANGOVAN, R. (2015). Energy harvesting through optical properties of TiO2 and C-TiO2 nanofluid for direct absorption solar collectors. *International Journal of Renewable Energy Research*, *5*(2), 542-547.

Alawi, O. A., & Kamar, H. M. (2020). Performance of Solar Thermal Collector Using Multi-Walled Carbon Nanotubes: Simulation Study. *Journal of Advanced Research in Micro and Nano Engineering*, *2*(1), 12-21.

Alawi, O. A., Kamar, H. M., Mallah, A. R., Kazi, S. N., & Sidik, N. A. C. (2019). Thermal efficiency of a flat-plate solar collector filled with Pentaethylene Glycol-Treated Graphene Nanoplatelets: An experimental analysis. *Solar Energy*, *191*, 360-370..

Alawi, O. A., Kamar, H. M., Mallah, A. R., Mohammed, H. A., Sabrudin, M. A. S., Newaz, K. M. S., ... & Yaseen, Z. M. (2021). Experimental and theoretical analysis of energy efficiency in a flat plate solar collector using monolayer graphene nanofluids. *Sustainability*, *13*(10), 5416.

Alem, A., Sarpoolaky, H., & Keshmiri, M. (2009). Sol–gel preparation of titania multilayer membrane for photocatalytic applications. *Ceramics International*, *35*(5), 1837-1843.

Ali, N., Teixeira, J. A., & Addali, A. (2019). Aluminium nanofluids stability: A comparison between the conventional two-step fabrication approach and the controlled sonication bath temperature method. Journal of Nanomaterials, 2019, 1-9.

Alicia, C. P. Y., Rashmi, W., Khalid, M., Rasheed, A. K., & Gupta, T. C. S. M. (2016). Synthesis and thermo-physical characterization of graphene based transformer oil. *J. Eng. Sci. Technol*, *11*(5), 140-152.

Amiri, A., Kazi, S. N., Shanbedi, M., Zubir, M. N. M., Yarmand, H., & Chew, B. T. (2015). Transformer oil based multi-walled carbon nanotube–hexylamine coolant with optimized electrical, thermal and rheological enhancements. *Rsc Advances*, *5*(130), 107222-107236.

Amiri, A., Sadri, R., Ahmadi, G., Chew, B. T., Kazi, S. N., Shanbedi, M., & Alehashem, M. S. (2015). Synthesis of polyethylene glycol-functionalized multi-walled carbon nanotubes with a microwave-assisted approach for improved heat dissipation. *RSC Advances*, *5*(45), 35425-35434.

Amiri, A., Shanbedi, M., Eshghi, H., Heris, S. Z., & Baniadam, M. (2012). Highly dispersed multiwalled carbon nanotubes decorated with Ag nanoparticles in water and experimental investigation of the thermophysical properties. *The Journal of Physical Chemistry C*, *116*(5), 3369-3375.

Arnold, A. J., & Matthews, D. R. (2002). Corporate financial disclosures in the UK, 1920–50: the effects of legislative change and managerial discretion. *Accounting and Business Research*, *32*(1), 3-16.

Arzani, H. K., Amiri, A., Kazi, S. N., Chew, B. T., & Badarudin, A. (2016). Experimental investigation of thermophysical properties and heat transfer rate of covalently functionalized MWCNT in an annular heat exchanger. *International Communications in Heat and Mass Transfer*, *75*, 67-77.

Asadi, A., Asadi, M., Rezaniakolaei, A., Rosendahl, L. A., Afrand, M., & Wongwises, S. (2018). Heat transfer efficiency of Al2O3-MWCNT/thermal oil hybrid nanofluid as a cooling fluid in thermal and energy management applications: An experimental and theoretical investigation. *International Journal of Heat and Mass Transfer*, *117*, 474-486.

Assael, M. J., Chen, C. F., Metaxa, I., & Wakeham, W. A. (2004). Thermal conductivity of suspensions of carbon nanotubes in water. *International Journal of Thermophysics*, *25*, 971-985.

Assael, M. J., Metaxa, I. N., Arvanitidis, J., Christofilos, D., & Lioutas, C. (2005). Thermal conductivity enhancement in aqueous suspensions of carbon multi-walled and double-walled nanotubes in the presence of two different dispersants. *International Journal of Thermophysics*, *26*, 647-664.

Babu, M. J., Sandeep, N., & Saleem, S. (2017). Free convective MHD Cattaneo-Christov flow over three different geometries with thermophoresis and Brownian motion. *Alexandria Engineering Journal*, *56*(4), 659-669.

Batchelor, G. K. (1977). The effect of Brownian motion on the bulk stress in a suspension of spherical particles. *Journal of fluid mechanics*, *83*(1), 97-117.

Bazdidi-Tehrani, F., Khabazipur, A., & Vasefi, S. I. (2018). Flow and heat transfer analysis of TiO2/water nanofluid in a ribbed flat-plate solar collector. *Renewable energy*, *122*, 406-418.

Berger, T., Monllor-Satoca, D., Jankulovska, M., Lana-Villarreal, T., & Gomez, R. (2012). The electrochemistry of nanostructured titanium dioxide electrodes. *ChemPhysChem*, *13*(12), 2824-2875.

Bergmann, C., Stumpf, A., Bergmann, C. P., & Stumpf, A. (2013). Ceramic Materials for Orthodontic Use. *Dental Ceramics: Microstructure, Properties and Degradation*, 23-29.

Bertocchi, R., Karni, J., & Kribus, A. (2004). Experimental evaluation of a non-isothermal high temperature solar particle receiver. *Energy*, *29*(5-6), 687-700.

Cambaz, Z. G., Yushin, G., Osswald, S., Mochalin, V., & Gogotsi, Y. (2008). Noncatalytic synthesis of carbon nanotubes, graphene and graphite on SiC. Carbon, 46(6), 841-849.

Cao, Q., Yu, Q., Connell, D. W., & Yu, G. (2013). Titania/carbon nanotube composite (TiO 2/CNT) and its application for removal of organic pollutants. *Clean Technologies and Environmental Policy*, *15*, 871-880.

Cham sa-ard, W., Fawcett, D., Fung, C. C., Chapman, P., Rattan, S., & Poinern, G. E. J. (2021). Synthesis, characterisation and thermo-physical properties of highly stable graphene oxide-based aqueous nanofluids for potential low-temperature direct absorption solar applications. Scientific Reports, 11(1), 16549.

Chandrasekar, M., Suresh, S., & Bose, A. C. (2010). Experimental investigations and theoretical determination of thermal conductivity and viscosity of Al2O3/water nanofluid. Experimental Thermal and Fluid Science, 34(2), 210-216.

Chen, H., Cong, T. N., Yang, W., Tan, C., Li, Y., & Ding, Y. (2009). Progress in electrical energy storage system: A critical review. *Progress in natural science*, *19*(3), 291-312.

Chng, E. L. K., & Pumera, M. (2011). Metallic impurities are responsible for electrocatalytic behavior of carbon nanotubes towards sulfides. *Chemistry-An Asian Journal*, *6*(9), 2304-2307.

Choi, S. U. S., Zhang, Z. G., Yu, W., Lockwood, F. E., & Grulke, E. A. (2001). Anomalous thermal conductivity enhancement in nanotube suspensions. *Applied physics letters*, *79*(14), 2252-2254.

Choi, S. U., & Eastman, J. A. (1995). *Enhancing thermal conductivity of fluids with nanoparticles* (No. ANL/MSD/CP-84938; CONF-951135-29). Argonne National Lab.(ANL), Argonne, IL (United States).

Chougule, S. S., & Sahu, S. K. (2015). Performance of carbon nanotubes–water nanofluid charged wickless heat pipe flat plate solar collectors having different filling ratio. *Journal of Solar Energy Engineering*, *137*(2), 024501.

Chougule, S. S., Sahu, S. K., & Pise, A. T. (2014). Thermal performance of two phase thermosyphon flat-plate solar collectors using nanofluid. *Journal of solar energy engineering*, *136*(1), 014503.

Das, S. K., Choi, S. U., Yu, W., & Pradeep, T. (2007). *Nanofluids: science and technology*. John Wiley & Sons.

Duffie, J. A., & Beckman, W. A. (2013). *Solar engineering of thermal processes*. John Wiley & Sons.

Duffie, W. A. Beckman, and J. McGowan, (**1985).** Solar Engineering of Thermal Processes, vol. 53, no. 4.

Eastman, J. A., Choi, U. S., Li, S., Thompson, L. J., & Lee, S. (1996). Enhanced thermal conductivity through the development of nanofluids. *MRS Online Proceedings Library (OPL)*, *457*, 3.

Ebrahimnia-Bajestan, E., Moghadam, M. C., Niazmand, H., Daungthongsuk, W., & Wongwises, S. (2016). Experimental and numerical investigation of nanofluids heat transfer characteristics for application in solar heat exchangers. *International Journal of Heat and Mass Transfer*, *92*, 1041-1052.

Ekramian, E. E. S. H. M., Etemad, S. G., & Haghshenasfard, M. (2014). Numerical analysis of heat transfer performance of flat plate solar collectors. *Journal of Fluid Flow, Heat and Mass Transfer (JFFHMT)*, *1*, 38-42.

Elsaid, K., Abdelkareem, M. A., Maghrabie, H. M., Sayed, E. T., Wilberforce, T., Baroutaji, A., & Olabi, A. G. (2021). Thermophysical properties of graphene-based nanofluids. *International Journal of Thermofluids*, *10*, 100073.

Eltaweel, M., & Abdel-Rehim, A. A. (2019). Energy and exergy analysis of a thermosiphon and forced-circulation flat-plate solar collector using MWCNT/Water nanofluid. *Case Studies in Thermal Engineering*, *14*, 100416.

Faizal, M. S. R. M. S., Saidur, R., Mekhilef, S., Hepbasli, A., & Mahbubul, I. M. (2015). Energy, economic, and environmental analysis of a flat-plate solar collector operated with SiO 2 nanofluid. *Clean Technologies and Environmental Policy*, *17*, 1457-1473.

Faizal, M., Saidur, R., & Mekhilef, S. (2013, June). Potential of size reduction of flat-plate solar collectors when applying MWCNT nanofluid. In *IOP Conference Series: Earth and Environmental Science* (Vol. 16, No. 1, p. 012004). IOP Publishing.

Farajollahi, B., Etemad, S. G., & Hojjat, M. (2010). Heat transfer of nanofluids in a shell and tube heat exchanger. International Journal of Heat and Mass Transfer, 53(1-3), 12-17.

Farajzadeh, E., Movahed, S., & Hosseini, R. (2018). Experimental and numerical investigations on the effect of Al2O3/TiO2H2O nanofluids on thermal efficiency of the flat plate solar collector. *Renewable Energy*, *118*, 122-130.

Farhana, K., Kadirgama, K., Rahman, M. M., Ramasamy, D., Noor, M. M., Najafi, G., ... & Mahamude, A. S. F. (2019). Improvement in the performance of solar collectors with nanofluids—A state-of-the-art review. Nano-Structures & Nano-Objects, 18, 100276.

Fathi, M., Mozafari, M. R., & Mohebbi, M. (2012). Nanoencapsulation of food ingredients using lipid based delivery systems. *Trends in food science & technology*, *23*(1), 13-27.

Fedele, L., Colla, L., & Bobbo, S. (2012). Viscosity and thermal conductivity measurements of water-based nanofluids containing titanium oxide nanoparticles. *International journal of refrigeration*, *35*(5), 1359-1366.

Fragneaud, B., Masenelli-Varlot, K., Gonzalez-Montiel, A., Terrones, M., & Cavaille, J. Y. (2008). Mechanical behavior of polystyrene grafted carbon nanotubes/polystyrene nanocomposites. *Composites Science and Technology*, *68*(15-16), 3265-3271.

Gupta, M., Singh, V., Kumar, R., & Said, Z. (2017). A review on thermophysical properties of nanofluids and heat transfer applications. *Renewable and Sustainable Energy Reviews*, *74*, 638-670.

Hajabdollahi, Z. O., Mirzaei, M., & Kim, K. C. (2019). Effects of a mixture of Cuo and Al 2 O 3 nanoparticles on the thermal efficiency of a flat plate solar collector at different mass flow rates. *Heat Transfer Research*, *50*(10).

Hawwash, A. A., Rahman, A. K. A., Nada, S. A., & Ookawara, S. (2018). Numerical investigation and experimental verification of performance enhancement of flat plate solar collector using nanofluids. *Applied Thermal Engineering*, *130*, 363-374.

He, Q., Zeng, S., & Wang, S. (2015). Experimental investigation on the efficiency of flat-plate solar collectors with nanofluids. *Applied Thermal Engineering*, *88*, 165-171.

Heris, S. Z., Ahmadi, F., & Mahian, O. (2013). Pressure drop and performance characteristics of water-based Al2O3 and CuO nanofluids in a triangular duct. *Journal of dispersion science and technology*, *34*(10), 1368-1375.

Hordy, N., Rabilloud, D., Meunier, J. L., & Coulombe, S. (2014). High temperature and long-term stability of carbon nanotube nanofluids for direct absorption solar thermal collectors. *Solar Energy*, *105*, 82-90.

Hou, C. Liu, and H. M. Cheng, "Purification of carbon nanotubes," *Carbon N. Y.*, vol. 46, no. 15, pp. 2003–2025, 2008.

Hussein, O. A., Habib, K., Nasif, M., Saidur, R., & Muhsan, A. S. (2020, May). Investigation of stability, dispersion, and thermal conductivity of functionalized multi-walled carbon nanotube based nanofluid. In *IOP Conference Series: Materials Science and Engineering* (Vol. 863, No. 1, p. 012012). IOP Publishing.

Hwang, T. Y., Kim, H. J., Ahn, Y., & Lee, J. W. (2010). Influence of twin screw extrusion processing condition on the properties of polypropylene/multi-walled carbon nanotube nanocomposites. *Korea-Australia Rheology Journal*, *22*(2), 141-148.

Hwang, Y., Lee, J. K., Lee, J. K., Jeong, Y. M., Cheong, S. I., Ahn, Y. C., & Kim, S. H. (2008). Production and dispersion stability of nanoparticles in nanofluids. *Powder Technology*, *186*(2), 145-153.

Javadi, A., Zheng, Q., Payen, F., Javadi, A., Altin, Y., Cai, Z., ... & Gong, S. (2013). Polyvinyl alcohol-cellulose nanofibrils-graphene oxide hybrid organic aerogels. ACS applied materials & interfaces, 5(13), 5969-5975.

Javadi, F. S., Saidur, R., & Kamalisarvestani, M. (2013). Investigating performance improvement of solar collectors by using nanofluids. *Renewable and Sustainable Energy Reviews*, *28*, 232-245.

Jesko, Ž. (2008). Classification of solar collectors. *rN*, *1*(21), 21.

Jha, N., & Ramaprabhu, S. (2008). Synthesis and thermal conductivity of copper nanoparticle decorated multiwalled carbon nanotubes based nanofluids. The Journal of Physical Chemistry C, 112(25), 9315-9319.

Jiang, L., Gao, L., & Sun, J. (2003). Production of aqueous colloidal dispersions of carbon nanotubes. *Journal of colloid and interface science*, *260*(1), 89-94.

Jouybari, H. J., Nimvari, M. E., & Saedodin, S. (2019). Thermal performance evaluation of a nanofluid-based flat-plate solar collector: An experimental study and analytical modeling. *Journal of Thermal Analysis and Calorimetry*, *137*, 1757-1774.

Jouybari, H. J., Saedodin, S., Zamzamian, A., Nimvari, M. E., & Wongwises, S. (2017). Effects of porous material and nanoparticles on the thermal performance of a flat plate solar collector: an experimental study. *Renewable Energy*, *114*, 1407-1418.

Kamanina, O. A., Saverina, E. A., Rybochkin, P. V., Arlyapov, V. A., Vereshchagin, A. N., & Ananikov, V. P. (2022). Preparation of hybrid sol-gel materials based on living cells of microorganisms and their application in nanotechnology. *Nanomaterials*, *12*(7), 1086.

Kang, W., Shin, Y., & Cho, H. (2017). Economic analysis of flat-plate and U-tube solar collectors using an Al2O3 nanofluid. *Energies*, *10*(11), 1911.

Kanti, P., Sharma, K. V., Ramachandra, C. G., & Gurumurthy, M. (2020, December). A CFD Study on fly ash nanofluid heat transfer behavior in a circular tube. In IOP Conference Series: Materials Science and Engineering (Vol. 1013, No. 1, p. 012030). IOP Publishing.

Karadimitriou, N. K., & Hassanizadeh, S. M. (2012). A review of micromodels and their use in two-phase flow studies. Vadose Zone Journal, 11(3).

Karami, M., Bahabadi, M. A., Delfani, S., & Ghozatloo, A. (2014). A new application of carbon nanotubes nanofluid as working fluid of low-temperature direct absorption solar collector. *Solar Energy Materials and Solar Cells*, *121*, 114-118.

Kashyap, Y., Singh, A., & Raja Sekhar, Y. (2018). Exergy analysis of a flat plate solar collector with grooved absorber tube configuration using aqueous ZnO–ethylene glycol. *Journal of Solar Energy Engineering*, *140*(6), 061011.

Khaledi, O., Saedodin, S., & Rostamian, S. H. (2023). Experimental investigation of thermal efficiency and thermal performance improvement of compound parabolic collector utilizing SiO2/ethylene glycol–water nanofluid. Environmental Science and Pollution Research, 30(5), 12169-12188.

Khan, M. M., Adil, S. F., & Al-Mayouf, A. (2015). Metal oxides as photocatalysts. *Journal of Saudi chemical society*, *19*(5), 462-464.

Khan, S., & Hossain, M. K. (2022). aOklahoma State University, Stillwater, OK, United States, bKyushu University, Fukuoka, Japan, cBangladesh Atomic Energy Commission, Dhaka, Bangladesh.

Kiliç, F., Menlik, T., & Sözen, A. (2018). Effect of titanium dioxide/water nanofluid use on thermal performance of the flat plate solar collector. *Solar Energy*, *164*, 101-108.

Kim, K. M., Choi, B. J., Shin, Y. C., Choi, S., & Hwang, C. S. (2007). Anode-interface localized filamentary mechanism in resistive switching of TiO2 thin films. *Applied physics letters*, *91*(1).

Koca, H. D., Doganay, S., & Turgut, A. (2017). Thermal characteristics and performance of Ag-water nanofluid: Application to natural circulation loops. *Energy Conversion and Management*, *135*, 9-20.

Kuang, Z., Chen, Y., Lu, Y., Liu, L., Hu, S., Wen, S., ... & Zhang, L. (2015). Fabrication of highly oriented hexagonal boron nitride nanosheet/elastomer nanocomposites with high thermal conductivity. Small, 11(14), 1655-1659.

Kumar, S., & Tien, C. L. (1990). Analysis of combined radiation and convection in a particulate-laden liquid film.

Lee, J. Y., Choi, H. J., Park, I. N., Hong, S. B., Oh, Y. M., Lim, C. M., ... & Shim, T. S. (2006). Comparison of two commercial interferon-γ assays for diagnosing Mycobacterium tuberculosis infection. European Respiratory Journal, 28(1), 24-30.

Lee, S., Choi, S. S., Li, S. A., & Eastman, J. A. (1999). Measuring thermal conductivity of fluids containing oxide nanoparticles..

Levshov, D. (2013). *Raman modes in index-identified individual single-walled and multi-walled carbon nanotubes* (Doctoral dissertation, Université Montpellier II-Sciences et Techniques du Languedoc; Rostovskij gosudarstvennyj universitet).

Li, W., Zou, C., & Li, X. (2018). Thermo-physical properties of cooling water-based nanofluids containing TiO2 nanoparticles modified by Ag elementary substance for crystallizer cooling system. *Powder Technology*, *329*, 434-444.

Li, Y., Zhu, G., Xu, X., Chen, L., Lu, T., Hill, J. P., ... & Yamauchi, Y. (2022). Embedding metal–organic frameworks for the design of flexible hybrid supercapacitors by electrospinning: synthesis of highly graphitized carbon nanofibers containing metal oxide nanoparticles. *Small Structures*, *3*(9), 2200015.

Liu, M. S., Lin, M. C. C., Huang, I. T., & Wang, C. C. (2005). Enhancement of thermal conductivity with carbon nanotube for nanofluids. *International communications in heat and mass transfer*, *32*(9), 1202-1210.

Liu, Z., Suenaga, K., Harris, P. J., & Iijima, S. (2009). Open and closed edges of graphene layers. *Physical review letters*, *102*(1), 015501.

Long, B., Manning, M., Burke, M., Szafranek, B. N., Visimberga, G., Thompson, D., ... & Quinn, A. J. (2012). Non-covalent functionalization of graphene using self-assembly of alkane-amines. Advanced Functional Materials, 22(4), 717-725.

Lu, Y., Li, J., Han, J., Ng, H. T., Binder, C., Partridge, C., & Meyyappan, M. (2004). Room temperature methane detection using palladium loaded single-walled carbon nanotube sensors. Chemical Physics Letters, 391(4-6), 344-348.

Luo, Y. Z., Tang, G. J., & Zhou, L. N. (2008). Hybrid approach for solving systems of nonlinear equations using chaos optimization and quasi-Newton method. *Applied Soft Computing*, *8*(2), 1068-1073.

Madhesh, D., Parameshwaran, R., & Kalaiselvam, S. (2014). Experimental investigation on convective heat transfer and rheological characteristics of Cu–TiO2 hybrid nanofluids. *Experimental Thermal and Fluid Science*, *52*, 104-115.

Mahian, O., Kianifar, A., Sahin, A. Z., & Wongwises, S. (2014). Performance analysis of a minichannel-based solar collector using different nanofluids. *Energy conversion and management*, *88*, 129-138.

Mahmoud, M. S. (2021). Numerical investigation of conjugate combined convective heat transfer for internal laminar flow of AL2O3/water nanofluid through tube–flat plate solar collector. *Journal of Engineering Science and Technology*, *16*(3), 2378-2393.

Mahmoud, M., Ramadan, M., Olabi, A. G., Pullen, K., & Naher, S. (2020). A review of mechanical energy storage systems combined with wind and solar applications. Energy Conversion and Management, 210, 112670.

Marconnet, A. M., Panzer, M. A., & Goodson, K. E. (2013). Thermal conduction phenomena in carbon nanotubes and related nanostructured materials. Reviews of Modern Physics, 85(3), 1295.

Mehrali, M., Latibari, S. T., Mehrali, M., Mahlia, T. M. I., & Metselaar, H. S. C. (2014). Effect of carbon nanospheres on shape stabilization and thermal behavior of phase change materials for thermal energy storage. *Energy conversion and management*, *88*, 206-213.

Michael, J. J., & Iniyan, S. (2015). Performance of copper oxide/water nanofluid in a flat plate solar water heater under natural and forced circulations. *Energy conversion and management*, *95*, 160-169.

Miller, F. J., & Koenigsdorff, R. W. (2000). Thermal modeling of a small-particle solar central receiver. *J. Sol. Energy Eng.*, *122*(1), 23-29.

Minardi, J. E., & Chuang, H. N. (1975). Performance of a "black" liquid flat-plate solar collector. *Solar Energy*, *17*(3), 179-183.

Moore, J. A., Jarding, B. P., Lograsso, B. K., & Anderson, I. E. (1995). Atmosphere control during debinding of powder injection molded parts. *Journal of materials engineering and performance*, *4*, 275-282.

Mukesh Kumar, P. C. (2017). Stability analysis of heat transfer MWCNT with different base fluids. Journal of Applied Fluid Mechanics, 10(Special Issue)), 51-59.

Mukesh, M. G., Katyal, P., & Kumar, R. (2020). A comparative study of nanofluid (Al2O3) and distilled water in terms of thermal conductivity. IJCS, 8(2), 1148-1154.

Naik, M. T., Janardana, G. R., & Sundar, L. S. (2013). Experimental investigation of heat transfer and friction factor with water–propylene glycol based CuO nanofluid in a tube with twisted tape inserts. *International Communications in Heat and Mass Transfer*, *46*, 13-21.

Namburu, P. K., Kulkarni, D. P., Misra, D., & Das, D. K. (2007). Viscosity of copper oxide nanoparticles dispersed in ethylene glycol and water mixture. *Experimental Thermal and Fluid Science*, *32*(2), 397-402.

Natarajan, E., & Sathish, R. (2009). Role of nanofluids in solar water heater. *The International Journal of Advanced Manufacturing Technology*, 1-5.

Nguyen, C. T., Desgranges, F., Roy, G., Galanis, N., Maré, T., Boucher, E., & Mintsa, H. A. (2007). Temperature and particle-size dependent viscosity data for water-based nanofluids–hysteresis phenomenon. *International journal of heat and fluid flow*, *28*(6), 1492-1506.

Niu, S., Han, B., Cao, W., & Zhang, S. (2009). Sensitive DNA biosensor improved by Luteolin copper (II) as indicator based on silver nanoparticles and carbon nanotubes modified electrode. *Analytica chimica acta*, *651*(1), 42-47.

Oh, D. W., Jain, A., Eaton, J. K., Goodson, K. E., & Lee, J. S. (2008). Thermal conductivity measurement and sedimentation detection of aluminum oxide nanofluids by using the 3ω method. *International Journal of Heat and Fluid Flow*, *29*(5), 1456-1461.

O'Hanley, H., Buongiorno, J., McKrell, T., & Hu, L. W. (2012). Measurement and model validation of nanofluid specific heat capacity with differential scanning calorimetry. Advances in Mechanical Engineering, 4, 181079.

Olayiwola, S. O., & Dejam, M. (2019). A comprehensive review on interaction of nanoparticles with low salinity water and surfactant for enhanced oil recovery in sandstone and carbonate reservoirs. *Fuel*, *241*, 1045-1057.

Pak, B. C., & Cho, Y. I. (1998). Hydrodynamic and heat transfer study of dispersed fluids with submicron metallic oxide particles. *Experimental Heat Transfer an International Journal*, *11*(2), 151-170.

Pan, D., Zhang, J., Li, Z., & Wu, M. (2010). Hydrothermal route for cutting graphene sheets into blue-luminescent graphene quantum dots. *Advanced materials*, *22*(6), 734-738.

Pantzali, M. N., Mouza, A. A., & Paras, S. V. (2009). Investigating the efficacy of nanofluids as coolants in plate heat exchangers (PHE). *Chemical Engineering Science*, *64*(14), 3290-3300.

Peng, Y., Zahedidastjerdi, A., Abdollahi, A., Amindoust, A., Bahrami, M., Karimipour, A., & Goodarzi, M. (2020). Investigation of energy performance in a U-shaped evacuated solar tube collector using oxide added nanoparticles through the emitter, absorber and transmittal environments via discrete ordinates radiation method. *Journal of Thermal Analysis and Calorimetry*, *139*, 2623-2631.

Poinern, G. E. J., Ali, N., & Fawcett, D. (2011). Progress in nano-engineered anodic aluminum oxide membrane development. Materials, 4(3), 487-526.

Postol, Y., & Struchaiev, M. (2020). Improving the pneumoreactive device for a wind generator.

Prasojo, I., Maseleno, A., & Shahu, N. (2020). Design of automatic watering system based on Arduino. Journal of Robotics and Control (JRC), 1(2), 59-63.

Qin, C., Kang, K., Lee, I., & Lee, B. J. (2017). Optimization of a direct absorption solar collector with blended plasmonic nanofluids. *Solar Energy*, *150*, 512-520.

Raj, P., & Subudhi, S. (2018). A review of studies using nanofluids in flat-plate and direct absorption solar collectors. *Renewable and Sustainable Energy Reviews*, *84*, 54-74.

Ramasamy, S., Balashanmugam, P., & Suresh, R.(2020) Evaluation of Solar Water Heater Performance Using Simulation. structure, 5762, 50K.

Ramires, M. L., Nieto de Castro, C. A., Nagasaka, Y., Nagashima, A., Assael, M. J., & Wakeham, W. A. (1995). Standard reference data for the thermal conductivity of water. *Journal of Physical and Chemical Reference Data*, *24*(3), 1377-1381.

Razi, M., Contreras-Mateus, M., Hashlamoun, K. W., & Nassar, N. N. (2022). Nanoparticles: Preparation, Stabilization, and Control Over Particle Size. In

Nanoparticles: An Emerging Technology for Oil Production and Processing Applications (pp. 1-40). Cham: Springer International Publishing.

Rohrig, B. **(2004).** The science of slime!. ChemMatters, 22(4), 13.

S. G. Benka,(2005). "Two-dimensional atomic crystals," Phys. Today, vol. 58, no. 9, pp. 9–9.

Sadeghi, G., Safarzadeh, H., & Ameri, M. (2019). Experimental and numerical investigations on performance of evacuated tube solar collectors with parabolic concentrator, applying synthesized Cu2O/distilled water nanofluid. *Energy for sustainable development*, *48*, 88-106.

Sadripour, S. (2017). First and second laws analysis and optimization of a solar absorber; using insulator mixers and MWCNTs nanoparticles. Global Journal of Researches in Engineering A: Mechanical and Mechanics, 17(5), 37-48.

Said, Z., Sabiha, M. A., Saidur, R., Hepbasli, A., Rahim, N. A., Mekhilef, S., & Ward, T. A. (2015). Performance enhancement of a flat plate solar collector using titanium dioxide nanofluid and polyethylene glycol dispersant. *Journal of Cleaner Production*, *92*, 343-353.

Said, Z., Saidur, R., Rahim, N. A., & Alim, M. A. (2014). Analyses of exergy efficiency and pumping power for a conventional flat plate solar collector using SWCNTs based nanofluid. *Energy and Buildings*, *78*, 1-9.

Said, Z., Saidur, R., Sabiha, M. A., Rahim, N. A., & Anisur, M. R. (2015). Thermophysical properties of Single Wall Carbon Nanotubes and its effect on exergy efficiency of a flat plate solar collector. *Solar Energy*, *115*, 757-769.

Saidur, R., Leong, K. Y., & Mohammed, H. A. (2011). A review on applications and challenges of nanofluids. *Renewable and sustainable energy reviews*, *15*(3), 1646-1668.

Saleh, R., Putra, N., Wibowo, R. E., Septiadi, W. N., & Prakoso, S. P. (2014). Titanium dioxide nanofluids for heat transfer applications. Experimental Thermal and Fluid Science, 52, 19-29.

Sarkar, B., Mandal, S., Tsang, Y. F., Kumar, P., Kim, K. H., & Ok, Y. S. (2018). Designer carbon nanotubes for contaminant removal in water and wastewater: a critical review. Science of the Total Environment, 612, 561-581.

Sarsam, W. S., Amiri, A., Kazi, S. N., & Badarudin, A. **(2016).** Stability and thermophysical properties of non-covalently functionalized graphene nanoplatelets nanofluids. *Energy conversion and management*, *116*, 101-111.

Sarsam, W. S., Kazi, S. N., & Badarudin, A. (2020). Thermal performance of a flat-plate solar collector using aqueous colloidal dispersions of graphene nanoplatelets with different specific surface areas. *Applied Thermal Engineering*, *172*, 115142.

Sarsam, W. S., Kazi, S. N., & Badarudin, A. (2022). Thermal performance of a flat-plate solar collector using aqueous colloidal dispersions of multi-walled carbon nanotubes with different outside diameters. *Experimental Heat Transfer*, *35*(3), 258-281.

Satish, J., & Satish, K. G. (2018, February). Preparation of magnesium metal matrix composites by powder metallurgy process. In IOP Conference Series: Materials Science and Engineering (Vol. 310, No. 1, p. 012130). IOP Publishing.

Schedin, F., Geim, A. K., Morozov, S. V., Hill, E. W., Blake, P., Katsnelson, M. I., & Novoselov, K. S. (2007). Detection of individual gas molecules adsorbed on graphene. Nature materials, 6(9), 652-655.

Sekhar, Y. R., & Sharma, K. V. (2015). Study of viscosity and specific heat capacity characteristics of water-based Al2O3 nanofluids at low particle concentrations. *Journal of experimental Nanoscience*, *10*(2), 86-102.

Shafieian, A., Khiadani, M., & Nosrati, A. **(2018).** A review of latest developments, progress, and applications of heat pipe solar collectors. *Renewable and Sustainable Energy Reviews*, *95*, 273-304

Sint, N. K. C., Choudhury, I. A., Masjuki, H. H., & Aoyama, H. (2017). Theoretical analysis to determine the efficiency of a CuO-water nanofluid based-flat plate solar collector for domestic solar water heating system in Myanmar. *Solar energy*, *155*, 608-619.

Solangi Khalid, H. **(2016).** Heat transfer to graphene nanoplatelets and metaloxides-studies in thermophysical properties and particle characterization/Solangi Khalid Hussain (Doctoral dissertation, Universiti Malaya).

Sridhar, V., Jeon, J. H., & Oh, I. K. (2010). Synthesis of graphene nano-sheets using eco-friendly chemicals and microwave radiation. *Carbon*, *48*(10), 2953-2957.

Sundar, L. S., Singh, M. K., Punnaiah, V., & Sousa, A. C. (2018). Experimental investigation of Al2O3/water nanofluids on the effectiveness of solar flat-plate collectors with and without twisted tape inserts. *Renewable energy*, *119*, 820-833.

Suslick, K. S. (1989). The chemical effects of ultrasound. *Scientific American*, *260*(2), 80-87.

Takabi, B., & Shokouhmand, H. (2015). Effects of Al 2 O 3–Cu/water hybrid nanofluid on heat transfer and flow characteristics in turbulent regime. *International Journal of Modern Physics C*, *26*(04), 1550047.

Tavakoli, A. H., Maram, P. S., Widgeon, S. J., Rufner, J., Van Benthem, K., Ushakov, S., ... & Navrotsky, A. (2013). Amorphous alumina nanoparticles: structure, surface energy, and thermodynamic phase stability. The Journal of Physical Chemistry C, 117(33), 17123-17130.

Thirugnanasambandam, M., Iniyan, S., & Goic, R. (2010). A review of solar thermal technologies. Renewable and sustainable energy reviews, 14(1), 312-322.

Ting-ting, H., Qing-tao, F., & Chen-guang, L. (2018, July). Synthesis and character investigation of magnetic alumina microspheres. In *IOP Conference Series: Materials Science and Engineering* (Vol. 392, No. 2, p. 022017). IOP Publishing.

Tomy, A. M., Ahammed, N., Subathra, M. S. P., & Asirvatham, L. G. (2016). Analysing the performance of a flat plate solar collector with silver/water nanofluid using artificial neural network. Procedia Computer Science, 93, 33-40.

Tsai, J. L., Tzeng, S. H., & Chiu, Y. T. (2010). Characterizing elastic properties of carbon nanotubes/polyimide nanocomposites using multi-scale simulation. *Composites Part B: Engineering*, *41*(1), 106-115.

Tyagi, H., Phelan, P., & Prasher, R. (2009). Predicted efficiency of a low-temperature nanofluid-based direct absorption solar collector.

Umar, S., Sulaiman, F., Abdullah, N., & Mohamad, S. N. (2018, November). Investigation of the effect of pH adjustment on the stability of nanofluid. In AIP Conference Proceedings (Vol. 2031, No. 1, p. 020031). AIP Publishing LLC.

Vaisman, L., Wagner, H. D., & Marom, G. (2006). The role of surfactants in dispersion of carbon nanotubes. *Advances in colloid and interface science*, *128*, 37-46.

Vajjha, R. S., & Das, D. K. (2009). Experimental determination of thermal conductivity of three nanofluids and development of new correlations. International Journal of Heat and Mass Transfer, 52(21-22), 4675-4682.

Vatani, A., & Mohammed, H. A. (2013). Turbulent nanofluidflow over periodic rib-grooved channels.Engineering Appli-cations of Computational Fluid Mechanics,7(3), 369–381.

Verma, S. K., Tiwari, A. K., & Chauhan, D. S. (2016). Performance augmentation in flat plate solar collector using MgO/water nanofluid. *Energy conversion and management*, *124*, 607-617.

Verma, S. K., Tiwari, A. K., & Chauhan, D. S. (2017). Experimental evaluation of flat plate solar collector using nanofluids. *Energy conversion and Management*, *134*, 103-115.

Verma, V., & Kundan, L. (2013). Thermal performance evaluation of a direct absorption flat plate solar collector (DASC) using Al2O3-H2O based nanofluids. IOSR J. Mech. Civ. Eng, 6, 29-35

Vijayakumar, S., Nagamuthu, S., & Muralidharan, G. (2013). Supercapacitor studies on NiO nanoflakes synthesized through a microwave route. *ACS applied materials & interfaces*, *5*(6), 2188-2196.

Vincely, D. A., & Natarajan, E. J. E. C. (2016). Experimental investigation of the solar FPC performance using graphene oxide nanofluid under forced circulation. Energy conversion and management, 117, 1-11..

Wang, D., Fan, B., Chen, Y., Han, Y., Liu, Y., Wang, Y., ... & Jiao, X. (2022). Comparative analysis of heat loss performance of flat plate solar collectors at different altitudes. Solar Energy, 244, 490-506

Wang, H. (2009). Dispersing carbon nanotubes using surfactants. *Current Opinion in Colloid & Interface Science*, *14*(5), 364-371.

Wang, X. J., & Zhu, D. S. (2009). Investigation of pH and SDBS on enhancement of thermal conductivity in nanofluids. *Chemical Physics Letters*, *470*(1-3), 107-111.

Wang, X. Q., & Mujumdar, A. S. (2008). A review on nanofluids-part I: theoretical and numerical investigations. *Brazilian journal of chemical engineering*, *25*, 613-630.

Wen, D., Lin, G., Vafaei, S., & Zhang, K. (2009). Review of nanofluids for heat transfer applications. *Particuology*, *7*(2), 141-150.

Wu, G. T., Wang, C. S., Zhang, X. B., Yang, H. S., Qi, Z. F., & Li, W. Z. (1998). Lithium insertion into CuO/carbon nanotubes. *Journal of Power Sources*, *75*(1), 175-179.

Xu, D., & Wang, Z. (2008). Role of multi-wall carbon nanotube network in composites to crystallization of isotactic polypropylene matrix. *Polymer*, *49*(1), 330-338.

Xu, J., Sheng, T., Hu, Y., Baig, S. A., Lv, X., & Xu, X. (2013). Adsorption–dechlorination of 2, 4-dichlorophenol using two specified MWCNTs-stabilized Pd/Fe nanocomposites. *Chemical engineering journal*, *219*, 162-173.

Yadav, S. K., & Cho, J. W. (2013). Functionalized graphene nanoplatelets for enhanced mechanical and thermal properties of polyurethane nanocomposites. *Applied surface science*, *266*, 360-367.

Yang, Y., Kaner, R. B., Tung, C. C., & Allen, M. J. (2015). U.S. Patent No. 9,105,403. Washington, DC: U.S. Patent and Trademark Office..

Yang, Z., Peng, H., Wang, W., & Liu, T. (2010). Crystallization behavior of poly (ε-caprolactone)/layered double hydroxide nanocomposites. *Journal of applied polymer science*, *116*(5), 2658-2667.

Yarmand, H., Gharehkhani, S., Shirazi, S. F. S., Amiri, A., Alehashem, M. S., Dahari, M., & Kazi, S. N. (2016). Experimental investigation of thermo-physical properties, convective heat transfer and pressure drop of functionalized graphene nanoplatelets aqueous nanofluid in a square heated pipe. Energy Conversion and Management, 114, 38-49.

Yousefi, N., Gudarzi, M. M., Zheng, Q., Aboutalebi, S. H., Sharif, F., & Kim, J. K. (2012). Self-alignment and high electrical conductivity of ultralarge graphene oxide–polyurethane nanocomposites. *Journal of Materials Chemistry*, *22*(25), 12709-12717.

Yousefi, T., Shojaeizadeh, E., Veysi, F., & Zinadini, S. (2012). An experimental investigation on the effect of pH variation of MWCNT–H2O nanofluid on the efficiency of a flat-plate solar collector. *Solar Energy*, *86*(2), 771-779.

Yousefi, T., Veisy, F., Shojaeizadeh, E., & Zinadini, S. (2012). An experimental investigation on the effect of MWCNT-H2O nanofluid on the efficiency of flat-plate solar collectors. *Experimental thermal and fluid science*, *39*, 207-212.

Yu, W., & Xie, H. (2012). A review on nanofluids: preparation, stability mechanisms, and applications. Journal of nanomaterials, 2012, 1-17.

Yuan, J., & Liew, K. M. (2009). Effects of vacancy defect reconstruction on the elastic properties of carbon nanotubes. *Carbon*, *47*(6), 1526-1533.

Zhang, T., Mubeen, S., Myung, N. V., & Deshusses, M. A. (2008). Recent progress in carbon nanotube-based gas sensors. *Nanotechnology*, *19*(33), 332001.

Zhu, C. L., Chou, S. W., He, S. F., Liao, W. N., & Chen, C. C. (2007). Synthesis of core/shell metal oxide/polyaniline nanocomposites and hollow polyaniline capsules. Nanotechnology, 18(27), 275604.

Zhu, H. T., Lin, Y. S., & Yin, Y. S. (2004). A novel one-step chemical method for preparation of copper nanofluids. *Journal of colloid and interface science*, *277*(1), 100-103.

Ziyadanogullari, N. B., Yucel, H. L., & Yildiz, C. (2018). Thermal performance enhancement of flat-plate solar collectors by means of three different nanofluids. *Thermal Science and Engineering Progress*, *8*, 55-65.

RESUME

Abdul Azeez Ahmed HAMEEDİ, I completed my primary education in (Al-Nahrain School for Boys) and joined (Al-Nahrain Secondary School for Boys) and both are located in the same city (Iraq - Salah Al-Din - Al-Sharqat / Left Coast). After graduating from secondary education in 2011, I joined (University of Tikrit - College of Engineering - Department of Mechanical Engineering) and in 2014 I graduated with an “acceptable” grade. I worked in private sector companies, then I joined (Karbuk University - Turkey) in 2021 to study a master’s degree in energy systems renewable and graduated in 2023.